UNIVERSITY OF CALIFORNIA, SAN DIEGO

Synthetic Advances for P_2N_2 Molecular Electrocatalysts with Pendant Bases in the Second Coordination Sphere

A dissertation submitted in partial satisfaction of the
requirements for the degree of Doctor of Philosophy

in

Chemistry

by

Michael David Doud

Committee in charge:

Professor Clifford P. Kubiak, Chair
Professor Katherine A. Barbeau
Professor Joshua S. Figueroa
Professor Michael J. Sailor
Professor Michael J. Tauber

2016

The dissertation of Michael David Doud is approved, and it is acceptable in quality and form for publication on microfilm and electronically:

_____

_____

_____

_____

_____

Chair

University of California, San Diego

2016

DEDICATION

This thesis is dedicated to

Manna, David, Valerie, Emma, and Theresa Doud

EPIGRAPH

1. Find a subject you care about.

2. Do not ramble, though.

3. Keep it simple.

4. Have the guts to cut.

5. Sound like yourself.

6. Say what you mean to say

7. Pity the readers.

-Kurt Vonnegut, Jr.

TABLE OF CONTENTS

Signature Page iii

Dedication iv

Epigraph v

Table of Contents vi

List of Figures x

List of Schemes xii

List of Tables xiii

Acknowledgements xiv

Vita xvii

Abstract of the Dissertation xix

CHAPTER 1
STORAGE OF RENEWABLE ENERGY AS A CHEMICAL FUEL: THE ROLE OF MOLECULAR ELECTROCATALYSTS 1

1.1 Introduction 1

1.2 Development of a renewable energy economy 1

1.3 Proton-Coupled Electron Transfer (PCET) and chemical fuel electrocatalysis 3

1.4 Design principles for molecular electrocatalysts 4

1.5 Nickel P_2N_2 complexes catalyze production of H_2 5

1.6 Hydricity and $Ni(P_2N_2)_2$ complexes 7

1.7 Description of Select Techniques 10

1.8 Summary 11

1.9 References 12

CHAPTER 2
S_N2 SYNTHESIS OF $P^R_2N^{R'}_2$ LIGANDS FOR MOLECULAR ELECTROCATALYSTS WITH PENDANT BASES IN THE SECOND COORDINATION SPHERE 16

2.1 Abstract 16

2.2 Introduction 16

2.3 Experimental 18

2.3.1 General Considerations 18

2.3.2 Preparation of tris(hydroxymethyl)phosphine (THP) 19

2.3.3 Synthesis of $P^{Me}_2N^{Ph}_2$ (3).....20

2.3.4 Synthesis of $P^{Et}_2N^{Ph}_2$ (4).....21

2.3.5 Synthesis of $P^{Bn}_2N^{Ph}_2$ (5).....22

2.3.6 Preparation of $Ni(P^{R}_2N^{Ph}_2)_2(CH_3CN)[BF_4]_2$.....22

2.3.7 Preparation of $Ni(P^{Me}_2N^{Ph}_2)_2[SO_3CF_3]_2$ (7) and X-ray Structure Determination.....23

2.3.8 Preparation of $Ni(P^{Et}_2N^{Ph}_2)_2[SO_3CF_3]_2$ (8) and X-ray Structure Determination.....23

2.4 Results and Discussion.....24

2.5 Conclusion.....31

2.6 References.....32

2.7 Appendix.....35

2.7.1 Crystallographic details for 7, $Ni(P^{Me}_2N^{Ph}_2)_2[SO_3CF_3]_2$.....35

2.7.2 Crystallographic details for 8, $Ni(P^{Et}_2N^{Ph}_2)_2(CH_3CN)[SO_3CF_3]_2$.....36

CHAPTER 3
SYNTHESIS OF P_2N_2 LIGANDS VIA MICHAEL ADDITION.....37

3.1 ABSTRACT.....37

3.2 Introduction.....37

3.3 Previously reported syntheses of P_2N_2 ligands.....39

3.4 Synthesis of P_2N_2 ligands via Michael Addition.....40

3.5 Nickel complexes of P_2N_2 ligands with carbonyl phosphine substituents.....41

3.6 Experimental Details.....46

3.6.1 General Considerations.....46

3.6.2 Synthesis of $P^{PA}_2N^{Ph}_2$ (6).....47

3.6.3 Synthesis of $P^{Amide}_2N^{Ph}_2$ (7).....48

3.6.4 Synthesis of $Ni(P^{PA}_2N^{Ph}_2)$ (10).....49

3.6.5 Synthesis of $Ni(P^{Amide}_2N^{Ph}_2)[BF_4]_2$ (11).....50

3.6.6 Synthesis of $P^{EtE}_2N^{Ph}_2$ (5).....50

3.6.7 Synthesis of $P^{EtE}_2N^{PhOMe}_2$ (6).....51

3.6.8 Preparation of $Ni(P^{EtE}_2N^{Ph}_2)Cl_2$ (12).....52

3.6.9 Preparation of $Ni(P^{EtE}_2N^{PhOMe}_2)Cl_2$ (13).....53

3.7 Conclusion 53
3.8 References 54
3.8 Appendix 58
3.8.1. Crystallographic details for 10, Ni($P^{PA}_2N^{Ph}_2$). 58
3.8.2 Crystallographic details for 11, [Ni(PAmide2NPh2)](BF4)2. 60
3.8.3 Crystallographic details of 12, Ni($P^{EtE}_2N^{Ph}_2$)Cl_2 62
3.8.4 Crystallographic details of 13, Ni($P^{EtE}_2N^{PhOMe}_2$)Cl_2. 64

CHAPTER 4
HYDROGEN EVOLUTION ELECTROCATALYSIS BY P_2N_2 COMPLEXES 66
4.1 Abstract 66
4.2 Introduction 66
4.3 Results and Discussion 69
4.4 Experimental 74
4.4.1 General Considerations 74
4.4.2 Synthesis of Ni($P^{Me}_2N^{Ph}_2$)$[BF_4]_2$ 75
4.4.3 Synthesis of Ni($P^{Et}_2N^{Ph}_2$)$[BF_4]_2$ 75
4.4.4 Synthesis of Ni($P^{Amide}_2N^{Ph}_2$) (11) 76
4.4.5 Preparation of Ni($P^{EtE}_2N^{Ph}_2$)Cl_2 (12) 76
4.4.6 Preparation of Ni($P^{EtE}_2N^{PhOMe}_2$)Cl_2 (13) 77
4.5 Conclusion 78
4.6 References 78

CHAPTER 5
FORMATE OXIDATION ELECTROCATALYSIS BY P_2N_2 COMPLEXES 81
5.1 Abstract 81
5.2 Introduction 81
5.3 Results and Discussion 83
5.4 Experimental 86
5.4.1 General Considerations 86
5.4.2 Synthesis of Ni($P^{PA}_2N^{Ph}_2$) (10) 87
5.4.3 Synthesis of Ni($P^{Amide}_2N^{Ph}_2$) (11) 88
5.4.4 Preparation of Ni($P^{EtE}_2N^{Ph}_2$)Cl_2 (12) 88

5.4.5 Preparation of Ni($P^{EtE}_2N^{PhOMe}_2$)Cl_2 (13) 89
5.5 Conclusion 89
5.6 References 90
CHAPTER 6
CONCLUSIONS AND FUTURE WORK 92
6.1 Introduction 92
6.2 Catalyst immobilization 92
6.3 Substitution of phosphine by S_N1 or Michael addition reagents ...93
6.4 Synthesis of asymmetric complexes 94
6.5 Testing of metal-P_4N_5 complexes as catalysts 96
6.6 The future of biomimetic catalysis 98
6.7 References 99
6.8 Appendix 101

LIST OF FIGURES

Figure 1.1. Current annual global energy consumption, total recoverable reserves of finite energy resources, and yearly potential yield of renewable resources.[5] 2

Figure 1.2. Diagram of PCET reactions for a hydrogen atom. Proton and electron transfer can be sequential (reactions depicted on edges) or concerted (reaction on diagonal). 4

Figure 1.3. Active site of [FeFe] Hydrogenase (A) and $Ni(P^{R}_{2}N^{R'}_{2})_{2}^{2+}$ (B) 5

Figure 1.4. Molecular orbital diagram for a typical nickel bis(diphosphine) hydride. As indicated above, the Ni^{2+} complex has 8 d-electrons, and the ligands are considered to donate 10 electrons. 8

Figure 1.5. Free energy change upon donation of H– (hydricities) by various [NiH(P2N2)]+ complexes, compared with their standard reduction potentials E0(NiII/I) 9

Figure 1.6. Diagram of an electrochemical cell for performing cyclic voltammetry (CV) and electrocatalytic measurements. 11

Figure 2.1 Structure of the FeFe Hydrogenase active site (1) and the $Ni(P^{R}_{2}N^{R'}_{2})_{2}^{2+}$ cation (2). 17

Figure 2.2 $P^{R}_{2}N^{Ph}_{2}$ ligands with methyl (3), ethyl (4), and benzyl (5) phosphine substituents synthesized from THPCl. 25

Figure 2.3 Cyclic voltammogram of 2.0 mM $Ni(P^{Me}_{2}N^{Ph}_{2})_{2}[BF_4]_2$ in benzonitrile/0.2 M Bu_4NPF_6 with a 1mm glassy carbon working electrode. Scan rate = 0.1 V s^{-1}. 28

Figure 2.4 Cyclic voltammogram of 1.0 mM 7 $[Ni(Et.Ph)_2](BF_4)_2$ with ferrocene added for internal reference in 0.2 M Bu_4NPF_6 in benzonitrile with a 1mm glassy carbon working electrode. Scan rate = 0.1 V s^{-1}. 29

Figure 2.5 X-ray crystal structure of $Ni(P^{Me}_{2}N^{Ph}_{2})_{2}[CF_3SO_3]_2$ with protons, co-crystallized solvent and counter ions excluded for clarity. Ellipsoids are shown at 50% probability.. 30

Figure 2.6 X-ray crystal structure of $Ni(P^{Et}_{2}N^{Ph}_{2})_{2}[CF_3SO_3]_2$ with protons, co-crystallized solvent and counter ions excluded for clarity. Ellipsoids are shown at 50% probability. 30

Figure 3.1 [FeFe] Hydrogenase active site (1) and $Ni(P^{R}_{2}N^{R'}_{2})_{2}^{2+}$ (2) 39

Figure 3.2 Newly synthesized P_2N_2 ligands with sodium 3-propanoate (6), 3-propanamide (7), and ethyl 3-propanoate (8, 9) phosphine substituents. 41

Figure 3.3 Molecular diagrams for complex 10, $Ni(P^{PA}_{2}N^{Ph}_{2})$. Thermal ellipsoids are shown at the 50% probability level. Hydrogens and phenyl- amine

substituents have been removed from this diagram for clarity. A and B show different orientations to clearly demonstrate the molecular geometry...43

Figure 3.4 Molecular diagrams for complex 11, [Ni($P^{Amide}_2N^{Ph}_2$)](BF_4)$_2$. Thermal ellipsoids are shown at the 50% probability level. Counterions, hydrogens, solvent molecules, and phenyl- amine substituents have been removed from this diagram for clarity.....43

Figure 3.5 Molecular structure of complex 12, Ni($P^{EtE}_2N^{Ph}_2$)Cl_2, as determined by X-ray diffraction studies. Thermal ellipsoids are shown at the 50% probability level. Hydrogens have been removed from this diagram for clarity. 46

Figure 3.6 Molecular structure of complex 13, Ni($P^{EtE}_2N^{PhOMe}_2$)Cl_2, as determined by X-ray diffraction studies. Thermal ellipsoids are shown at the 50% probability level. Hydrogens have been removed from this diagram for clarity. 46

Figure 3.7 Molecular diagram for complex 10, Ni($P^{PA}_2N^{Ph}_2$). Thermal ellipsoids are shown at the 50% probability level. Hydrogens have been removed from this diagram for clarity.....58

Figure 3.8 Molecular diagram for complex 11, [Ni($P^{Amide}_2N^{Ph}_2$)](BF_4)$_2$. Thermal ellipsoids are shown at the 50% probability level. Counterions, hydrogens, solvent molecules, and have been removed from this diagram for clarity. 60

Figure 3.9 Molecular structure of complex 12, Ni($P^{EtE}_2N^{Ph}_2$)Cl_2, as determined by X-ray diffraction studies. Thermal ellipsoids are shown at the 50% probability level. Hydrogens have been removed from this diagram for clarity. 62

Figure 3.10 Molecular structure of complex 13, Ni($P^{EtE}_2N^{PhOMe}_2$)Cl_2, as determined by X-ray diffraction studies. Thermal ellipsoids are shown at the 50% probability level. Hydrogens have been removed from this diagram for clarity. 64

Figure 4.1 Active sites of [Fe], [FeFe], and [NiFe] hydrogenases. Cys represents a cysteine amino acid residue, and GMP stands for a guanosine monophosphate moiety. 68

Figure 4.2 Homogeneous electrocatalysts for hydrogen evolution. 69

Figure 4.3 Hydrogen evolution catalyzed by 0.2 mM [Ni(Me.Ph)$_2$](CF_3SO_3)$_2$ in 0.2 M NBu_4PF_6 in benzonitrile with a 3mm gC working electrode and Pt wire counter. 1 M CF_3COOH in electrolyte solution was titrated in 10 uL aliquots.....71

Figure 4.4 Hydrogen evolution catalyzed by 0.2 mM [Ni(Et.Ph)$_2$](CF_3SO_3)$_2$ in 0.2 M NBu_4PF_6 in benzonitrile with a 3mm gC working electrode and Pt wire counter. 1 M CF_3COOH in electrolyte solution was titrated in 10 uL aliquots.....72

Figure 4.5 Hydrogen evolution catalyzed by 0.2 mM $[Ni(EtE.Ph)_2](BF_4)_2$ in 0.2 M NBu_4PF_6 in benzonitrile with a 3mm gC working electrode and Pt wire counter. 1 M CF_3COOH in electrolyte solution was titrated in 10 uL aliquots. 72

Figure 4.6 Hydrogen evolution catalyzed by 0.2 mM $[Ni(EtE.PhOMe)_2](PF_6)_2$ in 0.2 M NBu_4PF_6 in acetonitrile with a 3mm gC working electrode and Pt wire counter. 1 M CF_3COOH in electrolyte solution was titrated in 10 uL aliquots. 73

Figure 5.1 Active sites of NiFe, CuMo, and NiNi carbon monoxide dehydrogenase (CODH).[12] 82

Figure 5.2 Formate oxidation electrocatalysis of $Ni(Me.Ph)_2[BF_4]_2$. 1.0 mM $Ni(Me.Ph)_2[BF_4]_2$ in 0.2 M NBu_4PF_6, formate added in 5 uL aliquots of 1.0 M $HNEt_3OCHO$. 3.0 mm gC working electrode, Pt wire counter electrode. $CoCp_2$ is included as an internal reference. 84

Figure 5.3 Electrocatalytic oxidation of formate by $Ni(Et.Ph)_2[CF_3SO_3]$. 1.0 mM $Ni(Et.Ph)_2[CF_3SO_3]_2$ in 0.2 M NBu_4PF_6, formate added in 5 uL aliquots of 1.0 M $HNEt_3OCHO$. 3.0 mm gC working electrode, Pt wire counter electrode. $CoCp_2$ is included as an internal reference. 84

Figure 6.1 Active sites of NiFe, CuMo, and NiNi carbon monoxide dehydrogenase (CODH).[9] 95

Figure 6.2 Molecular diagram for complex 16, $Ni(P^{nPr}{}_4N^{Ph}{}_5)[PF_6]_2$. Thermal ellipsoids are shown at the 50% probability level. Counterions and hydrogens have been removed for clarity. Only the N-C atoms of phenyl-amine substituents have been shown for clarity. 97

Figure 6.3 Molecular diagram for complex 17, $Ni(P^{EtE}{}_4N^{PhOMe}{}_5)[BF_4]_2$. Thermal ellipsoids are shown at the 50% probability level. Counterions and hydrogens have been removed for clarity. Only the N-C atoms of 4-methoxyphenyl- amine substituents have been shown for clarity. 98

LIST OF SCHEMES

Scheme 2.1 Traditional $P^{R}_{2}N^{R'}_{2}$ ligand synthesis. 18

Scheme 2.2 $P^{R}_{2}N^{R'}_{2}$ synthesis via dehydroxymethylation and alkylation of THPCl. .24

Scheme 2.3 Synthesis of homoleptic nickel complexes of $P^{R}_{2}N^{R'}_{2}$ ligands. 26

Scheme 3.1 Previously reported $P^{R}_{2}N^{R'}_{2}$ ligand syntheses. 39

Scheme 3.2 $P^{R}_{2}N^{R'}_{2}$ synthesis via Michael Addition of THP. 40

Scheme 3.3 Ligation of $P^{R}_{2}N^{R'}_{2}$ ligands to nickel. 42

Scheme 4.1 Hydrogen evolution at the standard hydrogen electrode (SHE). The SHE utilizes the hydrogen evolution from platinum as an absolute reference potential.....66

Scheme 4.2 The potential mechanisms for electrocatalytic hydrogen evolution on heterogeneous electrodes. 67

Scheme 4.3 Purification and Isolation for $P^{EtE}_{2}N^{R'}_{2}$ Attachment to Nickel (R' = Ph, PhOMe). 70

Scheme 6.1 Synthesis of $Ni(P^{R}_{4}N^{R'}_{5})X_2$ complexes. 96

LIST OF TABLES

Table 2.1 Reduction potentials for the series of complexes $Ni(P^{R}_{2}N^{Ph}_{2})_2(CH_3CN)[BF_4]_2$ in benzonitrile.....27

Table 2.2 X-ray determination details for 7.....35

Table 2.3 X-ray determination details for 8.....36

Table 3.1 Selected Bond Lengths(Å), Bond Angles (°), and Dihedral angles (°) of $Ni(P_2N_2)X_2$ Complexes.....45

Table 3.2 Crystal data and structure refinement for 10, $Ni(P^{PA}_{2}N^{Ph}_{2})$.....59

Table 3.3 Crystal data and structure refinement for 11, $[Ni(P^{Amide}_{2}N^{Ph}_{2})](BF_4)_2$.....61

Table 3.4 Crystal data and structure refinement for 12, $Ni(P^{EtE}_{2}N^{Ph}_{2})Cl_2$.....63

Table 3.5 Crystal data and structure refinement for 13, $Ni(P^{EtE}_{2}N^{PhOMe}_{2})Cl_2$.....65

Table 4.1 Electrocatalytic rates for $Ni(P_2N_2)^{2+}$ complexes for proton-coupled electron transfer reactions.....69

Table 5.1 Reduction potentials for the series of complexes $[Ni(P^{R}_{2}N^{Ph}_{2})_2(CH_3CN)]X_2$ in benzonitrile. ($X=PF_6^-$ or BF_4^-).....85

Table 5.2 Formate oxidation electrocatalytic rates for the series of complexes $[Ni(P^{R}_{2}N^{Ph}_{2})_2(CH_3CN)]X_2$ in benzonitrile. ($X=PF_6^-$ or BF_4^-).....86

Table 6.1 Crystal data and structure refinement for complex 1.....101

Table 6.2 Crystal data and structure refinement for complex 2.....102

ACKNOWLEDGEMENTS

"I am glad you are here with me. Here, at the end of all things…"

-J.R.R Tolkien

A wise hobbit once noted that the completion of his task was only fulfilled through the improbable intervention of his friends, and that what might seem to be a personal journey in actuality represented the total effort of a universe of characters. While I cannot claim to have vanquished any true demons, I recognize that the accomplishment of this thesis and my diploma could only be possible with the help and support of virtually everyone I know.

I'd first like to thank Professor Kubiak and my committee for taking the time to sincerely evaluate my work in both my defense and thesis. I value your time greatly, and I appreciate your effort in helping to train me to be a better scientist and a better student.

My family has been so incredibly supportive of me through my entire life. Every decision I've made, mom and dad have supported me the whole way. Life can take you in many directions, and it can be difficult to understand the currents and eddies along the way, but talking with my family always helps me to remember my own internal direction and drive. Emma and Theresa have likewise been such great support for me, and I hope that once I'm done with graduate school I will have the time (and money!) to be a more thoughtful son and brother.

I've also been extremely fortunate to have met the love of my life during graduate school. Manna has been a constant source of support and love for me, and I consider myself incredibly smart and lucky to have introduced myself at that Halloween party. Thanks to Manna and Brutus, I was able to complete this dissertation with some semblance of sanity.

Professor Kubiak has been a living fount of knowledge and support since he was kind enough to let me join his lab. It has been such a valuable experience to be able just to listen to him, and has helped me value chemical knowledge and the value of asking the right questions. I hope I can make him proud with my future in chemistry.

I was extremely fortunate to have several incredibly patient mentors to work with in lab. I really appreciate Dr. Candace Seu for taking the time to really teach me not only the techniques of electrochemistry and air-free synthesis, but also to teach me the value of thoughtfulness for science and research. I only hope I can possibly meet someone as kind and patient as Candace sometime in the rest of my life. I was also fortunate enough to have Professor Kyle Grice help me during his postdoctoral appointment at UCSD. He taught me the value of hard work and a constant appraisal of the literature. I literally have no idea where I would be without the incredible help I received from Candace and Kyle.

Another benefit of working in Cliff's lab is all the amazing coworkers I've had the pleasure of working with over the past 6 years. I've been lucky to watch people like Starla Glover, Eric Benson, John Goeltz, Jon Smieja, Julia Schöffel, Sayak Roy, Aaron Sathrum, Jerry Lin, and Daniel Sieh work in lab. My close labmate cohorts Gabe, Jesse, Mark, Tram, Jane, Alyssia, and Alissa have made working in lab a true pleasure and a genuine learning experience every time I set foot in the office or go out to a delicious work lunch. I've had the great fortune of seeing brilliant students enter the lab, including Matt, Mark, Alma, Jason, Dr. Charles Machan, Melissa, Steven, Daphne, Gwen, and Tyler, and I hope I gave as much help as I could.

Finally, I've also had the great fortune of making friends from San Diego who made the whole experience great. I was fortunate enough to enter grad school with my great friend Travis Blaine, who is doing amazing stuff with his non-chemistry life, just like we all knew he would. I was lucky to meet Jose, Sonia, Ryan, and Pearl at my first apartment here in San Diego, and I greatly appreciate how they taught me to appreciate the importance of taking a step back and approaching problems with careful consideration.

Chapter 2: The majority of the material for this chapter comes directly from a manuscript entitled “Versatile Synthesis of $P^{R}_{2}N^{R'}_{2}$ Ligands for Molecular Electrocatalysts with Pendant Bases in the Second Coordination Sphere," by Michael D. Doud, Kyle A. Grice, Alyssia M. Lilio, Candace S. Seu, and Clifford P. Kubiak, published in *Organometallics*, **2012**, *31*, 779-782. The dissertation author is the primary author of this manuscript.

Chapter 3: The majority of the material for this chapter comes directly from a manuscript entitled “Synthesis of P_2N_2 Ligands via Michael Addition" by Michael D. Doud, Curtis E. Moore, Arnold L. Rheingold, and Clifford P. Kubiak, to be submitted to *Organometallics*. The dissertation author is the primary author of this manuscript.

Chapter 4: Parts of the Results and Discussion and Experimental sections for this chapter come directly from a manuscript entitled “Electrocatalytic behavior of alkyl-substituted P_2N_2 complexes" by Michael D. Doud and Clifford P. Kubiak, to be submitted. The dissertation author is the primary author of this manuscript.

Chapter 5: Parts of the Results and Discussion and Experimental sections for this chapter come directly from a manuscript entitled “Electrocatalytic behavior of alkyl-substituted P_2N_2 complexes" by Michael D. Doud and Clifford P. Kubiak, to be submitted. The dissertation author is the primary author of this manuscript.

VITA

2009	B.S., Chemistry Purdue University
2009	B.S., Biology Purdue University
2011	M.S., Chemistry University of California, San Diego
2016	Ph.D., Chemistry, University of California, San Diego

PUBLICATIONS

Doud, M.; Kubiak, C. Electrocatalytic behavior of alkyl-substituted P_2N_2 complexes. *Manuscript in preparation.*

Doud, M.; Moore, C.; Rheingold, A.; Kubiak, C. Synthesis of P_2N_2 ligands via Michael Addition. *Manuscript submitted.*

Doud, M.; Grice, K.; Lilio, A.; Seu, C.; Kubiak, C. Versatile synthesis of $P_2N'_2$ ligands for molecular electrocatalysts with pendant bases in the second coordination sphere. *Organometallics*, **2012,** *31*, p 779

Hamaguchi, T.; **Doud, M.**; Kubiak, C.; Structural and electrochemical behavior of nickel dimer complexes with pendant bases in the scond coordination sphere. *In preparation.*

Hamaguchi, T.; **Doud, M.**; Hilgar, J.; Rinehart, J.; Kubiak, C. Competing ferro- and antiferromagnetic interactions in a hexagonal bipyramidal nickel sulfide cluster. *Submitted.*

Seu, C.; Ung, D.; **Doud, M.**; Moore, C.; Rheingold, A.; Kubiak, C. Synthesis, structural, and electrocatalytic reduction studies of $[Pd(P_2N_2)_2]^{2+}$ complexes. *Organometallics*, **2013**, *32*, p. 4556

Seu, C., Appel, A., **Doud, M.**, Dubois, D., Kubiak, C.; Formate oxidation *via* β-deprotonation in $[Ni(P_2N_2)_2(CH_3CN)]^{2+}$complexes. *Energy Environ. Sci.*, **2012**, *5*, p 6480

FIELDS OF STUDY

Major Field: Inorganic Chemistry

Studies in Inorganic Synthesis and Electrocatalysis

Professor Clifford P. Kubiak, Chair

ABSTRACT OF THE DISSERTATION

Synthetic Advances for P_2N_2 Molecular Electrocatalysts with Pendant Bases in the Second Coordination Sphere

by

Michael David Doud

Doctor of Philosophy in Chemistry

University of California, San Diego, 2016

Professor Clifford P. Kubiak, Chair

Efficient electrocatalytic reduction of small molecules such as CO_2, N_2, and even protons relies upon the precise delivery of electrons and protons to an active site. The coordination of these reactions can involve sophisticated ligands controlling the coordination spheres around a reactive center. The incorporation of a pendant base for proton shuttling is one way to achieve such control. In order to explore the

reactivities of a class of complexes, Ni(P_2N_2), versatile syntheses are required.

Seven 1,5-diaza-3,7-diphosphacyclooctane (P_2N_2) ligands with alkyl- and carbonyl- substituted phosphines have been synthesized via two versatile methods that allows for improved control of the phosphine substituent. The methyl-, ethyl-, benzyl-, 3-propanoic acid, 3-propanamide, and ethyl 3-propanoate-phosphino- substituted phosphine P_2N_2 ligands ($P^{Me}{}_2N^{Ph}{}_2$, $P^{Et}{}_2N^{Ph}{}_2$, $P^{Bn}{}_2N^{Ph}{}_2$, $P^{PA}{}_2N^{Ph}{}_2$, $P^{Amide}{}_2N^{Ph}{}_2$, $P^{EtE}{}_2N^{Ph}{}_2$, $P^{EtE}{}_2N^{PhOMe}{}_2$) were synthesized and characterized by $^{31}P\{^1H\}$ NMR, ^1H NMR, and elemental analysis, and their corresponding $[Ni(P^R{}_2N^{Ph}{}_2)_2](BF_4)_2$ complexes were synthesized and characterized by $^{31}P\{^1H\}$ NMR, ^1H NMR, and electrochemistry, and their corresponding $Ni(P^R{}_2N^{R'}{}_2)X_2$ (X= Cl^-, BF_4^-, $CF_3SO_3^-$, PF_6^-) complexes have been synthesized and characterized by $^{31}P\{^1H\}$ NMR, ^1H NMR, X-ray crystallography, and elemental analysis.

The nickel complexes of P_2N_2 ligands synthesized and characterized by these new methods were investigated for hydrogen evolution and formate oxidation electrocatalysis. The newly synthesized complexes with alkyl- and carbonyl- phosphine substituents rapidly evolve hydrogen and oxidize formate more slowly than previously synthesized cyclohexyl- and phenyl- substituted phosphine ligands, due to a more negative reduction potential leading to a decrease in the driving force of formate oxidation and increase for that of hydrogen evolution.

CHAPTER 1
STORAGE OF RENEWABLE ENERGY AS A CHEMICAL FUEL: THE ROLE OF MOLECULAR ELECTROCATALYSTS

1.1 Introduction

A crucial challenge of science in this generation is the development of a sustainable energy economy. Chemists play an essential role in meeting this challenge.[1] This thesis describes studies of molecular catalysts that mimic the natural enzyme hydrogenase. Like the role of hydrogenase in nature, the molecular catalysts described herein may contribute to energy storage and conversion schemes of the future.

1.2 Development of a renewable energy economy

Fossil fuels account for over 80% of the energy that humans consume.[2] A result of this fuel usage has been unprecedented increases in atmospheric and oceanic carbon dioxide levels.[3] Harnessing renewable energy sources would reduce carbon dioxide emissions. Figure 1.1 indicates that renewable sources of energy have plenty of capacity to meet world needs. Clean electricity can be generated efficiently and on a large scale using solar and wind power. Part of the new energy economy involves the efficient storage of electrical energy generated from renewable sources. Many such energy storage systems are under investigation worldwide, including advanced battery and chemical fuel technology.[4] However, many important functions require energy-dense liquid fuels, such as flight and long-distance shipping.

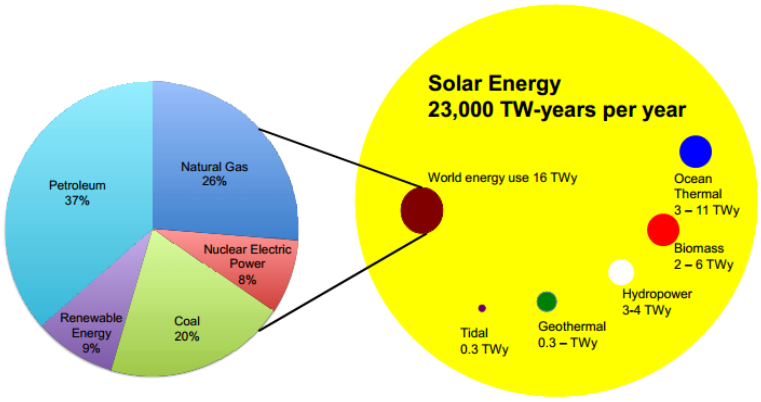

Figure 1.1. Current annual global energy consumption, total recoverable reserves of finite energy resources, and yearly potential yield of renewable resources.[5]

Chemical fuels have specific energy (J/kg) and energy density (J/m^3) that greatly exceed those of batteries.[6] Chemical reactions capable of producing energy-dense fuels like hydrogen or hydrocarbon fuels under mild conditions are crucial to the future of a renewable energy economy. The key challenge from a chemical standpoint is the development of efficient catalysts for the synthesis of chemical fuels from renewable resources. The conversion of carbon dioxide into chemical fuels is a particularly attractive goal because CO_2 is a greenhouse gas, and because it is a waste product of industrial processes. The next section discusses the chemical reduction of carbon dioxide. Efficient catalysts are important for this reaction because CO_2 is relatively unreactive.

1.3 Proton-Coupled Electron Transfer (PCET) and chemical fuel electrocatalysis

Carbon dioxide is abundant, and a potential feedstock for the synthesis of more reduced forms of carbon that are known chemical fuels. However, transformations such as the direct single-electron reduction of carbon dioxide to form an anion is thermodynamically unfavorable.[7] If CO_2 is reduced and protons are also transferred in a proton-coupled electron transfer (PCET) process, the thermodynamics are greatly improved. The reduction potentials for these reactions are compared in Table 1.1.

Table 1.1. Reduction potentials of carbon dioxide and PCET processes.

Reaction	Reduction Potential (V vs. NHE)
$CO_2 + e^- \rightarrow CO_2^{\cdot -}$	$E^0 = -1.90$ V
$CO_2 + 2H^+ + 2e^- \rightarrow CO + H_2O$	$E^0 = -0.53$ V
$CO_2 + 2H^+ + 2e^- \rightarrow HCO_2H$	$E^0 = -0.61$ V
$CO_2 + 4H^+ + 4e^- \rightarrow HCHO + H_2O$	$E^0 = -0.48$ V
$CO_2 + 6H^+ + 6e^- \rightarrow CH_3OH + H_2O$	$E^0 = -0.38$ V
$CO_2 + 8H^+ + 8e^- \rightarrow CH_4 + 2H_2O$	$E^0 = -0.24$ V

pH 7 in aqueous solution, 25 °C, 1 atmosphere gas pressure, and 1 M for other solutes

PCET reactions can occur sequentially or concertedly (e.g. Figure 1.2).[8] Building inorganic metal catalysts that facilitate both proton and electron transfer requires a complex molecular system. Fortunately, examples of ligands that participate in catalytic PCET reactions are abundant in natural enzymes.

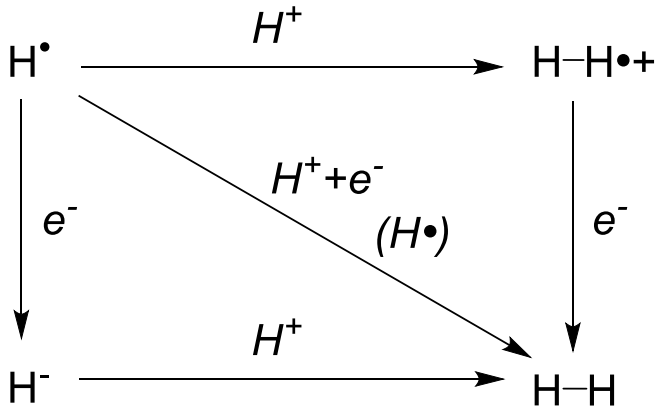

Figure 1.2. Diagram of PCET reactions for a hydrogen atom. Proton and electron transfer can be sequential (reactions depicted on edges) or concerted (reaction on diagonal).

1.4 Design principles for molecular electrocatalysts

Enzymes have evolved over billions of years to efficiently catalyze a wide variety of important reactions. These include the reversible oxidation of dihydrogen gas,[9] reduction of carbon dioxide to formate,[10] reduction of dinitrogen gas to ammonia,[11] and formation of carbamate from carbon dioxide.[12] Biochemists have noted that the structure of enzyme active sites, and particularly the ligand framework, is critical to their catalytic abilities.[13] For example, cytochrome P450, an iron based protein, uses its redox-active porphyrin in the functionalization of a wide variety of biological compounds.[14] Tyrosine can act as a redox-active ligand, as in galactose oxidase.[15] Other enzymes, such as cinnamyl alcohol dehydrogenase, coordinate proton transfer from a substrate to a ligand that positions a base near the active site. The [FeFe] hydrogenase enzyme features two iron atoms in the active site and has a unique azadithiolate ligand. This ligand positions a nitrogen over the iron active site and allows it to accept a proton.[16]

Biological systems have inspired much synthetic work in the design of inorganic catalysts. For these catalysts to have multiple functions, ligands must incorporate specific

active motifs. Research has focused on controlling electron and proton transfer to and from ligands, by tuning their redox potentials,[17] or adding proton channels,[18] electron reservoirs[19] and mediators.[20] Ligands that can control proton transfer to the active site are important in the electrocatalytic reduction of small molecules. The active site of [FeFe] hydrogenase (Figure 1.3 A) has inspired much research into detailed active site mimics, particularly by C. J. Pickett[21] and S. Ott.[22] Other research has focused on mimicking specific ligand functionality, such as the addition of phenolic substituents to iron-porphyrin catalysts for carbon dioxide reduction.[23] The goal of this work is not necessarily to precisely replicate the structure of the enzyme, but to use the fundamental chemical lessons from these enzymes to increase the rates of inorganic catalysts. This thesis focuses on one such system, nickel-P_2N_2 complexes.

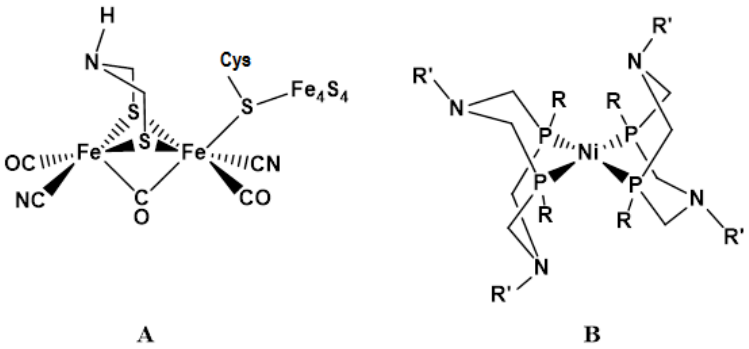

Figure 1.3. Active site of [FeFe] Hydrogenase (A) and $Ni(P^R_2N^{R'}_2)_2^{2+}$ (B)

1.5 Nickel P_2N_2 complexes catalyze production of H_2

Hydrogen is the simplest chemical fuel, and several enzymes catalyze its production.[24] The active sites of [FeFe] (Figure 1.3) and [NiFe] hydrogenases indicate

that iron and nickel metal complexes can catalyze the hydrogen evolution reaction (HER).[25] 1,5-diaza-3,7-diphosphacyclooctane (P_2N_2) ligands contain two phosphine atoms that can form a bond to a metal atom, and two nitrogen atoms, each with a lone pair of electrons that can reversibly accept the transfer of a proton from a substrate. The coordination of P_2N_2 ligands via the phosphines to both iron and nickel cations yield complexes with pendant nitrogen bases in the second coordination sphere (Figure 1.3 B), but only the nickel complexes show an ability to produce hydrogen.[26,27] These complexes have demonstrated fast rates for the electrocatalytic, proton-coupled processes of H_2 oxidation,[28] proton reduction to H_2,[29] O_2 reduction,[30] and the oxidation of formate.[31]

The utility of these nickel-P_2N_2 complexes is expanded by the ability to vary substituents of both the tertiary phosphine and amine. The basicity of the amine can be tuned via substitution at R',[32] while the thermodynamic parameters of the metal center, such as the reduction potentials and hydride donor ability ("hydricity") of the Ni–H, can be tuned most directly via substitution at R (Figure 1.3 B). For example, a more donating substituent at R results in a nickel center with more negative reduction potentials. The steric effects of R also affect the bite angle and dihedral angles of the two ligands on the metal center, which can have a substantial effect on the hydricity and reduction potentials of the nickel complex.[33] P_2N_2 ligands have been coordinated to many metals, including Ni, Co,[34] and Mn.[35] These complexes have diverse molecular structures,[36] [34] [37] and facilitate a wide variety of electrocatalytic reactions.

1.6 Hydricity and $Ni(P_2N_2)_2$ complexes

Nickel-P_2N_2 electrocatalysts show the fastest rates for formate oxidation[38] and have some of the fastest rates for hydrogen evolution.[39] The catalytic cycles in formate oxidation and hydrogen production involve many steps, and modifying a catalyst to increase the rate of one specific step often causes a different step to slow down.[40] For hydrogen oxidation by $[Ni(P_2N_2)_2]^{2+}$ complexes, the rate limiting step is the initial binding of H_2 to nickel, as the rotational and translational freedom lost by the hydrogen molecule is not offset by the enthalpy lost upon forming a Ni-H_2 bond. The presence of an amine base in the second coordination sphere facilitates the subsequent hydrogen splitting, in which the H-H bond splits heterolytically to form hydride (bound to nickel) and a proton (bound to nitrogen).

The nickel-(P_2N_2)-hydride complexes mentioned above [should be able to?][are expected to?] transfer a hydride (PCET) to a molecule like carbon dioxide. The rate of hydride transfer can be tuned bythe phosphine ligands. Electron donating substituents on these ligands enhance the electron density in the metal hydride sigma bond and the ability of the complex to donate a hydride, i.e. its 'hydricity' is increased. The $[MH(P_2N_2)_2]^{+}$ species adopt a trigonal bipyramidal molecular structure,[37] with the hydride at an equatorial position, and the Ni-H bond has dz^2 character (Figure 1.4). Nickel(II) has eight *d* electrons, so the lowest unoccupied molecular orbital is the antibonding (σ^*) orbital for the Ni-H bond. By comparison, in analogous Fe^{2+} compounds, the lowest unoccupied molecular orbital would be a Fe-P antibonding orbital, because Fe^{2+} only has six *d* electrons. This difference makes $[FeH(P_2N_2)_2]^{+}$ complexes more stable and less reactive.

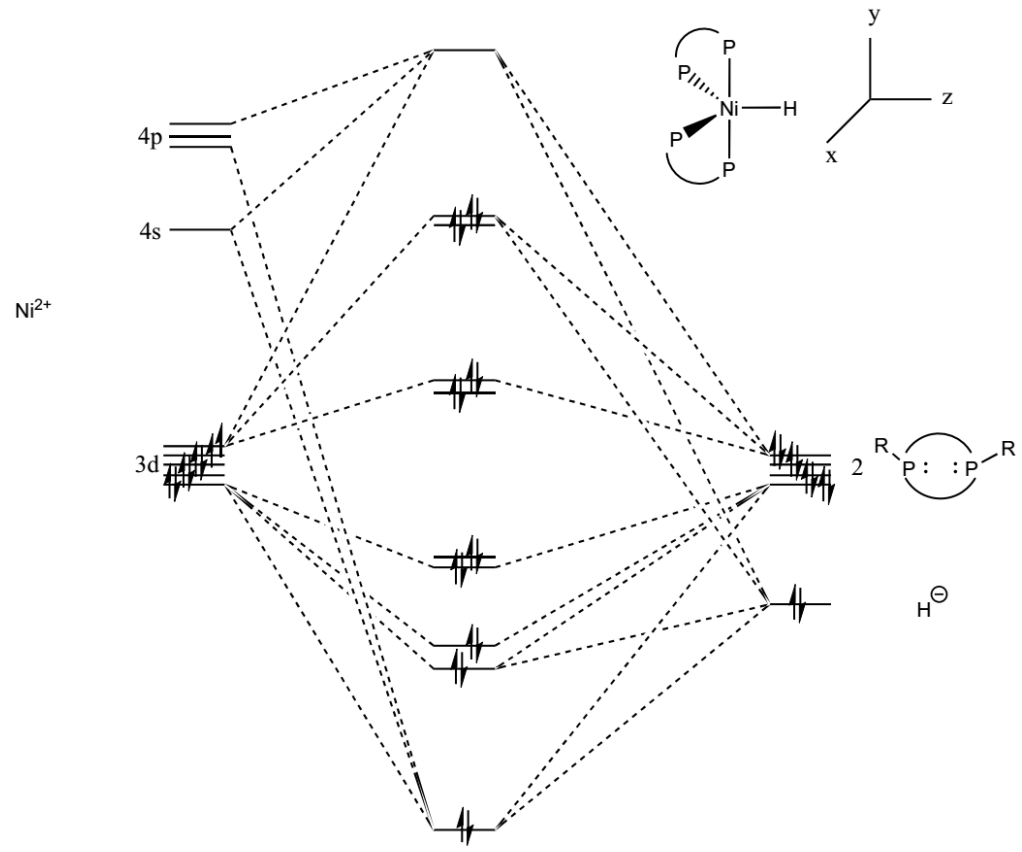

Figure 1.4. Molecular orbital diagram for a typical nickel bis(diphosphine) hydride. As indicated above, the Ni^{2+} complex has 8 d-electrons, and the ligands are considered to donate 10 electrons.

The hydride donor abilities of various $[NiH(P_2N_2)_2]^+$ complexes can be expressed as the free energy change of the hydride transfer step (ΔG_{H^-}). For various $[NiH(P_2N_2)_2]^+$ complexes this correlates with the standard electrode potential, E^0, as shown in Figure 1.4. It is possible to make reduction potentials more negative (as needed to reduce CO_2) by altering the phosphine and amine substituents. So far the reduction potentials of these complexes have only been modifiable through an indirect interaction involving the amine

substituent of P_2N_2.[41] To create systems with even more negative reduction potentials, new syntheses enabling substitution at the phosphorus are required.

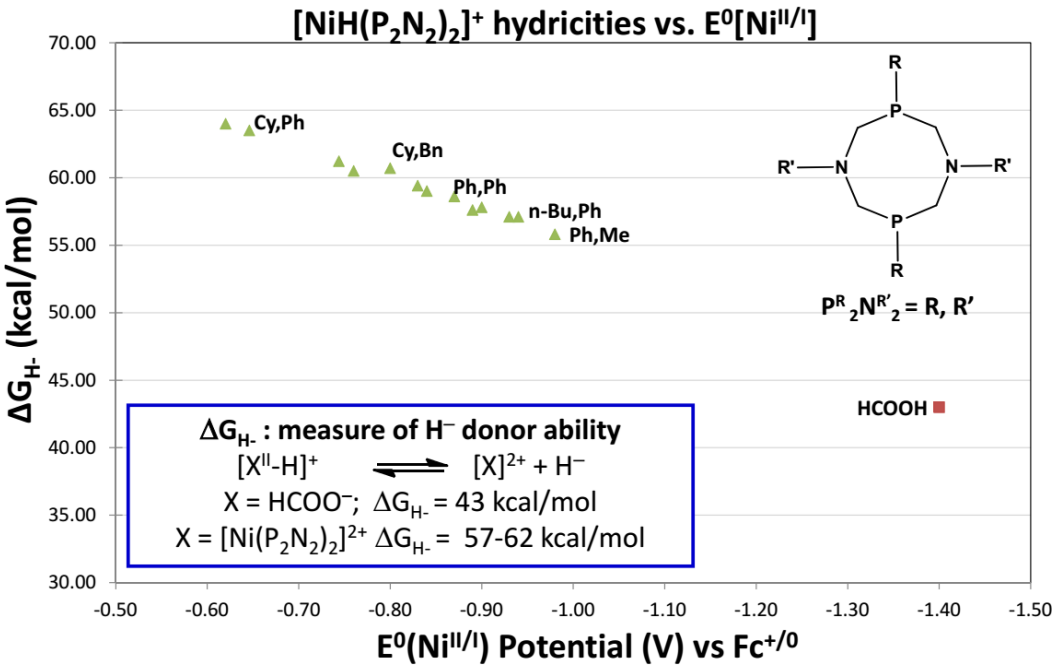

Figure 1.5. Free energy change upon donation of H– (hydricities) by various [NiH(P2N2)]+ complexes, compared with their standard reduction potentials E0(NiII/I)

The exceptional ability of $[Ni(P_2N_2)_2]^{2+}$ complexes in catalytic hydrogen oxidation and the relatively underexplored topic of new phosphorus substituents lead to fertile ground for synthetic chemistry research. Chapters 2 and 3 describe two new syntheses of P_2N_2 complexes with increased hydricity. The effect of these new ligands on the electrocatalytic hydrogen evolution reaction (HER) and formate oxidation will be discussed in chapters 4 and 5, respectively.

1.7 Description of Select Techniques

P_2N_2 complexes oxidize rapidly and irreversibly upon exposure to oxygen gas, so the exposure of the ligands and precursors to the atmosphere to be minimized. New P_2N_2 compounds described in this thesis were synthesized using inert atmosphere glovebox and Schlenk double-manifold techniques.

The compounds are characterized by techniques that include nuclear magnetic resonance (NMR) and X-ray crystallography. One NMR technique, proton-decoupled phosphorus-31 NMR ($\{^1H\}^{31}P$-NMR), was especially useful for probing the electronic environment of the phosphorus nuclei. It is also useful for the identification of reaction intermediates, side products, and monitoring product formation.[42]

Cyclic voltammetry (CV) is employed to study the capability and efficiency of substances for electrocatalytic transformations. CV requires an electrochemical cell (Figure 1.6). Detailed information about the electrochemical reversibility of a system can be determined by scanning the potential between the working and counter electrodes in a cyclic fashion. An electrocatalyst is also characterized by its overpotential and catalytic rate. The overpotential of a reaction is the difference between the thermodynamically determined standard potential for the reaction and the potential at which the redox event is observed to occur experimentally. The rate of electrocatalysis can be derived from the current passed from the electrode through the catalysts to the substrate. These redox potentials and electrocatalytic rates are important for understanding the behavior of electrocatalysts.

The products of these electrocatalytic reactions can be identified through controlled potential electrolysis (CPE). In a typical CPE experiment, the potential of the working

electrode is held constant. After a given amount of time, typically 20 to 30 minutes, the space above the liquid within the electrochemical cell (or “headspace”) can be sampled and tested for any gases produced. Liquid or soluble products can be discovered through nuclear magnetic resonance or mass spectrometry.

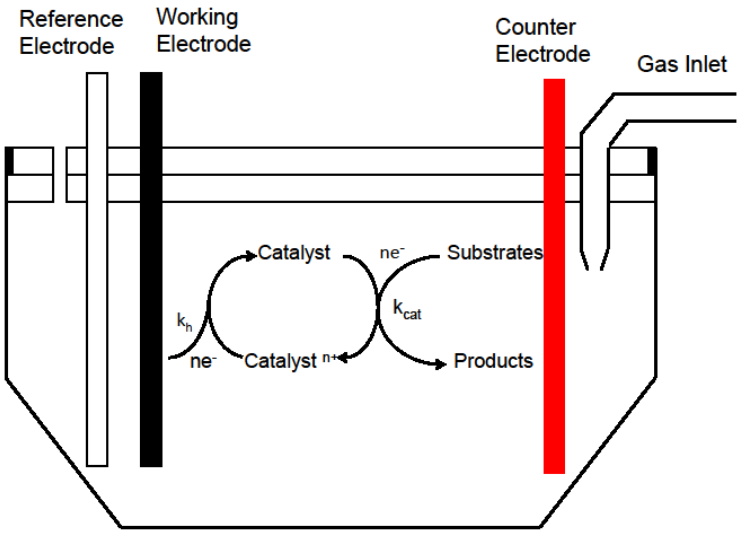

Figure 1.6. Diagram of an electrochemical cell for performing cyclic voltammetry (CV) and electrocatalytic measurements.

1.8 Summary

The work in this thesis expands the synthetic routes available for P_2N_2 ligands and complexes; these syntheses allow a wide range of phosphorus substituents to be incorporated. The new complexes demonstrate improved electrocatalytic rates for

hydrogen evolution, and offer new insights into the mechanisms for other electrocatalytic reactions, particularly oxidation of formate.

1.9 References

(1) Höök, M.; Tang, X. *Energy Policy* **2013**, *52*, 797.

(2) Meinshausen, M.; Meinshausen, N.; Hare, W.; Raper, S. C. B.; Frieler, K.; Knutti, R.; Frame, D. J.; Allen, M. R. *Nature* **2009**, *458*, 1158.

(3) Andres, R. J.; Boden, T. A.; Breon, F. M.; Ciais, P.; Davis, S.; Erickson, D.; Gregg, J. S.; Jacobson, A.; Marland, G.; Miller, J.; Oda, T.; Oliver, J. G. J.; Raupach, M. R.; Rayner, P.; Treanton, K. *Biogeosciences* **2012**, *9*, 1845.

(4) Barton, J. P.; Infield, D. G. *IEEE Transactions on Energy Conversion* **2004**, *19*, 441.

(5) Perez, R.; Perez, M. *The IEA SHC Solar Update* **2009**, *50*.

(6) Turner, J. W. G.; Pearson, R. J.; Dekker, E.; Iosefa, B.; Johansson, K.; ac Bergström, K. *Applied Energy* **2013**, *102*, 72.

(7) Sullivan, B. P.; Krist, K.; Guard, H. *Electrochemical and electrocatalytic reactions of carbon dioxide*; Elsevier, 2012.

(8) Hammes-Schiffer, S.; Soudackov, A. V. *The Journal of Physical Chemistry B* **2008**, *112*, 14108.

(9) Chenevier, P.; Mugherli, L.; Darbe, S.; Darchy, L.; DiManno, S.; Tran, P. D.; Valentino, F.; Iannello, M.; Volbeda, A.; Cavazza, C.; Artero, V. *Comptes Rendus Chimie* **2013**, *16*, 491.

(10) Bassegoda, A.; Madden, C.; Wakerley, D. W.; Reisner, E.; Hirst, J. *Journal of the American Chemical Society* **2014**, *136*, 15473.

(11) Hoffman, B. M.; Lukoyanov, D.; Dean, D. R.; Seefeldt, L. C. *Accounts of Chemical Research* **2013**, *46*, 587.

(12) Cleland, W. W.; Andrews, T. J.; Gutteridge, S.; Hartman, F. C.; Lorimer, G. H. *Chemical reviews* **1998**, *98*, 549.

(13) Benkovic, S. J.; Hammes-Schiffer, S. *Science* **2003**, *301*, 1196.

(14) Rittle, J.; Green, M. T. *Science* **2010**, *330*, 933.

(15) Müller, J.; Weyhermüller, T.; Bill, E.; Hildebrandt, P.; Ould-Moussa, L.; Glaser, T.; Wieghardt, K. *Angewandte Chemie International Edition* **1998**, *37*, 616.

(16) Simmons, T. R.; Berggren, G.; Bacchi, M.; Fontecave, M.; Artero, V. *Coordination Chemistry Reviews* **2014**, *270–271*, 127.

(17) Garrido-Barros, P.; Funes-Ardoiz, I.; Drouet, S.; Benet-Buchholz, J.; Maseras, F.; Llobet, A. *Journal of the American Chemical Society* **2015**, *137*, 6758.

(18) Dutta, A.; Lense, S.; Hou, J.; Engelhard, M. H.; Roberts, J. A. S.; Shaw, W. J. *Journal of the American Chemical Society* **2013**, *135*, 18490.

(19) Lyaskovskyy, V.; de Bruin, B. *ACS Catalysis* **2012**, *2*, 270.

(20) Lin, J.; Hou, Y.; Zheng, Y.; Wang, X. *Chemistry – An Asian Journal* **2014**, *9*, 2468.

(21) Tard, C.; Liu, X.; Ibrahim, S. K.; Bruschi, M.; Gioia, L. D.; Davies, S. C.; Yang, X.; Wang, L.-S.; Sawers, G.; Pickett, C. J. *Nature* **2005**, *433*, 610.

(22) Schwartz, L.; Eilers, G.; Eriksson, L.; Gogoll, A.; Lomoth, R.; Ott, S. *Chemical Communications* **2006**, 520.

(23) Costentin, C.; Drouet, S.; Robert, M.; Savéant, J.-M. *Science* **2012**, *338*, 90.

(24) Lubitz, W.; Tumas, W. *Chemical reviews* **2007**, *107*, 3900.

(25) Marr, A. C.; Spencer, D. J. E.; Schröder, M. *Coordination Chemistry Reviews* **2001**, *219–221*, 1055.

(26) Jacobsen, G. M.; Shoemaker, R. K.; McNevin, M. J.; Rakowski DuBois, M.; DuBois, D. L. *Organometallics* **2007**, *26*, 5003.

(27) Wilson, A. D.; Newell, R. H.; McNevin, M. J.; Muckerman, J. T.; Rakowski DuBois, M.; DuBois, D. L. *Journal of the American Chemical Society* **2006**, *128*, 358.

(28) Yang, J. Y.; Chen, S. T.; Dougherty, W. G.; Kassel, W. S.; Bullock, R. M.; DuBois, D. L.; Raugei, S.; Rousseau, R.; Dupuis, M.; DuBois, M. R. *Chemical Communications* **2010**, *46*, 8618.

(29) Wilson, A. D.; Shoemaker, R. K.; Miedaner, A.; Muckerman, J. T.; DuBois, D. L.; DuBois, M. R. *Proceedings of the National Academy of Sciences of the United States of America* **2007**, *104*, 6951.

(30) Yang, J. Y.; Bullock, R. M.; Dougherty, W. G.; Kassel, W. S.; Twamley, B.; DuBois, D. L.; DuBois, M. R. *Dalton Transactions* **2010**, *39*, 3001.

(31) Galan, B. R.; Schoffel, J.; Linehan, J. C.; Seu, C.; Appel, A. M.; Roberts, J. A. S.; Helm, M. L.; Kilgore, U. J.; Yang, J. Y.; DuBois, D. L.; Kubiak, C. P. *Journal of the American Chemical Society* **2011**, *133*, 12767.

(32) Kilgore, U. J.; Roberts, J. A. S.; Pool, D. H.; Appel, A. M.; Stewart, M. P.; DuBois, M. R.; Dougherty, W. G.; Kassel, W. S.; Bullock, R. M.; DuBois, D. L. *Journal of the American Chemical Society* **2011**, *133*, 5861.

(33) Fraze, K.; Wilson, A. D.; Appel, A. M.; DuBois, M. R.; DuBois, D. L. *Organometallics* **2007**, *26*, 3918.

(34) Jacobsen, G. M.; Yang, J. Y.; Twamley, B.; Wilson, A. D.; Bullock, R. M.; DuBois, M. R.; DuBois, D. L. *Energy & Environmental Science* **2008**, *1*, 167.

(35) Welch, K. D.; Dougherty, W. G.; Kassel, W. S.; DuBois, D. L.; Bullock, R. M. *Organometallics* **2010**, *29*, 4532.

(36) Das, P.; Stolley, R. M.; van der Eide, E. F.; Helm, M. L. *European Journal of Inorganic Chemistry* **2014**, *2014*, 4611.

(37) Franz, J. A.; O'Hagan, M.; Ho, M.-H.; Liu, T.; Helm, M. L.; Lense, S.; DuBois, D. L.; Shaw, W. J.; Appel, A. M.; Raugei, S.; Bullock, R. M. *Organometallics* **2013**, *32*, 7034.

(38) Seu, C. S.; Appel, A. M.; Doud, M. D.; DuBois, D. L.; Kubiak, C. P. *Energy & Environmental Science* **2012**, *5*, 6480.

(39) Wiese, S.; Kilgore, U. J.; DuBois, D. L.; Bullock, R. M. *ACS Catalysis* **2012**, *2*, 720.

(40) Raugei, S.; Helm, M. L.; Hammes-Schiffer, S.; Appel, A. M.; O'Hagan, M.; Wiedner, E. S.; Bullock, R. M. *Inorganic Chemistry* **2016**, *55*, 445.

(41) O'Hagan, M.; Shaw, W. J.; Raugei, S.; Chen, S.; Yang, J. Y.; Kilgore, U. J.; DuBois, D. L.; Bullock, R. M. *Journal of the American Chemical Society* **2011**, *133*, 14301.

(42) Iggo, J. A. *NMR Spectroscopy in Inorganic Chemistry*; Oxford Science Publications, 2000.

CHAPTER 2
S_N2 SYNTHESIS OF $P^R{}_2N^{R'}{}_2$ LIGANDS FOR MOLECULAR ELECTROCATALYSTS WITH PENDANT BASES IN THE SECOND COORDINATION SPHERE

2.1 Abstract

Three 1,5-diaza-3,7-diphosphacyclooctane (P_2N_2) ligands with alkyl-substituted phosphines have been synthesized via a versatile method that allows for improved control of the phosphine substituent. The methyl-, ethyl-, and benzyl-substituted phosphine P_2N_2 ligands ($P^{Me}{}_2N^{Ph}{}_2$, $P^{Et}{}_2N^{Ph}{}_2$, and $P^{Bn}{}_2N^{Ph}{}_2$) were synthesized and characterized by $^{31}P\{^1H\}$ NMR, ^1H NMR, and elemental analysis, and their corresponding $[Ni(P^R{}_2N^{Ph}{}_2)_2](BF_4)_2$ complexes were synthesized and characterized by $^{31}P\{^1H\}$ NMR, ^1H NMR, and electrochemistry. The structures of the complex $[Ni(P^{Me}{}_2N^{Ph}{}_2)_2](CF_3SO_3)_2$ and $[Ni(P^{Et}{}_2N^{Ph}{}_2)_2](CF_3SO_3)_2$ were characterized by X-ray crystallography.

2.2 Introduction

The catalytic reductions of small molecules such as protons, CO_2, and N_2 pose significant chemical challenges. Transformations of these molecules are often hindered by high kinetic barriers for the formation of reduction intermediates; however, these reactions can be facilitate by proton-coupled electron transfer (PCET) reduction processes.[1] Many enzymes take advantage of PCET to manage electron transfers at low potentials.[2] One particularly interesting example is the enzyme [FeFe] hydrogenase (**1**), which contains an azadithiolate ligand whose nitrogen base is poised to deliver or accept

a proton during the reversible oxidation of H_2, as shown in Figure 2.1.[3] Many groups have developed and studied mimics of this active site, incorporating various pendant bases to supply hydrogen bonds for H_2 activation and otherreactions.[4,5] One of the most successful functional models of the hydrogenase enzyme is the $[Ni(P^R_2N^{R'2})_2]^{2+}$ system (2), also shown in Figure 2.1. These complexes have shown excellent electrocatalytic rates for the proton-coupled processes of H_2 oxidiation,[6] proton reduction to H_2,[7] O_2 reduction,[8] and more recently, the oxidation of formate.[9]

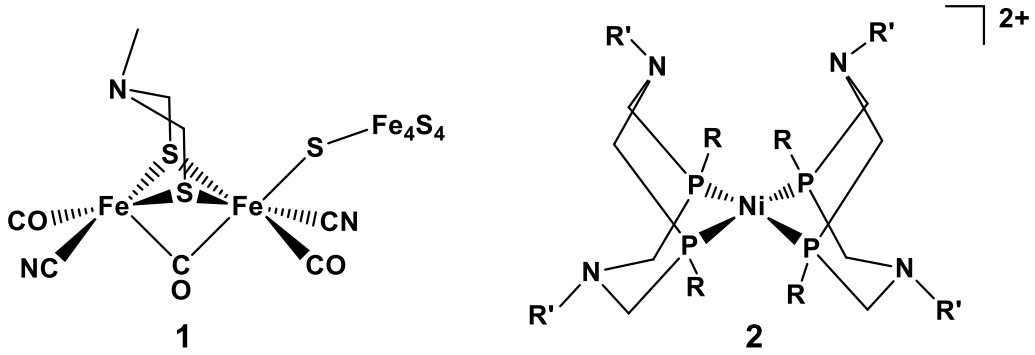

Figure 2.1 Structure of the FeFe Hydrogenase active site (1) and the $Ni(P^R_2N^{R'}_2)_2^{2+}$ cation (2).

One reason $P^R_2N^{R'}_2$ systems exhibit high performance lies in their ability to take on multiple conformations that orient the nitrogen bases into ideal locations for proton-coupled processes.[10] The utility of these complexes is expanded by the ability to vary the substituents of both the tertiary phosphine and amine of the ligand. The basicity of the amine can be tuned via substitution at R',[11] while the redox potentials of the metal center can be modified via substitution at R, and to a lesser extent at R'. More donating substituents at R generally lead to more negative reduction potentials for the metal complexes. The steric effects of R also affect the bite angle and dihedral angles of the two ligands on the metal center, which have a substantial effect on the hydricity and

reduction potentials of the metal complexes.[12] The development of new $P^{R}_{2}N^{R'}_{2}$ catalysts has been hampered by the limited availability of starting materials in the usual ligand synthesis. This arises from the fact that the first step in the literature synthesis is the dihydroxymethylation of a primary phosphine (**Scheme 2.1**).[13]

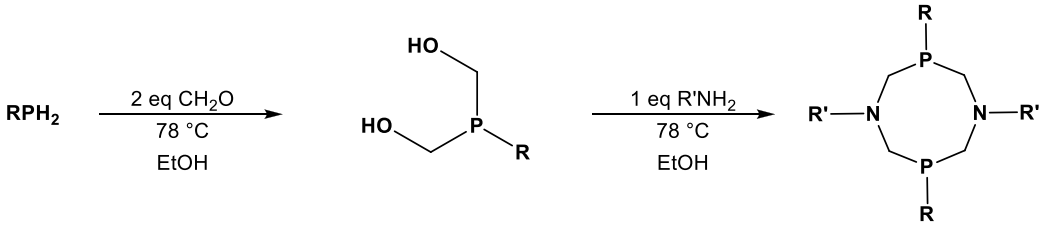

Scheme 2.1 Traditional $P^{R}_{2}N^{R'}_{2}$ ligand synthesis.

Primary phosphines are highly air-sensitive, noxious, toxic, and often pyrophoric chemicals whose commercial availability in bulk quantities is limited to cyclohexyl and phenyl phosphine. While some primary phosphines can be synthesized via alkylation of PH_3 or via the Arbuzov reaction followed by reduction, these routes require that the primary phosphine be isolated from the reactions prior to use in the synthesis of P_2N_2 ligands.[14] Ideally, ligand syntheses should be concise, use stable and commercially available reactants, and be scalable for the production of large quantities.

2.3 Experimental

2.3.1 General Considerations

Unless otherwise noted, all reactions and manipulations were performed under a N_2 atmosphere using standard glovebox or Schlenk line techniques. Glassware was dried in an oven overnight prior to use. Acetonitrile and tetrahydrofuran (THF) were purified via passage through alumina and molecular sieves. Ethanol was dried over 4 Å molecular

sieves. Aniline and triethylamine were distilled from CaH_2 prior to use. Tetrabutylammonium hexafluorophosphate was crystallized from methanol and dried under vacuum prior to use. Benzyl chloride was purified by passage through alumina. Methyl iodide was distilled from $CaCl_2$. $Ni(P^{Ph}{}_2N^{Ph}{}_2)_2[BF_4]_2$ was prepared according to literature methods.[11] All other chemicals were used as obtained from commercial suppliers. Electrochemical measurements were performed on a Gamry potentiostat in an air-tight cell with a glassy carbon working electrode, a Pt counter electrode, and a $Ag^{+/0}$ wire pseudo reference electrode. Benzonitrile was used as the solvent and 0.2M tetrabutylammonium hexafluorophosphate was used as the supporting electrolyte. ^1H and $^{31}P\{^1H\}$ NMR spectra were obtained on a 300MHz Varian or a 500MHz Joel spectrometer. ^1H NMR spectral data are referenced against the residual solvent signal and are reported in ppm downfield of tetramethylsilane ($\delta = 0$). $^{31}P\{^1H\}$ NMR spectral data were referenced against an external H_3PO_4 ($\delta = 0$) reference. Elemental Analyses were performed by Midwest Microloab in Indianapolis, IN or by NuMega Labs in San Diego, CA.

2.3.2 PREPARATION OF TRIS(HYDROXYMETHYL)PHOSPHINE (THP)

A large quantity of THP was prepared and isolated for use in the subsequent alkylation reactions. 20 mL of THPCl (80% in water, 110 mmol) were dried under vacuum in a 250 mL Schlenk flask. To the resulting oily residue was added 100 mL triethylamine, which precipitated triethylammonium chloride. The supernatant was filtered via cannula into a 250 mL Schlenk flask and dried under vacuum at 40°C overnight to remove excess formaldehyde via sublimation. The resulting oil was

dissolved in 10 mL methanol, to which was added 100 mL diethyl ether. This flask was then placed in a freezer at –40 °C for a week, after which a white precipitate, THP, was observed. This was filtered via cannula, rinsed with ether, and dried to yield 6.58 g (53 mmol, 48% yield). Spectral data matched reported values.[15]

2.3.3 SYNTHESIS OF $P^{Me}{}_2N^{Ph}{}_2$ (3)

A 100 mL Schlenk flask was charged with 6.0 mL of a solution of tetrakis(hydroxymethyl)phosphonium chloride (80% in water, 33 mmol) and the volatiles were removed under vacuum overnight. The resulting oil was dissolved in 50 mL triethylamine and stirred overnight at room temperature, precipitating triethylammonium chloride as a fine white solid. The supernatant was filtered via cannula into a 100 mL Schlenk flask and the volatiles were removed under vacuum. The resulting oil was dissolved in 20 mL THF. To this stirring solution of tris(hydroxymethyl)phosphine, 1.9 mL (30 mmol) of CH_3I was slowly added at –40 °C via syringe and the reaction was allowed to warm to room temperature overnight. The volatiles were removed under vacuum and the residue was redissolved in 20 mL triethylamine. The solution was stirred overnight, and the precipitation of the triethylammonium iodide salt was observed. The supernatant was filtered via cannula and dried under vacuum to yield $CH_3P(CH_2OH)_2$ as an oil. This was dissolved in 50 mL dry ethanol, to which was added 2.3 mL aniline (25 mmol). This mixture was stirred at room temperature for one week. A white solid precipitated, and the supernatant was removed via cannula. The solid was rinsed with absolute ethanol and dried to give 3.29 g of 3,7-dimethyl-1,5-diphenyl-1,5-diaza-3,7-diphosphacyclooctane ($P^{Me}{}_2N^{Ph}{}_2$) (10 mmol, 63% yield). A sample was prepared for

elemental analysis by recrystallization from toluene. Calculated CHN values: 65.44% C, 7.32% H, 8.48% N. Found CHN values: 65.47% C, 7.43% H, 8.47% N. ^{1}H NMR (400MHz, CD_3CN): δ = 7.22 (m, Ar*H*, 4H), 6.70 (m, Ar*H*, 6H), 4.17 (t, *J* = 14.3 Hz, CH_2, 4H), 3.44 (dd, *J* = 14.8 Hz, *J* = 4.6 Hz, CH_2, 8H), 1.02 (d, *J* = 4.4 Hz, CH_3, 6H). ^{31}P{^{1}H} NMR (162MHz, CD_3CN): δ = -61.8 ppm (s).

2.3.4 SYNTHESIS OF $P^{Et}_2N^{Ph}_2$ (4)

In an oven-dried 25 mL Schlenk flask, THPC (4.49 g, 23.6 mmol) was dissolved in ethanol. To this stirring mixture, solid sodium hydroxide (NaOH, 0.960 g, 24.0 mmol) was carefully added under positive N_2 pressure, precipitating sodium chloride. The supernatant was isolated in another oven-dried 25 mL Schlenk flask via cannula filtration. To this stirring mixture, bromoethane (EtBr, 5.2 mL, 70.1 mmol) was added via syringe. The reaction was stirred on a sand bath at 50°C, and monitored by ^{31}P{^{1}H} NMR by observing the appearance and growth of a peak at 30.6 ppm. Upon completion of the reaction, potassium hydroxide (KOH, 1.28 g, 22.8 mmol) was added to the stirring mixture. A white precipitate (KBr) formed. The supernatant was isolated by cannula filtration to another oven-dried 25 mL Schlenk flask. To this stirring solution, aniline (2.0 mL, 21.9 mmol) was added and stirred on a sand bath at 50°C. After three hours, a voluminous white precipitate formed, and the supernatant was removed via cannula filtration. The solid was rinsed with absolute ethanol (10 mL) and three times with acetonitrile (10 mL) and dried to yield **4**, 3,7-diethyl-1,5-diphenyl-1,5-diaza-3,7-diphosphacyclooctane ($P^{Et}_2N^{Ph}_2$) (2.2 g, 6.1 mmol, 28% yield). ^{1}H NMR (300MHz, $CDCl_3$): δ = 7.29 (m, Ar*H*, 4H), 6.70 (m, Ar*H*, 6H), 4.17 (t, *J* = 14.3 Hz, CH_2, 4H), 3.44

(dd, J = 14.8 Hz, J = 4.6 Hz, CH_2, 8H), 1.02 (d, J = 4.4 Hz, CH_3, 6H). $^{31}P\{^1H\}$: δ = -46.86 ppm. Calculated M/z for $[C_{22}H_{30}N_4O_2P_2Na]^+$: 467.1736; Found: 467.1738.

2.3.5 SYNTHESIS OF $P^{Bn}{}_2N^{Ph}{}_2$ (5)

0.58 grams (4.6 mmol) of tris(hydroxymethyl)phosphine and 0.53 mL (4.6 mmol) benzyl chloride were dissolved in tetrahydrofuran and stirred overnight in a 100 mL Schlenk flask. This reaction mixture was dried under vacuum and dissolved in triethylamine, and the immediate precipitation of triethylammonium chloride was observed. The supernatant was filtered via cannula into another 100 mL Schlenk flask and dried under vacuum to yield 0.61 grams of oily benzylbis(hydroxymethyl)phosphine. This was dissolved in dry ethanol and refluxed with 0.30 mL (3.2 mmol) of aniline overnight, precipitating the ligand 3,7-dibenzyl-1,5-diphenyl-1,5-diaza-3,7-diphosphacyclooctane ($P^{Bn}{}_2N^{Ph}{}_2$) as a white solid. This was filtered via cannula, washed with ethanol, and dried under vacuum, yielding 0.15 grams of $P^{Bn}{}_2N^{Ph}{}_2$ (0.31 mmol, 13% yield). Spectral data matched reported values.[16]

2.3.6 PREPARATION OF $Ni(P^R{}_2N^{Ph}{}_2)_2(CH_3CN)[BF_4]_2$

The nickel complexes $Ni(P^R{}_2N^{Ph}{}_2)_2(CH_3CN)[BF_4]_2$ (R = Me (**5**), Et (**6**) and Bn (**7**)) were prepared following the same procedure. The following is a representative example for $Ni(P^{Me}{}_2N^{Ph}{}_2)_2[BF_4]_2$. 370 mg of $P^{Me}{}_2N^{Ph}{}_2$ (1.1 mmol) was added to a solution of $Ni(CH_3CN)_6[BF_4]_2$ (340 mg, 0.71 mmol) in 50 mL acetonitrile. The color of this solution immediately turned deep red. This mixture was stirred overnight and solid was precipitated by layering with diethyl ether. The solid is filtered via cannula, rinsed with diethyl ether, and dried under vacuum to yield 0.45 g of microcrystalline red

$Ni(P^{Me}{}_2N^{Ph}{}_2)_2[BF_4]_2$ (0.48 mmol, 86% yield) ^1H NMR (500MHz, CD_3CN): δ = 7.34 (t, *J* = 8.0 Hz, Ar*H*, 8H), 7.09 (d, *J* = 8.0 Hz, Ar*H*, 8H), 7.03 (t, *J* = 7.3 Hz, Ar*H*, 4H), 3.74 (d, *J* = 14.0 Hz, CH_2, 8H), 3.68 (d, *J* = 14.0 Hz, CH_2, 8H), 1.83 (s, CH_3, 12H). $^{31}P\{^1H\}$ NMR (202.5MHz, CD_3CN): δ = 1.2 ppm (s). Calculated M/z for $[Ni(P^{Me}{}_2N^{Ph}{}_2)_2]^{2+}$: 359.1091 ; Found: 359.1088. Spectral data for complex **6** matched literature values.[16]

2.3.7 Preparation of $Ni(P^{Me}{}_2N^{Ph}{}_2)_2[SO_3CF_3]_2$ (7) and X-ray Structure Determination

In a 20 mL scintillation vial, 0.107 g $P^{Me}{}_2N^{Ph}{}_2$ (0.386 mmol) was added to a solution of 0.116 g $Ni(CH_3CN)_6[CF_3SO_3]_2$ (0.192 mmol) in 10 mL acetonitrile. The color of this solution immediately turned deep red. This mixture was stirred overnight. Attempts to isolate solid $Ni(P^{Me}{}_2N^{Ph}{}_2)[CF_3SO_3]_2$ failed as the complex oils out of solution upon layering of diethyl ether into acetonitrile. An analogous microscale reaction performed in a J Young NMR tube (2.2 mg $P^{Me}{}_2N^{Ph}{}_2$, 2.0 mg $Ni(CH_3CN)_6[CF_3SO_3]_2$ provided spectroscopic evidence for the complex with a broad peak in the $^{31}P\{^1H\}$ NMR spectrum with δ = 1.4 ppm. X-ray quality crystals of **7** were grown by vapor diffusion of diethyl ether into acetontrile. Single crystal X-ray structural data was collected at 100K on a Kappa diffractometer equipped with a Bruker Apex detector. The structure was solved by direct methods using SHELXS-97 and refined with full-matrix least-squares procedures using SHELXL-97.

2.3.8 Preparation of $Ni(P^{Et}{}_2N^{Ph}{}_2)_2[SO_3CF_3]_2$ (8) and X-ray Structure Determination

In a 20 mL scintillation vial, 0.14 g $P^{Et}{}_2N^{Ph}{}_2$ (0.386 mmol) was added to a solution of 0.11 g $Ni(CH_3CN)_6[CF_3SO_3]_2$ (0.192 mmol) in acetonitrile (10 mL). The color of this

solution immediately turned deep red. This mixture was stirred overnight. The supernatant was isolated via syringe filtration, and X-ray quality crystals of **8** were grown by vapor diffusion of diethyl ether into acetonitrile. Single crystal X-ray structural data was collected at 100K on a Kappa diffractometer equipped with a Bruker Apex detector. The structure was solved by direct methods using SHELXS-97 and refined with full-matrix least-squares procedures using SHELXL-97.(REF = Sheldrick, G. *Acta Cryst. A* **2008**, *64*, 112)

2.4 Results and Discussion

We presently report a synthetic route which meets these requirements. A report by Griffiths and coworkers indicates that alkyl(bis-hydroxymethyl)phophines can be synthesized utilizing a cheap, commercially available, and air-stable reagent: tetrakis(hydroxymethyl)phosphonium chloride (THPCl).[17,18] This route removes the need to synthesize or utilize a primary phosphine. Here, we demonstrate the use of THPCl to synthesize the $P^{R}{}_{2}N^{R'}{}_{2}$ ligands with methyl and benzyl substituents on the phosphine (Scheme 2.2).

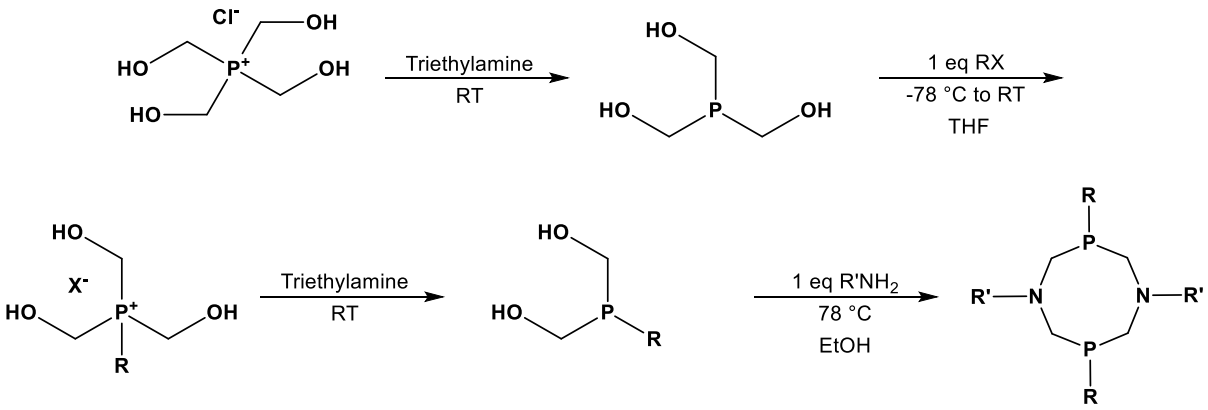

Scheme 2.2 $P^{R}{}_{2}N^{R'}{}_{2}$ synthesis via dehydroxymethylation and alkylation of THPCl.

Dehydroxymethylation of THPCl under basic conditions in neat triethylamine or KOH in ethanol yields tris(hydroxymethyl)phosphine (THP).[19] This phosphine reacts with alkyl halides, yielding the alkyltris(hydroxymethyl)phosphonium halide salt. Methyl iodide and benzyl chloride were successfully used as alkylating agents for this reaction. This selection of compounds demonstrates the versatility of the synthesis: alkylating agents can be chosen irrespective of the halide leaving group and with concern for safety, utility, and expense. After alkylation, the compound is once more dehydroxymethylated in neat triethylamine to form the alkylbis(hydroxymethyl)phosphine. Here the synthesis of the $P^{R}{}_{2}N^{Ph}{}_{2}$ ligands **3**, **4**, and **5** proceeds in the same fashion as the traditional ligand synthesis, as this phosphine is treated with one equivalent of a primary amine ($R'NH_2$, aniline for **3**, **4**, and **5**) to form the corresponding $P^{R}{}_{2}N^{R'}{}_{2}$.

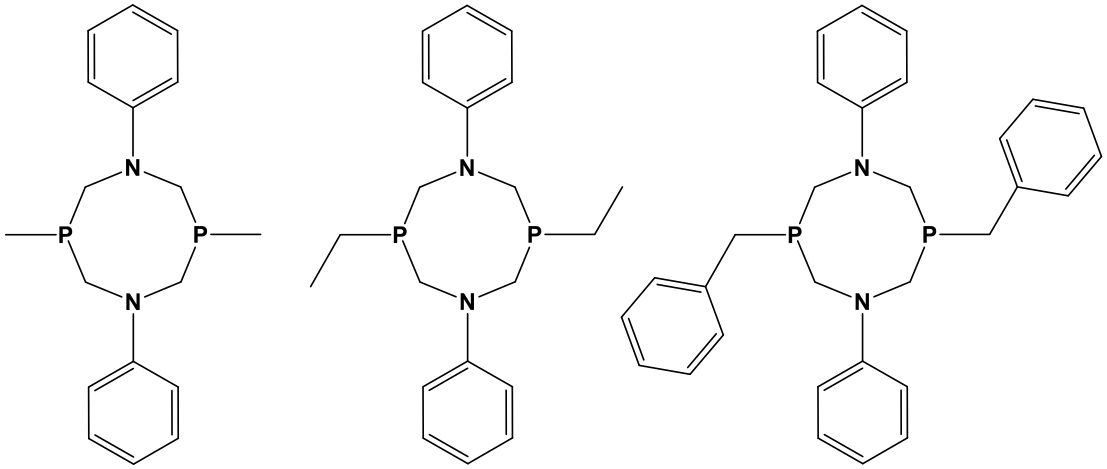

Figure 2.2 $P^{R}{}_{2}N^{Ph}{}_{2}$ ligands with methyl (3), ethyl (4), and benzyl (5) phosphine substituents synthesized from THPCl.

Ligands **3**, **4**, and **5**, shown in Figure 2.2, were isolated and characterized by elemental analysis, ^{1}H NMR and $^{31}P\{^{1}H\}$ NMR. We have used these ligands to prepare

their homoleptic nickel complexes, whose cyclic voltammograms were examined to study how these alkyl-substituted P_2N_2 ligands affect the reduction potentials of the associated complexes, $Ni(P^R_2N^{Ph}_2)_2[BF_4]_2$. The electrochemical properties of similar $Ni(P^R_2N^{Ph}_2)_2^{2+}$ complexes with R = Ph and Cy are well documented in the literature.[7-11] The nickel complexes $Ni(P^R_2N^{Ph}_2)_2[BF_4]_2$ (R = Me, **6**; R = Et, **7**; R = Bn, **8**) were synthesized analogously to the previously reported complexes (Scheme 2.3).[16]

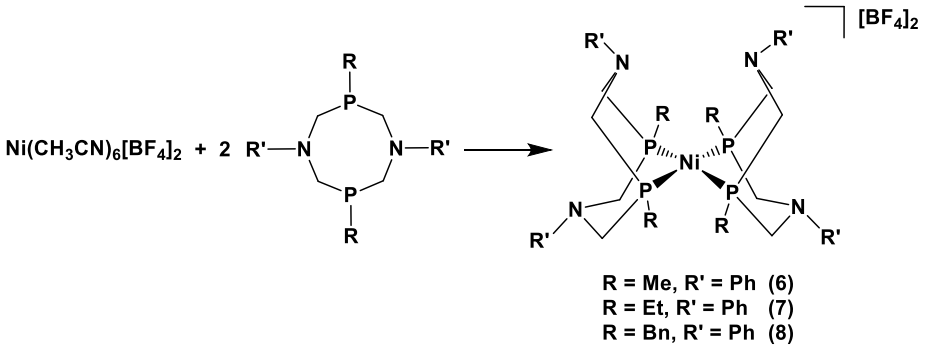

Scheme 2.3 Synthesis of homoleptic nickel complexes of $P^R_2N^{R'}_2$ ligands.

Table 2.1 Reduction potentials for the series of complexes $Ni(P^{R}_{2}N^{Ph}_{2})_2(CH_3CN)[BF_4]_2$ in benzonitrile.

Ligand	$E°(Ni^{II/I})$ (V vs $Cp_2Fe^{+/0}$)	$E°(Ni^{I/0})$ (V vs $Cp_2Fe^{+/0}$)
Me,Ph[a]	–1.01	–1.30
Et,Ph	-0.91	-1.25
Bn,Ph[a]	–0.78	–1.16
Ph,Ph[a]	–0.79	–1.00
Cy,Ph[b]	–0.60	–1.10

[a] This work. [b] Ref 7

These complexes typically give cyclic voltammograms consisting of two reversible 1-electron redox processes associated with $E°(Ni^{I/0})$ and $E°(Ni^{II/I})$, exemplified by the $Ni(P^{Me}_{2}N^{Ph}_{2})_2[BF_4]_2$ shown in Figure 2.3. Table 2.1 compares the reduction potentials in benzonitrile for previously reported complexes with the complexes synthesized in this work. The methyl-substituted phosphine ligands on $[Ni(P^{Me}_{2}N^{Ph}_{2})_2]^{2+}$ shift both reduction potentials of the nickel complex farther negative against the $FeCp_2^{+/0}$ reference when compared to the previously reported $[Ni(P^{Ph}_{2}N^{Ph}_{2})_2]^{2+}$ and $[Ni(P^{Cy}_{2}N^{Ph}_{2})_2]^{2+}$ complexes. The electron donating character of the alkyl phosphines (R = Me, Et, Bn) is expected to be greater than that of the aryl phosphine (R=Ph). However, it is notable that the benzyl-substituted P_2N_2 complex is more easily reduced than the phenyl-substituted complex. The decrease in steric bulk at R as compared to the

cyclohexyl phosphine-substituted P_2N_2 ligands may have the effect of reducing the distortion toward a tetrahedral geometry in the Ni(II) state. The partial tetrahedral distortion in complexes ligated with the bulky cyclohexyl phosphine P_2N_2 ligands lowers the Ni(II) reduction potential and stabilizes the Ni(I) state. Less bulky alkyl substituents may favor a square planar geometry in the Ni(II) state, which raises the Ni(II) reduction potential and destabilizes the Ni(I) state.[10] Indeed, from Table 2.1 it can be seen that as the steric bulk of the phosphine groups increases (Me<Ph<Bn<Cy), the potential required for the $E°(Ni^{II/I})$ reduction couple decreases (Me<Ph<Bn<Cy).

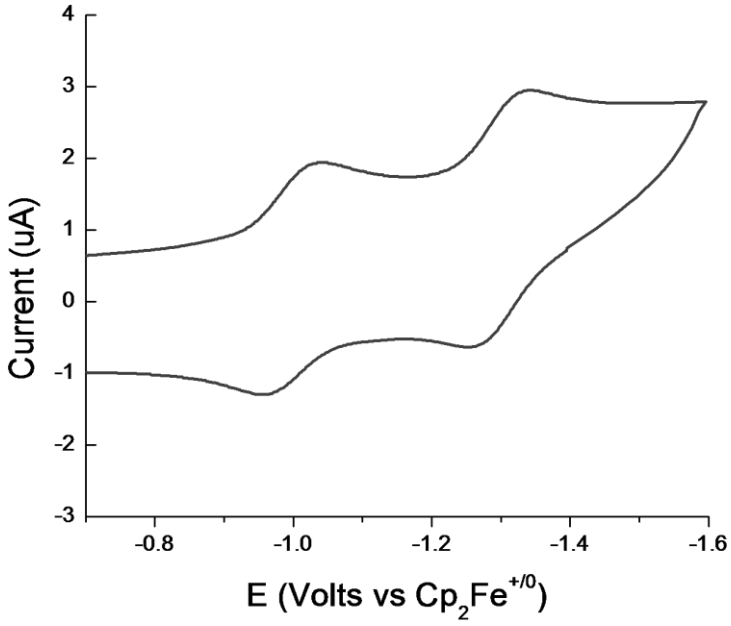

Figure 2.3 Cyclic voltammogram of 2.0 mM $Ni(P^{Me}_2N^{Ph}_2)_2[BF_4]_2$ in benzonitrile/0.2 M Bu_4NPF_6 with a 1mm glassy carbon working electrode. Scan rate = 0.1 V s^{-1}.

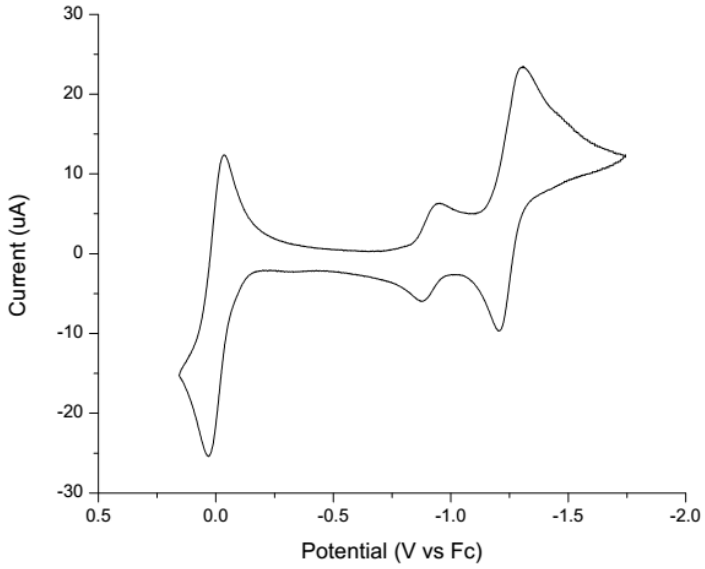

Figure 2.4 Cyclic voltammogram of 1.0 mM 7 $[Ni(Et.Ph)_2](BF_4)_2$ with ferrocene added for internal reference in 0.2 M Bu_4NPF_6 in benzonitrile with a 1mm glassy carbon working electrode. Scan rate = 0.1 V s^{-1}.

The importance of the steric effect exerted by the phosphine substitutent is illustrated by the X-ray crystal structure of the $Ni[(P^{Me}{}_2N^{Ph}{}_2)_2]^{2+}$ complex. X-ray quality crystals were obtained for $Ni(P^{Me}{}_2N^{Ph}{}_2)_2[CF_3SO_3]_2$ (**7**) (Figure 2.5) by vapor diffusion of diethyl ether into acetonitrile. The non-coordinative nature of both the $[BF_4]^-$ and $[CF_3SO_3]^-$ anions allow for reasonable comparisons between the active $[Ni(P^R{}_2N^{R'}{}_2)]^{2+}$ cations. This structure differs from most previous $[Ni(P^R{}_2N^{R'}{}_2)_2]^{2+}$ complexes in that acetonitrile is not coordinated to the metal center in the crystal structure. The reduced steric impetus exerted by the methyl substituent yields a distorted square planar structure for the $[Ni(P^{Me}{}_2N^{Ph}{}_2)_2]^{2+}$ cation, which is a significant variation from the reported structures of the $[Ni(P^{Bn}{}_2N^{Ph}{}_2)_2(CH_3CN)]^{2+}$ and $[Ni(P^{n\text{-}Bu}{}_2N^{Ph}{}_2)_2(CH_3CN)]^{2+}$ cations, which exhibit distorted trigonal bipyramidal structures.[16] The structure of **9** deviates

slightly from a square planar geometry, with a dihedral angle of 16.16° between the two P–Ni–P planes.

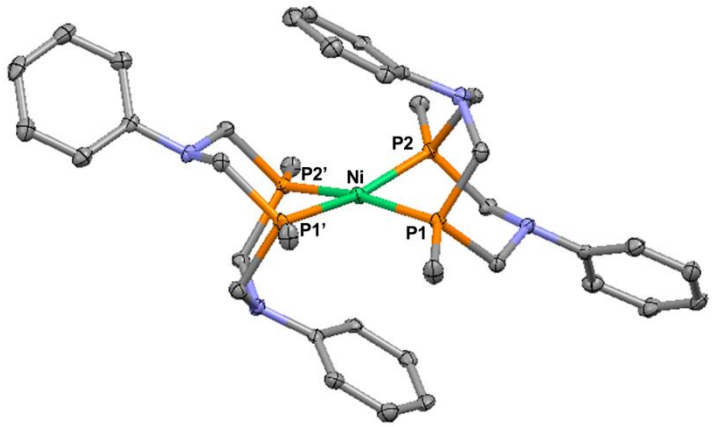

Figure 2.5 X-ray crystal structure of $Ni(P^{Me}{}_2N^{Ph}{}_2)_2[CF_3SO_3]_2$ with protons, co-crystallized solvent and counter ions excluded for clarity. Ellipsoids are shown at 50% probability. Selected bond distances (Å) and angles (°): Ni–P1 = 2.2393(11), Ni–P1' = 2.2393(11), Ni–P2 = 2.2088(12), Ni–P2' = 2.2089(12), P1–Ni–P2 = 83.16(4), P1–Ni–P1' = 99.64(6), P1'–Ni–P2' = 83.16(5), P2–Ni–P2' = 96.06(6). P1 and P1' and P2 and P2' are related by symmetry.

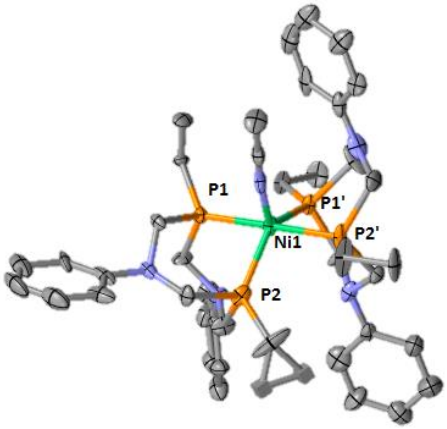

Figure 2.6 X-ray crystal structure of $Ni(P^{Et}{}_2N^{Ph}{}_2)_2[CF_3SO_3]_2$ with protons, co-crystallized solvent and counter ions excluded for clarity. Ellipsoids are shown at 50% probability.

2.5 Conclusion

We have demonstrated a versatile synthetic route for the production of P_2N_2-type ligands that avoids the use of primary phosphines. This synthesis gives unprecedented control over the substitution at the phosphorus atoms in the ligand, which directly modifies the donating character of the ligand and the redox potentials of the associated metal complexes. The homoleptic nickel complexes of the $P^{Me}{}_2N^{Ph}{}_2$, $P^{Et}{}_2N^{Ph}{}_2$, $P^{Bn}{}_2N^{Ph}{}_2$ ligands have been synthesized and characterized, and the reduction potentials of two complexes are compared with previously reported $P^{R}{}_2N^{Ph}{}_2$ complexes (R = Ph and Cy). A nickel $P^{Me}{}_2N^{Ph}{}_2$ complex has also been characterized by X-ray crystallography.

This synthesis invites the potential to generate P_2N_2 ligands with a multitude of substituents on the phosphine. We are in the process of employing this control to impart further functionality on P_2N_2 ligands and their metal complexes. While previous studies have attempted to attach P_2N_2 catalysts to electrode surfaces, they have been limited by the traditional synthesis via functionalization of the amine.[20] Attaching the amine to a surface limits the flexibility of the pendant base, which has been shown to be critical to the electrocatalytic activity of the P_2N_2 complexes.[10] By combining the synthesis described in this report with electrode surface modification techniques, the freedom of the pendant base should be preserved while attachment of an appropriate functional group to the phosphine substituent will enable a direct connection between the electrode and the catalytic site.

In addition, we are using this synthesis to modify the electrocatalytic activity of $P^{R}{}_2N^{R'}{}_2$ complexes of nickel and other metals. By increasing the electron donation character of the phosphine substituent, the redox potentials of the metal $P^{R}{}_2N^{R'}{}_2$

complexes are pushed more negative, and the hydricity (hydride donation ability) of the $[NiH(P^{R}_{2}N^{R'}_{2})]^{+}$ complexes should also increase.[21] This thermodynamic property can be used to predict whether a complex will oxidize H_2 or reduce protons under given reaction conditions.[22] Our goal is to find a similar balance in the new complexes with regards to formate oxidation and carbon dioxide reduction. Adding more electronically donating and less sterically bulky substituents increases the hydride donation ability and pushes the formate oxidation catalysis towards its microscopic reverse, the single proton-coupled two-electron reduction of carbon dioxide to formate or further reduction products. Further studies of P_2N_2 ligands synthesized with this method and their corresponding metal complexes will be reported in due course.

The majority of the material for this chapter comes directly from a manuscript entitled "Versatile Synthesis of $P^{R}_{2}N^{R'}_{2}$ Ligands for Molecular Electrocatalysts with Pendant Bases in the Second Coordination Sphere," by Michael D. Doud, Kyle A. Grice, Alyssia M. Lilio, Candace S. Seu, and Clifford P. Kubiak, published in *Organometallics,* **2012**, *31,* 779-782. The dissertation author is the primary author of this manuscript.

2.6 References

(1) Benson, E. E.; Kubiak, C. P.; Sathrum, A. J.; Smieja, J. M. *Chem. Soc. Rev.* **2009**, *38*, 89.

(2) Reece, S. Y.; Hodgkiss, J. M.; Stubbe, J.; Nocera, D. G. *Philosophical Transactions of the Royal Society B: Biological Sciences* **2006**, *361,* 1351.

(3) Nicolet, Y.; de Lacey, A. L.; Vernède, X.; Fernandez, V. M.; Hatchikian, E. C.; Fontecilla-Camps, J. C. *J. Am. Chem. Soc.* **2001**, *123*, 1596.

(4) Schwartz, L.; Eilers, G.; Eriksson, L.; Gogoll, A.; Lomoth, R.; Ott, S. *Chem. Commun.* **2006**, 520.

(5) Tard, C.; Liu, X.; Ibrahim, S. K.; Bruschi, M.; Gioia, L. D.; Davies, S. C.; Yang, X.; Wang, L.-S.; Sawers, G.; Pickett, C. J. *Nature* **2005**, *433*, 610.

(6) Yang, J. Y.; Chen, S.; Dougherty, W. G.; Kassel, W. S.; Bullock, R. M.; DuBois, D. L.; Raugei, S.; Rousseau, R.; Dupuis, M.; DuBois, M. R. *Chemical Communications* **2010**, *46*, 8618.

(7) Wilson, A. D.; Shoemaker, R. K.; Miedaner, A.; Muckerman, J. T.; DuBois, D. L.; DuBois, M. R. *Proceedings of the National Academy of Sciences* **2007**, *104*, 6951.

(8) Yang, J. Y.; Bullock, R. M.; Dougherty, W. G.; Kassel, W. S.; Twamley, B.; DuBois, D. L.; Rakowski DuBois, M. *Dalton Transactions* **2010**, *39*, 3001.

(9) Galan, B. R.; Schöffel, J.; Linehan, J. C.; Seu, C.; Appel, A. M.; Roberts, J. A. S.; Helm, M. L.; Kilgore, U. J.; Yang, J. Y.; DuBois, D. L.; Kubiak, C. P. *J. Am. Chem. Soc.* **2011**, *133*, 12767.

(10) Wilson, A. D.; Newell, R. H.; McNevin, M. J.; Muckerman, J. T.; Rakowski DuBois, M.; DuBois, D. L. *J. Am. Chem. Soc.* **2006**, *128*, 358.

(11) Kilgore, U. J.; Roberts, J. A. S.; Pool, D. H.; Appel, A. M.; Stewart, M. P.; DuBois, M. R.; Dougherty, W. G.; Kassel, W. S.; Bullock, R. M.; DuBois, D. L. *J. Am. Chem. Soc.* **2011**, *133*, 5861.

(12) Fraze, K.; Wilson, A. D.; Appel, A. M.; Rakowski DuBois, M.; DuBois, D. L. *Organometallics* **2007**, *26*, 3918.

(13) G. Märkl, V.; Jin, G. Y.; Schoerner, C. *Tetrahedron Letters* **1980**, *21*, 1409.

(14) Van Hooijdonk, M. C. J. M.; Gerritsen, G.; Brandsma, L. *Phosphorus, Sulfur, and Silicon and the Related Elements* **2000**, *162*, 39.

(15) Chatt, J.; Leigh, G. J.; Slade, R. M. *J. Chem. Soc., Dalton Trans.* **1973**, 2021.

(16) Kilgore, U. J.; Stewart, M. P.; Helm, M. L.; Dougherty, W. G.; Kassel, W. S.; DuBois, M. R.; DuBois, D. L.; Bullock, R. M. *Inorganic Chemistry* **2011**, *50*, 10908.

(17) Griffiths, D. V.; Groombridge, H. J.; Salt, M. C. *Phosphorus, Sulfur, and Silicon and the Related Elements* **2008**, *183*, 473.

(18) Petrov, K.; Parshina, V.; Luzanova, M. *JOURNAL OF GENERAL CHEMISTRY USSR* **1962**, *32*, 542.

(19) Caporali, M.; Gonsalvi, L.; Zanobini, F.; Peruzzini, M. *Inorg Synth* **2010**, *35*, 96.

(20) Le Goff, A.; Artero, V.; Jousselme, B.; Tran, P. D.; Guillet, N.; Metaye, R.; Fihri, A.; Palacin, S.; Fontecave, M. *Science* **2009**, *326*, 1384.

(21) Berning, D. E.; Noll, B. C.; DuBois, D. L. *J. Am. Chem. Soc.* **1999**, *121*, 11432.

(22) Berning, D. E.; Miedaner, A.; Curtis, C. J.; Noll, B. C.; Rakowski DuBois, M. C.; DuBois, D. L. *Organometallics* **2001**, *20*, 1832.

2.7 Appendix

2.7.1 Crystallographic details for 7, $Ni(P^{Me}_2N^{Ph}_2)_2[SO_3CF_3]_2$

Table 2.2 X-ray determination details for 7.

Empirical formula	C42 H54 F6 N6 Ni O6 P4 S2	
Formula weight	1099.62	
Temperature	100(2) K	
Wavelength	0.71073 Å	
Crystal system	Orthorhombic	
Space group	C222(1)	
Unit cell dimensions	a = 9.599(4) Å	□= 90°.
	b = 19.149(9) Å	□= 90°.
	c = 26.346(10) Å	□ = 90°.
Volume	4843(3) $Å^3$	
Z	4	
Density (calculated)	1.508 Mg/m^3	
Absorption coefficient	0.695 mm^{-1}	
F(000)	2280	
Crystal size	0.20 x 0.20 x 0.10 mm^3	
Theta range for data collection	2.13 to 25.43°.	
Index ranges	-10<=h<=11, -22<=k<=23, -30<=l<=31	
Reflections collected	14015	
Independent reflections	4418 [R(int) = 0.0404]	
Completeness to theta = 25.00°	99.8 %	
Absorption correction	Semi-empirical from equivalents	
Max. and min. transmission	0.9338 and 0.8735	
Refinement method	Full-matrix least-squares on F^2	
Data / restraints / parameters	4418 / 0 / 306	
Goodness-of-fit on F^2	1.142	
Final R indices [I>2sigma(I)]	R1 = 0.0316, wR2 = 0.0725	
R indices (all data)	R1 = 0.0427, wR2 = 0.1000	
Absolute structure parameter	0.024(17)	
Largest diff. peak and hole	0.479 and -0.369 $e.Å^{-3}$	

2.7.2 CRYSTALLOGRAPHIC DETAILS FOR 8, $Ni(P^{Et}{}_2N^{Ph}{}_2)_2(CH_3CN)[SO_3CF_3]_2$

Table 2.3 X-ray determination details for 8.

Empirical formula	C46 H61 F6 N7 Ni O6 P4 S2	
Formula weight	1168.73	
Temperature	100(2) K	
Wavelength	0.71073 Å	
Crystal system	Monoclinic	
Space group	P21/c	
Unit cell dimensions	a = 11.172(1) Å	□= 90°.
	b = 18.010(2) Å	□= 98.802(4)°.
	c = 25.152(3) Å	□ = 90°.
Volume	5001(2) $Å^3$	
Z	4	
Density (calculated)	1.476 Mg/m^3	
Absorption coefficient	0.673 mm^{-1}	
F(000)	2308	
Crystal size	0.30 x 0.10 x 0.10 mm^3	
Theta range for data collection	2.41 to 20.74°.	
Index ranges	-10<=h<=11, -22<=k<=19, -30<=l<=26	
Independent reflections	6413 [R(int) = 0.0573]	
Completeness to theta = 25.00°	99.4 %	
Absorption correction	Semi-empirical from equivalents	
Max. and min. transmission	0.9338 and 0.8735	
Refinement method	Full-matrix least-squares on F^2	
Data / restraints / parameters	4418 / 0 / 306	
Goodness-of-fit on F^2	1.142	
Final R indices [I>2sigma(I)]	R1 = 0.0316, wR2 = 0.0725	
R indices (all data)	R1 = 0.0427, wR2 = 0.1000	
Absolute structure parameter	0.024(17)	
Largest diff. peak and hole	0.479 and -0.369 $e.Å^{-3}$	

CHAPTER 3
SYNTHESIS OF P_2N_2 LIGANDS VIA MICHAEL ADDITION

3.1 ABSTRACT

A series of 1,5-diaza-3,7-diphosphacyclooctane (P_2N_2) ligands with carbonyl phosphine substituents has been synthesized via a new method involving the Michael Addition of a phosphine precursor which allows functionalization of the phosphine substituents on the P_2N_2 ligands. Acrylic acid, acrylamide, and ethyl acrylate were used to synthesize the 3-propanoic acid, 3-propanamide, and ethyl 3-propanoate-phosphino-substituted P_2N_2 ligands ($P^{PA}{}_2N^{Ph}{}_2$, $P^{Amide}{}_2N^{Ph}{}_2$, $P^{EtE}{}_2N^{Ph}{}_2$, $P^{EtE}{}_2N^{PhOMe}{}_2$), respectively. These ligands were synthesized and characterized by $^{31}P\{^1H\}$ NMR and ^1H NMR, and their corresponding $Ni(P^R{}_2N^{R'}{}_2)X_2$ ($X= Cl^-$, BF_4^-) complexes have been synthesized and characterized by $^{31}P\{^1H\}$ NMR, ^1H NMR, X-ray crystallography, and elemental analysis.

3.2 Introduction

The development of efficient catalysts for the conversion of electrical energy to chemical energy and the reverse process is a pressing challenge for the development of a renewable energy economy.[1,2] The reduction of such species as CO_2, N_2, and even protons are often hindered by high kinetic barriers for the formation of reduced intermediates.[3] Catalysts can lower these barriers by using proton-coupled reduction processes.[4-6] Enzymes have evolved to take advantage of this;[7] for example, the active site of [FeFe] hydrogenase possesses a unique azadithiolate cofactor (Figure 3.1) in

which the nitrogen base is positioned to deliver or accept a proton during the reversible oxidation of H_2.[8,9]

Homogeneous catalysis offers possibilities to harness these proton-coupled electron transfer (PCET) reactions. Molecular catalysts can be designed to mimic structures that are found to be effective,[10] and a diverse array of spectroscopic and synthetic methods can be used to characterize, study, and iterate catalyst design.[11,12] One of the most rigorously studied examples of bio-inspired catalyst design is that of the DuBois-type $Ni(P^R_2N^{R'}_2)_2^{2+}$ system, also shown in Figure 3.1.[13] D. L. DuBois and his coworkers began by studying the relationship between the hydricities of $[Ni(diphosphine)_2]^{2+}$ complexes and their ability to heterolytically split H_2.[14] By incorporating a nitrogen base into a "PNP" ligand framework, they synthesized a functional hydrogenase model containing both hydride- and proton- acceptor sites.[15] These complexes demonstrated promising activity, but were limited by poor positioning of the pendant base owing to the geometry of the metallaheterocycle in the chair conformation where the N atom is further away from the metal center. By instead using a heterocyclic diphosphine "P_2N_2" ligand, the pendant base is constrained to the more active boat conformation, leading to much greater activities for hydrogen oxidation and evolution.[16]

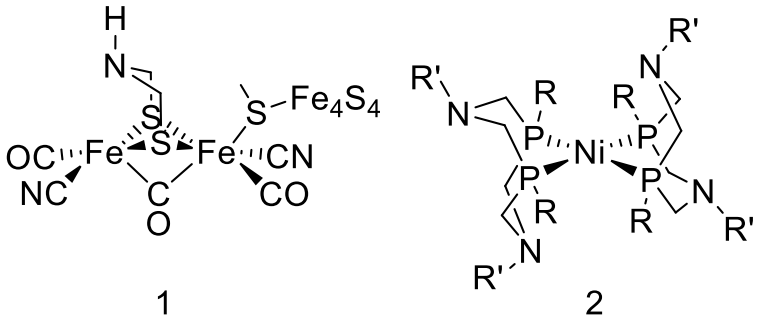

Figure 3.1 [FeFe] Hydrogenase active site (1) and $Ni(P^{R}_{2}N^{R'}_{2})_{2}^{2+}$ (2)

3.3 Previously reported syntheses of P_2N_2 ligands

Unfortunately, the conventional synthesis of these ligands (Scheme 3.1a) utilizes primary phosphines, [17] which are unstable and pyrophoric materials; and at the time this article was written the commercial availability of primary phosphine precursors was limited to cyclohexyl, phenyl, and *tert*-butyl phosphine. Other primary phosphines can be made from the alkylation of PH_3 but require isolation of the potentially gaseous primary phosphine before further synthesis.[18] In view of the widespread interest in P_2N_2 type ligands, we sought to develop alternative synthetic procedures to prepare them from more readily available starting materials and diversify the pool of available functional groups.

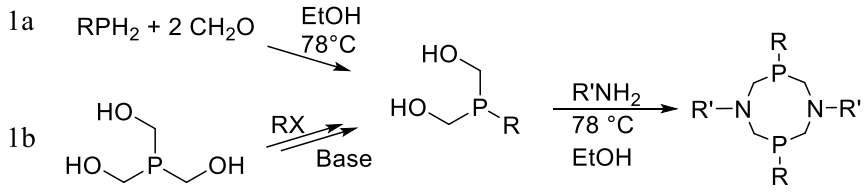

Scheme 3.1 Previously reported $P^{R}_{2}N^{R'}_{2}$ ligand syntheses.

Previously, we used the S_N2 substitution of tris(hydroxymethyl)phosphine (THP) to synthesize $P^{R}_{2}N^{R'}_{2}$ ligands with methyl and benzyl substituents on the phosphine (Scheme 3.1b).[19] This route removes the need to synthesize or utilize a primary

phosphine, and offers new synthetic pathways to P_2N_2 ligands. For example, the Michael Addition of phosphines to α,β-unsaturated carbonyls has been explored in the synthesis of industrial chemicals,[20] ligands,[21] ionic liquids,[22] and biomolecular crosslinkers.[23] W.J. Vullo reported that THP also undergoes Michael Addition reactions with acrylic acid, acrylamide, acrylonitrile, and ethylene oxide.[20] Using this reaction, we have implemented a new synthetic procedure for P_2N_2 ligands containing β-ethyl ester or amide substituents at the phosphorus centers using THP under relatively mild conditions, obviating the need for volatile primary phosphine reagents (Scheme 3.2).

3.4 Synthesis of P_2N_2 ligands via Michael Addition

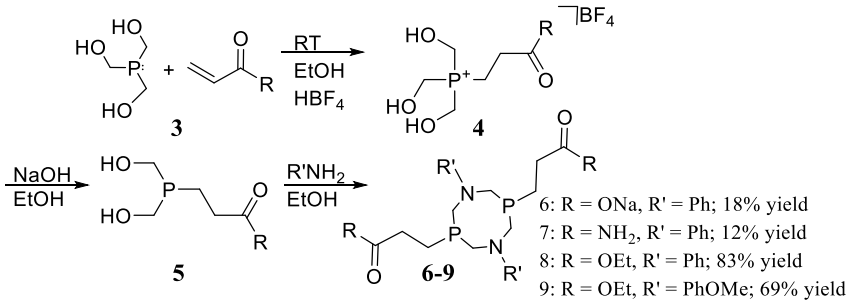

Scheme 3.2 $P^R_2N^{R'}_2$ synthesis via Michael Addition of THP.

THP has been demonstrated previously as a suitable nucleophile for Michael Additions with ethylene oxide, acrylonitrile, acrylamide, and acrylic acid.[24] We expanded on these known reactions, using acrylic acid, acrylamide, and ethyl acrylate to synthesize four new P_2N_2 ligands with carbonyl-functionalized phosphine substituents. In the initial step of the general synthetic procedure, THP is added to the α,β-unsaturated carbonyl with at least 1.5 equivalent of tetrafluoroboric acid (HBF_4, 48% aq. Solution), to form a phosphonium tetrafluoroborate salt (**4**). This salt can be subsequently dehydroxymethylated with a base after neutralization of the solution to form the

carbonyl-substituted bis(hydroxymethyl)phosphine (**5**). The addition of 1 equivalent of a primary amine (e.g. aniline) yields the corresponding $P^{R}{}_{2}N^{R'}{}_{2}$ heterocycle.

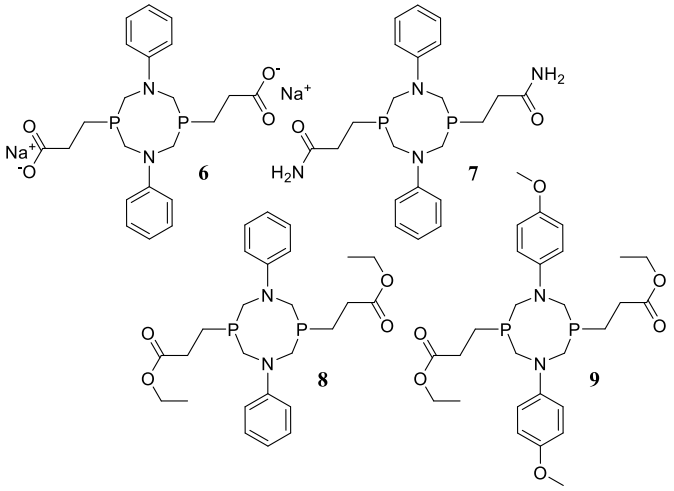

Figure 3.2 Newly synthesized P_2N_2 ligands with sodium 3-propanoate (6), 3-propanamide (7), and ethyl 3-propanoate (8, 9) phosphine substituents.

3.5 Nickel complexes of P_2N_2 ligands with carbonyl phosphine substituents

The corresponding nickel complexes of ligands **6**, **7**, **8**, and **9** were isolated and characterized by X-ray crystallography, elemental analysis, ^{1}H NMR and ^{31}P{^{1}H} NMR. The propionate- and propanamide- ligands $P^{PA}{}_{2}N^{Ph}{}_{2}$ (**6**) and $P^{Amide}{}_{2}N^{Ph}{}_{2}$ (**7**) were isolated and purified by rinsing with ethanol and acetonitrile following the primary amine addition step to close the macrocycle, *vide supra*. Metallation of these ligands with nickel was done according to well-established previous protocols;[25] however, instead of the expected bis-diphosphine complex (scheme 3.3a), tetradentate mono-P_2N_2 nickel(II) complexes, as shown in scheme 3.3b, were isolated. Crystals of complexes **10** and **11** suitable for X-ray diffraction studies were grown, and the molecular structures were consistent with all other characterization data (Figure 3.3). The binding modes displayed

here are highly unusual with few precedents in the chemical literature.[26,27] Bidentate P-O phosphine-amide carbonyl binding has previously been observed in an X-ray structure of a palladium complex.[28] Carboxylates have been observed binding to nickel, including T. Tada's report of an organometallic nickel carboxylate species formed from acrylic acid reacting with a nickel phosphine complex.[29] G.L. Hillhouse and E. Wenger have also reported nickel diphosphine dicarboxylate structures synthesized by CO_2 reactions with nickel-carbene[30] and nickel-benzyne[31] complexes, respectively.

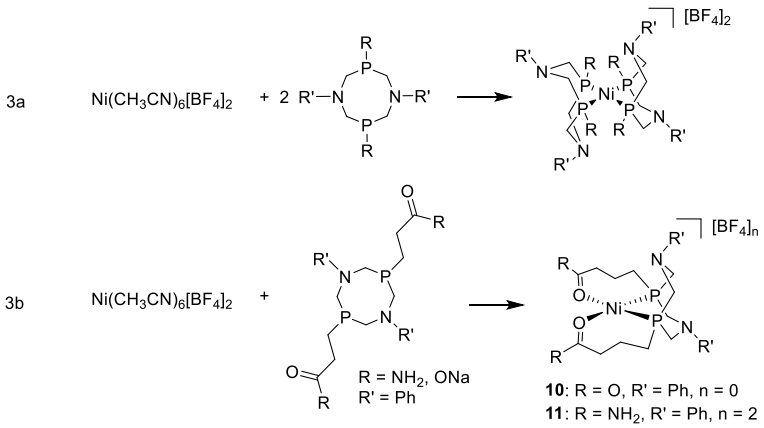

Scheme 3.3 Ligation of $P^{R}_{2}N^{R'}_{2}$ ligands to nickel.

X-ray crystallography of **10** reveals a tetradentate binding mode of the dianionic ligand **6** in a nearly square planar geometry around Ni, with an average deviation from the least-squares plane of 0.049 Å. The P-Ni-P bond angle is 83.06°, and the O-Ni-P bond angles are 94.73° and 94.41°. The crystal structure of **11** incorporates two complexes in the asymmetric unit (Z' = 2). The deviation of these nickel centers from square planar was almost identical, with dihedral angles of 6.25° and 6.18° and an average distance from the least-squares plane of 0.042 Å. Other key parameters are

reported in Table 3.1. To our knowledge, these are the first reports of a tetradentate dicarbonyl diphosphine ligand on any metal.

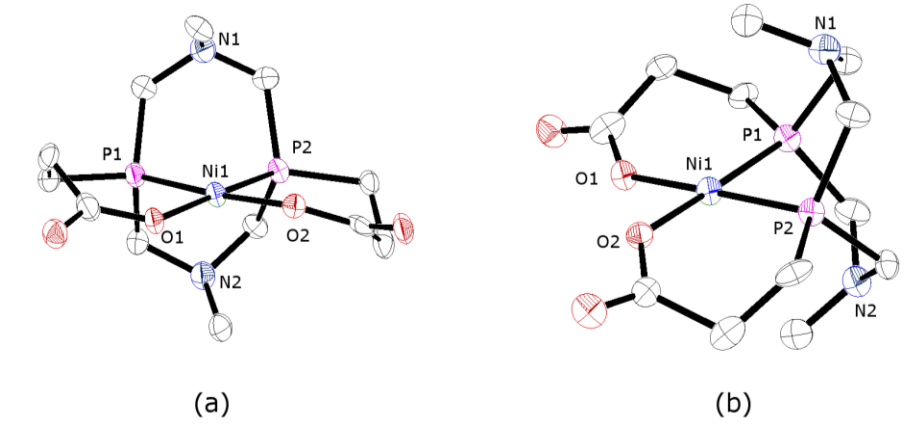

Figure 3.3 Molecular diagrams for complex 10, Ni($P^{PA}_2N^{Ph}_2$). Thermal ellipsoids are shown at the 50% probability level. Hydrogens and phenyl- amine substituents have been removed from this diagram for clarity. A and B show different orientations to clearly demonstrate the molecular geometry.

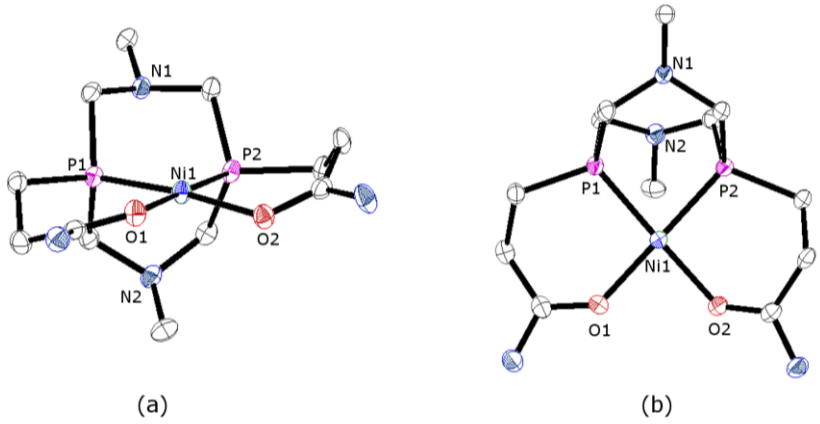

Figure 3.4 Molecular diagrams for complex 11, [Ni($P^{Amide}_2N^{Ph}_2$)](BF_4)$_2$. Thermal ellipsoids are shown at the 50% probability level. Counterions, hydrogens, solvent molecules, and phenyl- amine substituents have been removed from this diagram for clarity. A and B show different orientations to clearly demonstrate the molecular geometry.

The ethyl ester ligands **8** and **9** were ligated to nickel(II) chloride ($NiCl_2$) by combining the crude ligand product with 1 equivalent anhydrous $NiCl_2$ in acetonitrile, after which the pure nickel(II) mono-P_2N_2 chloride salt was isolated in the supernatant upon filtration. Single crystals of $Ni(P^{EtE}{}_2N^{Ph}{}_2)Cl_2$ (**12**) and $Ni(P^{EtE}{}_2N^{PhOMe}{}_2)Cl_2$ (**13**) suitable for X-ray diffraction studies were grown by vapor diffusion of ethyl ether into acetonitrile. The structures of **12** and **13** have similar geometric parameters. Both structures show a slightly distorted square planar geometry, **12** displaying an average variation from the least-squares plane of 0.134 Å and **13** a variation of 0.048 Å. The crystal structure of **13** includes two complexes in the asymmetric unit ($Z' = 2$), with varying dihedral angles of 1.54° and 7.39° in the geometry of the primary coordination sphere. Similar $NiCl_2$diphosphine complexes have been observed, including $Ni(dppe)Cl_2$[32] and a related chiral diphosphine complex.[33] These complexes require two related steps to form the well-studied nickel(II) bis-P_2N_2 complex: the exchange of the chloride anions for non-coordinating anions, and the disproportionation of the mono-P_2N_2 complexes to the bis-P_2N_2 complexes. Unfortunately, conventional anion exchange techniques, such as metathesis reactions with sodium, potassium, thallium(I), and silver(I) salts of non-coordinating anions lead to complex degradation.

Table 3.1 Selected Bond Lengths(Å), Bond Angles (°), and Dihedral angles (°) of $Ni(P_2N_2)X_2$ Complexes.

Length/Angle	**10**	**11**	**12**	**13**
Ni(1)-P(1)	2.127(2)	2.1026(8)	2.1443(11)	2.1752(16)
Ni(1)-P(2)	2.127(2)	2.1199(8)	2.1731(11)	2.1426(16)
Ni(1)-O(1)	1.911(6)	1.9214(18)	2.2178(10)	2.1919(16)
Ni(1)-O(2)	1.912(6)	1.9234(17)	2.2064(11)	2.2250(15)
P(1)-Ni(1)-P(2)	83.06(8)	83.13(3)	84.21(4)	83.07(6)
O(1)-Ni(1)-P(1)	94.73(19)	95.52(6)	92.26(4)	93.36(6)
O(2)-Ni(1)-P(2)	94.41(19)	95.45(6)	91.20(4)	91.27(6)
Dihedral	4.27	6.25	10.27	1.54
Ni(1')-P(1')		2.1136(8)		2.1334(16)
Ni(1')-P(2')		2.1041(7)		2.1692(16)
Ni(1')-O(1')		1.9350(17)		2.2120(16)
Ni(1')-O(2')		1.9038(17)		2.2070(15)
P(2')-Ni(1')-P(1')		83.53(3)		83.25(6)
O(1')-Ni(1')-P(1')		94.91(6)		90.70(6)
O(2')-Ni(1')-P(2')		96.16(6)		93.69(6)
Dihedral’		6.18		7.39

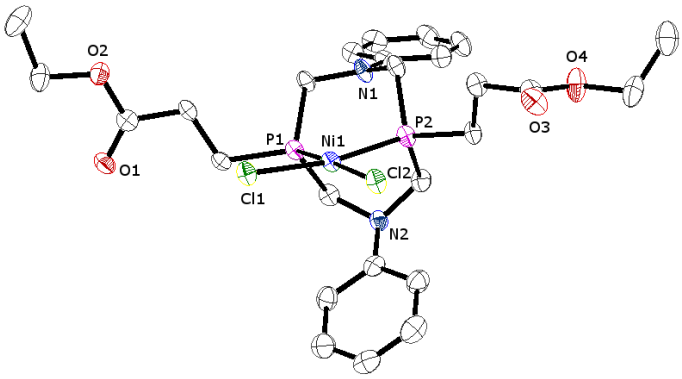

Figure 3.5 Molecular structure of complex 12, Ni($P^{EtE}_2N^{Ph}_2$)Cl_2, as determined by X-ray diffraction studies. Thermal ellipsoids are shown at the 50% probability level. Hydrogens have been removed from this diagram for clarity.

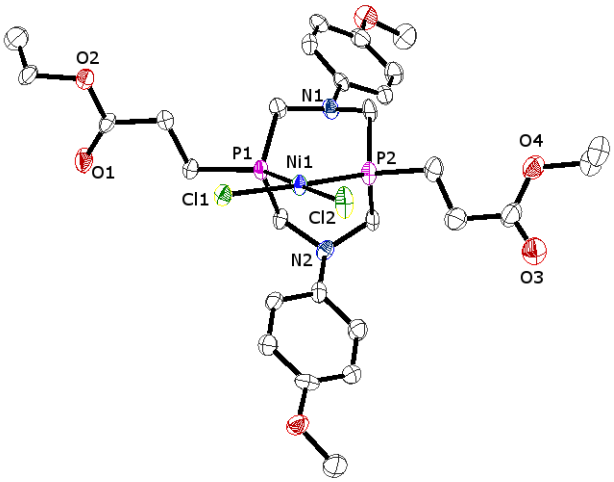

Figure 3.6 Molecular structure of complex 13, Ni($P^{EtE}_2N^{PhOMe}_2$)Cl_2, as determined by X-ray diffraction studies. Thermal ellipsoids are shown at the 50% probability level. Hydrogens have been removed from this diagram for clarity.

3.6 Experimental Details

3.6.1 General Considerations

Unless otherwise noted, all reactions and manipulations were performed under a N_2 atmosphere using standard glovebox or Schlenk line techniques. Glassware was dried in an oven (120°C) overnight prior to use. Acetonitrile and tetrahydrofuran (THF) were purified via passage through alumina and molecular sieves. Ethanol was dried over 4 Å

molecular sieves. Aniline and triethylamine were distilled from CaH_2. Tris(hydroxymethyl)phosphine (THP) was used as obtained from Acros Organics. All other chemicals were used as obtained from commercial suppliers. ^1H and $^{31}P\{^1H\}$ NMR spectra were obtained on a 300 MHz Varian or a 500 MHz Jeol spectrometer. ^1H and $^{31}P\{^1H\}$ NMR spectral data are referenced against the residual solvent signal and are reported in ppm downfield of tetramethylsilane and 85% phosphoric acid, respectively (δ = 0). Elemental analyses were performed by NuMega Labs in San Diego, CA. Mass spectrometry was performed at the UCSD Molecular Mass Spectrometry Facilty.

3.6.2 Synthesis of $P^{PA}_2N^{PH}_2$ (6)

An oven-dried 100 mL Schlenk flask with a stir bar was charged with tetrakis(hydroxymethyl)phosphonium chloride (6.18 g, 32.4 mmol; THPC) and ethanol (10 mL). While stirring under N_2 atmosphere, approximately 1 equiv NaOH (1.31 g, 32.8 mmol) was added to the mixture and stirred overnight. During this time a white precipitate (NaCl) formed. The supernatant was filtered via cannula into an oven-dried 50 mL Schlenk flask under N_2 atmosphere. While stirring on ice, acrylic acid (2.2 mL, 32 mmol) dissolved in ethanol (10 mL) was slowly added via cannula. Within five minutes, a white precipitate formed, the zwitterionic 3-(tris(hydroxymethyl)phosphino) propanoate (THPP) . The THPP product was again filtered via cannula to remove the supernatant and dried, yielding THPP (6.08 g, 95.7% yield). Methanol (20 mL) was added to the isolated THPP, and the flask was sonicated to suspend and partially dissolve the white precipitate. To this suspension, NaOH (1.29 g, 32.3 mmol) was added and the reaction stirred overnight under N_2 atmosphere. Reaction progress was monitored by $^{31}P\{^1H\}$ NMR to

observe the growth of a peak at -21.25 ppm corresponding to the bis(hydroxymethyl)phosphine species. Upon completion, the supernatant was filtered via cannula into a 50 mL Schlenk flask. Aniline (2.6 mL, 29 mmol) was added via syringe, and the reaction mixture was refluxed at 64°C for 2 days, after which a white precipitate was observed. The resulting suspension was cooled to room temperature and the supernatant removed via cannula filtration. After vacuum drying, (analytically pure 3,7-di(3,3'-propanoate(Na^+))-1,5-diphenyl-1,5-diaza-3,7-diphosphacyclooctane ($P^{PA(Na)}{}_2N^{Ph}{}_2$; 1.41 g, 2.8 mmol) was isolated (17.7% yield). ^{1}H NMR (300 MHz, D_2O): δ = 7.08 (t, *J* = 7.5 Hz, Ar*H*, 8H), 6.66 (d, *J* = 8.3 Hz, Ar*H*, 8H), 6.52 (t, *J* = 6.9 Hz, Ar*H*, 4H), 3.28 (d, *J* = 10.3 Hz, PC*H*$_2$N, 8H), 3.68 (dt, *J* = 14.0 Hz, *J* =12.3 Hz, PC*H*$_2$CH$_2$, 8H), 0.90 (t, *J* = 10.0 Hz, C*H*$_2$COONa, 8H). ^{31}P{^{1}H}(D_2O): δ = -51.90 ppm (s). Calculated M/z for $[C_{22}H_{27}N_4O_2P_2]^-$: 445.1452; Found: 445.1451.

3.6.3 Synthesis of $P^{Amide}{}_2N^{Ph}{}_2$ (7)

An oven-dried 100 mL Schlenk flask with stir bar was charged with THP (0.868 g; 7.00 mmol) in a glovebox under N_2 atmosphere. The white solid was dissolved in ethanol (20 mL) and stirred at room temperature (22°C). To this solution, HBF_4 (0.91 mL 48 wt% in H_2O, 7.0 mmol) was added via syringe. After 20 minutes, 0.50 g (7.0 mmol) acrylamide was dissolved in ethanol (5 mL) and transferred via cannula into the reaction mixture. This mixture was allowed to stir for 5 hours, and monitored via ^{31}P{^{1}H} NMR to observe the growth of a peak at 31.28 ppm. Upon completion of the reaction, volatiles were removed by vacuum drying, yielding a pale yellow oil. The oil was dissolved in ethanol (15 mL), to which NaOH (0.287 g, 7.18 mmol) dissolved in ethanol (25 mL) was

added. A white precipitate ($NaBF_4$) immediately formed. After stirring the reaction for 1 hour, the contents were filtered via cannula into another oven-dried 100 mL Schlenk flask, followed by two rinses of ethanol (5 mL). To this stirring mixture, aniline (0.53 mL, 5.8 mmol) was added via syringe. A white precipitate formed after stirring for 5 days. This precipitate was rinsed sequentially with acetonitrile and water. Upon vacuum drying, this precipitate was characterized as 3,7-di(3,3'-propanamide)-1,5-diphenyl-1,5-diaza-3,7-diphosphacyclooctane ($P^{Amide}{}_2N^{Ph}{}_2$) was isolated. (0.36 g, 0.43 mmol; 12% yield) ^{1}H NMR (500MHz, DMSO): δ = 7.43 (br, N*H*$_2$, 2H), 7.09 (t, *J* = 8.0 Hz, Ar*H*, 4H), 6.91 (br, N*H*$_2$, 2H), 6.61 (d, *J* = 8.2 Hz, Ar*H*, 4H), 6.52 (t, *J* = 7.2 Hz, Ar*H*, 2H), 4.08 (t, *J* = 13.8 Hz, C*H*$_2$CONH$_2$, 4H), 3.38 (d, *J* = 7.0 Hz, PC*H*$_2$N, 8H), 3.82 (dd, *J* = 15.0 Hz, *J* = 5.8 Hz, PC*H*$_2$C, 4H). ^{31}P{^{1}H}: δ = -52.01 ppm. Calculated M/z for $[C_{22}H_{30}N_4O_2P_2Na]^+$: 467.1736; Found: 467.1738.

3.6.4 Synthesis of Ni($P^{PA}{}_2N^{PH}{}_2$) (10)

In an oven-dried 10 mL Schlenk flask, **6** (88 mg, 0.18 mmol) was combined with $Ni(CH_3CN)_6[BF_4]_2$ (67 mg, 0.14 mmol) in acetonitrile (3 mL). To this cloudy mixture, deoxygenated water (3 mL) was added. Upon stirring overnight, the suspension clarified into a yellow solution. Volatiles were removed by evacuation. Yellow, rhomboid crystals suitable for X-ray diffraction were grown by vapor diffusion of acetone into acetonitrile:water (1:1). ^{31}P{^{1}H} (CD_3CN:D_2O) δ = +20.39 ppm. ^{1}H NMR (500MHz, CD_3CN:D_2O): δ = 7.20 (t, *J* = 7.9 Hz, Ar*H*, 4H), 7.04 (d, *J* = 8.2 Hz, Ar*H*, 4H), 6.78 (t, *J* = 7.2 Hz, Ar*H*, 2H), 3.33 (d, *J* = 7.0 Hz, PC*H*$_2$N, 8H), 2.46 (br, PC*H*$_2$CH$_2$, 4H), 1.04 (t, *J*

= 7.0 Hz, C*H*$_2$COONa, 4H). Calculated M/z for $[C_{22}H_{27}N_2O_4P_2Ni]^+$: 503.0800; Found: 503.0797.

3.6.5 Synthesis of Ni($P^{Amide}_2N^{Ph}_2$)[BF_4]$_2$ (11)

In an oven-dried 10 mL Schlenk flask with a stir bar, Ni(CH_3CN)$_6$[BF_4]$_2$ (42 mg, 0.088 mmol) was combined with **7** (46 mg, 0.10 mmol) in acetonitrile (5 mL). Upon stirring, the solution turned light red with slight precipitation. After stirring overnight, the solution was filtered and dried to yield **11** (63 mg, 0.094 mmol), a yellow-orange powder (99.5% yield). Yellow, rod-like crystals suitable for X-ray diffraction were grown by vapor diffusion of diethyl ether into acetonitrile. ^{1}H NMR (500MHz, DMSO): δ = 7.47 (br, N*H*$_2$, 2H), 7.44 (t, *J* = 7.9 Hz, Ar*H*, 4H), 7.16 (d, *J* = 8.3 Hz, Ar*H*, 4H), 7.09 (t, *J* = 7.3 Hz, Ar*H*, 2H), 6.96 (br, N*H*$_2$, 2H), 4.12 (d, *J* = 14.5 Hz, PC*H*$_2$N, 8H), 3.71 (dt, *J* = 14.3 Hz, *J* = 4.9 Hz, PC*H*$_2$C, 4H), 2.13 (t, *J* = 13.9 Hz, C*H*$_2$CO, 4H). ^{31}P{^{1}H} (CD_3CN): δ = 19.76 ppm. Calculated M/z for $[C_{22}H_{29}P_2N_4O_2Ni]^+$: 501.1114; Found: 501.1115.

3.6.6 Synthesis of $P^{EtE}_2N^{Ph}_2$ (5)

An oven-dried 100 mL Schlenk flask with a stir bar was charged with THP (0.63 g, 5.1 mmol) in a glovebox under N_2 atmosphere. The white solid was dissolved in ethanol (20 mL) and stirred at room temperature (22°C). To this solution, HBF_4 (48 wt% in H_2O, 1.0 mL, 7.7 mmol) was added via syringe. After 20 minutes, ethyl acrylate (0.54 mL, 5.1 mmol) was added via syringe. This mixture was allowed to stir overnight, and monitored via ^{31}P{^{1}H} NMR to observe the growth of a peak at 31.28 ppm. Upon completion of the reaction, volatiles were removed by vacuum drying, yielding clear oil.

This was dissolved in ethanol (10 mL), to which NaOH (0.39 g, 9.8 mmol) dissolved in ethanol (15 mL) was added. A white precipitate ($NaBF_4$) immediately formed. After stirring the reaction for 1 hour, the supernatant was filtered via cannula into another oven-dried 50 mL Schlenk flask, followed by two rinses of ethanol (5 mL). To this stirring mixture, aniline (0.42 mL, 4.6 mmol) was added via syringe. This mixture was stirred at room temperature (22°C) for 2 days, until voluminous white precipitate was observed. The supernatant was removed via cannula and the precipitate dried via vacuum to yield a white powder, 3,7-di(3,3'-ethylpropanoyl)-1,5-diphenyl-1,5-diaza-3,7-diphosphacyclooctane ($P^{EtE}{}_2N^{Ph}{}_2$, 1.06 g, 2.11 mmol). (83.4% yield). ^1H NMR: δ = $^{31}P\{^1H\}$ (CD_3CN): δ = -54.78 ppm. Calculated M/z for $[C_{26}\,H_{37}\,N_2\,O_4\,P_2]^+$: 503.2223; Found: 503.2226.

3.6.7 Synthesis of $P^{EtE}{}_2N^{PhOMe}{}_2$ (6)

An oven-dried 25 mL Schlenk flask with a stir bar was charged with THP (0. 354 g, 2.86 mmol) in a glovebox under N_2 atmosphere. The white solid was dissolved in ethanol (10 mL) and stirred at room temperature (22°C). To this solution, HBF_4 (48 wt% in H_2O, 0.57 mL, 4.3 mmol) was added via syringe. After 5 minutes, ethyl acrylate (0.31 mL, 2.9 mmol) was added via syringe. This mixture was allowed to stir for 2 hours at room temperature, and monitored via $^{31}P\{^1H\}$ NMR to observe the growth of a peak at 31.28 ppm. Upon completion of the reaction, volatiles were removed by vacuum drying, yielding a clear oil. This was dissolved in ethanol (5 mL), to which NaOH (0.183 g, 4.59 mmol) dissolved in ethanol (10 mL) was added. A white precipitate ($NaBF_4$) immediately formed. After stirring the reaction for 2 hours at room temperature, the

supernatant was filtered via cannula into another oven-dried 25 mL Schlenk flask containing anisidine (0.326 g, 2.65 mmol). White solid precipitated after five minutes. The reaction was stirred overnight at room temperature (22°C). The supernatant was removed via cannula, and the precipitate was dried via vacuum to yield **6**, a white powder 3,7-di(3,3'-ethylpropanoyl)-1,5-di(4-methoxyphenyl)-1,5-diaza-3,7-diphosphacyclooctane ($P^{EtE}_2N^{PhOMe}_2$, 0.55 g, 0.98 mmol). (69% yield) ^{1}H NMR: δ = ^{31}P{^{1}H} (CD_3CN): δ = -55.40 ppm. Calculated M/z for $[C_{28}H_{41}N_2O_6P_2]^+$: 563.2434; Found: 563.2438.

3.6.8 Preparation of Ni($P^{EtE}_2N^{PH}_2$)Cl_2 (12)

In an oven-dried 20 mL scintillation vial with a stir bar, **5** (54 mg, 0.11 mmol) was combined with approximately 1 equiv anhydrous $NiCl_2$ (13 mg, 0.099 mmol). Upon addition of acetonitrile (5 mL), mixture was stirred at room temperature and over the course of 10 minutes became dark red. The solution was stirred overnight, then filtered and vacuum dried. The resulting residue was rinsed three times with water (10 mL) to remove excess $NiCl_2$. After vacuum drying, **12** (56 mg, 0.089 mmol) was isolated (90.6% yield). Crystals suitable for X-ray diffraction were grown from vapor diffusion of diethyl ether into acetonitrile. ^{1}H NMR (CD_3CN): δ = 7.13 (d, *J* = 8.9 Hz, Ar*H*, 4H), 6.94 (t, *J* = 9.1 Hz, Ar*H*, 4H), 6.80 (d, *J* = 8.6 Hz, Ar*H*, 2H), 4.08 (q, *J* = 7.1 Hz, -OC*H*$_2$CH$_3$, 4H), 3.91 (d, *J* = 14, P-C*H*$_2$-N, 8H), 3.76 (dt, *J* = 7.2 Hz, *J* = 3.09 Hz, PC*H*$_2$CH$_2$, 4H), 1.92 (t, *J* = 2.4 Hz, -C*H*$_2$COO-, 4H), 1.21 (t, *J* = 7.1 Hz, COOCH$_2$C*H*$_3$, 6H). ^{31}P{^{1}H} (CD_3CN): δ = +3.54 ppm. Calculated M/z for $[C_{26}H_{36}ClP_2N_2O_4Ni]^+$: 595.1187; Found: 595.1193.

3.6.9 Preparation of $Ni(P^{EtE}_2N^{PhOME}_2)Cl_2$ (13)

In an oven-dried 20 mL scintillation vial with a stir bar, **6** (104 mg, 0.19 mmol) was combined with approximately 1 equiv anhydrous $NiCl_2$ (20 mg, 0.15 mmol). Upon addition of acetonitrile (5 mL), mixture was stirred at room temperature and over the course of 10 minutes became brown-red. The solution was stirred overnight, then filtered and vacuum dried. This residue was rinsed three times with water (10 mL) to remove excess $NiCl_2$. After vacuum drying, **13** (0.11 g, 0.16 mmol) was isolated (91% yield). Crystals suitable for X-ray diffraction were grown from vapor diffusion of diethyl ether into acetonitrile. $^{31}P\{^1H\}$ (CD_3CN): δ = +1.35 ppm. ^1H NMR: δ = 7.16 (t, *J* = 6.5 Hz, Ar*H*, 4H), 7.00 (d, *J* = 8.8 Hz, Ar*H*, 4H), 6. 84 (t, *J* = 8.4 Hz, Ar*H*, 2H), 4.15 (q, *J* = 7.0 Hz, -OC$H_2$$CH_3$, 4H), 3.96 (d, *J* = 14, P-CH_2-N, 8H), 3.77 (dt, *J* = 21 Hz, *J* = 5.5 Hz, PC$H_2$$CH_2$, 4H), 2.66 (s, ArC$H_3$, 6H), 1.97 (t, *J* = 2.3 Hz, -CH_2COO-, 4H), 1.25 (t, *J* = 5.7 Hz, $COOCH_2C$$H_3$, 6H). Calculated M/z for $[C_{26}H_{36}ClP_2N_2O_4Ni]^+$: 655.1398; Found: 655.1409. Anal. Calcd for $C_{28}H_{40}Cl_2N_2NiO_6P_2(H_2O)_2(CH_3CN)_{0.5}$: C, 46.58; H, 6.12; N, 4.68. Found: C, 46.43; H, 5.95; N, 4.83

3.7 Conclusion

We have demonstrated a new synthetic route for the production of P_2N_2-type ligands that installs β-ethyl ester or amide groups as the phosphorus substituent. Nickel complexes of the new $P^R_2N^{R'}_2$ ligands have been synthesized and characterized. This new synthetic route accesses a variety of new functional carbonyl substituents on the phosphine of P_2N_2 ligands that were not previously isolated. We are using this control to impart further functionality on the ligand and its complexes, e.g. incorporating electron

reservoirs for multi-electron catalysis[34] and forming cooperative multimetallic catalyst complexes.[35] A prime focus is the covalent attachment of these molecular catalysts to electrode surfaces, or heterogenization. Previous studies have successfully attached $Ni(P^{R}_{2}N^{R'}_{2})_{2}^{2+}$ catalysts to electrodes, but the conventional synthesis limited covalent attachment through the amine substituent.[36,37] Attaching the amine to a surface could limit the flexibility of the pendant base, which has been shown to be critical to the electrocatalytic activity of the P_2N_2 complexes.[38] By combining this synthesis with electrode surface modification techniques, the freedom of the pendant base should be preserved, while the phosphine substituent offers a direct route between the electrode and the catalytic site.

The majority of the material for this chapter comes directly from a manuscript entitled “Synthesis of P_2N_2 Ligands via Michael Addition" by Michael D. Doud, Curtis E. Moore, Arnold L. Rheingold, and Clifford P. Kubiak, to be submitted to *Organometallics*. The dissertation author is the primary author of this manuscript.

3.8 References

(1) Chu, S.; Majumdar, A. *Nature* **2012**, *488*, 294.

(2) Anderson, J. S.; Rittle, J.; Peters, J. C. *Nature* **2013**, *501*, 84.

(3) Keene, F. R. In *Electrochemical and Electrocatalytic Reactions of Carbon Dioxide*; Sullivan, B. P., Ed.; Elsevier: Amsterdam, 1993, p 1.

(4) Benson, E. E.; Kubiak, C. P.; Sathrum, A. J.; Smieja, J. M. *Chemical Society Reviews* **2009**, *38*, 89.

(5) Solis, B. H.; Hammes-Schiffer, S. *Inorganic Chemistry* **2014**, *53*, 6427.

(6) Bediako, D. K.; Solis, B. H.; Dogutan, D. K.; Roubelakis, M. M.; Maher, A. G.; Lee, C. H.; Chambers, M. B.; Hammes-Schiffer, S.; Nocera, D. G. *Proceedings of the National Academy of Sciences* **2014**, *111*, 15001.

(7) Weinberg, D. R.; Gagliardi, C. J.; Hull, J. F.; Murphy, C. F.; Kent, C. A.; Westlake, B. C.; Paul, A.; Ess, D. H.; McCafferty, D. G.; Meyer, T. J. *Chemical Reviews* **2012**, *112*, 4016.

(8) Nicolet, Y.; de Lacey, A. L.; Vernede, X.; Fernandez, V. M.; Hatchikian, E. C.; Fontecilla-Camps, J. C. *Journal of the American Chemical Society* **2001**, *123*, 1596.

(9) Cornish, A. J.; Gärtner, K.; Yang, H.; Peters, J. W.; Hegg, E. L. *Journal of Biological Chemistry* **2011**, *286*, 38341.

(10) Bachmeier, A.; Armstrong, F. *Current Opinion in Chemical Biology* **2015**, *25*, 141.

(11) Burello, E.; Rothenberg, G. *International Journal of Molecular Sciences* **2006**, *7*, 375.

(12) Schunk, S. A.; Bohmer, N.; Futter, C.; Kuschel, A.; Prasetyo, E.; Roussiere, T. In *Catalysis: Volume 25*; The Royal Society of Chemistry: 2013; Vol. 25, p 172.

(13) DuBois, D. L.; Bullock, R. M. *European Journal of Inorganic Chemistry* **2011**, *2011*, 1017.

(14) Curtis, C. J.; Miedaner, A.; Ellis, W. W.; DuBois, D. L. *Journal of the American Chemical Society* **2002**, *124*, 1918.

(15) Curtis, C. J.; Miedaner, A.; Ciancanelli, R.; Ellis, W. W.; Noll, B. C.; DuBois, M. R.; DuBois, D. L. *Inorganic Chemistry* **2003**, *42*, 216.

(16) Wilson, A. D.; Newell, R. H.; McNevin, M. J.; Muckerman, J. T.; DuBois, M. R.; DuBois, D. L. *Journal of the American Chemical Society* **2006**, *128*, 358.

(17) Markl, G.; Jin, G. Y.; Schoerner, C. *Tetrahedron Letters* **1980**, *21*, 1409.

(18) Van Hooijdonk, M. C. J. M.; Gerritsen, G.; Brandsma, L. *Phosphorus Sulfur and Silicon and the Related Elements* **2000**, *162*, 39.

(19) Doud, M. D.; Grice, K. A.; Lilio, A. M.; Seu, C. S.; Kubiak, C. P. *Organometallics* **2012**, *31*, 779.

(20) Vullo, W. J. *Industrial & Engineering Chemistry Product Research and Development* **1966**, *5*, 346.

(21) Babahan, I.; Engle, J. T.; Kumar, N.; Ziegler, C. J.; Jia, L. *Polyhedron* **2014**, *69*, 156.

(22) Ma, K.; Lee, K.-M.; Minkova, L.; Weiss, R. G. *The Journal of Organic Chemistry* **2009**, *74*, 2088.

(23) Lim, D. W.; Nettles, D. L.; Setton, L. A.; Chilkoti, A. *Biomacromolecules* **2007**, *8*, 1463.

(24) Enders, D.; Saint-Dizier, A.; Lannou, M.-I.; Lenzen, A. *European Journal of Organic Chemistry* **2006**, *2006*, 29.

(25) Wilson, A. D.; Shoemaker, R. K.; Miedaner, A.; Muckerman, J. T.; DuBois, D. L.; DuBois, M. R. *Proceedings of the National Academy of Sciences of the United States of America* **2007**, *104*, 6951.

(26) Marinho, V. R. D.; Ramalho, J. P. P.; Rodrigues, A. I.; Burke, A. J. *Chirality* **2011**, *23*, 383.

(27) Sánchez, G.; García, J.; Liu, M.; García, L.; Pérez, J.; Pérez, E.; Serrano, J. L. *Journal of Coordination Chemistry* **2013**, *66*, 2919.

(28) Amatore, C.; Jutand, A.; Mensah, L.; Ricard, L. *Journal of Organometallic Chemistry* **2007**, *692*, 1457.

(29) Yamamoto, T.; Sano, K.; Osakada, K.; Komiya, S.; Yamamoto, A.; Kushi, Y.; Tada, T. *Organometallics* **1990**, *9*, 2396.

(30) Mindiola, D. J.; Hillhouse, G. L. *Journal of the American Chemical Society* **2002**, *124*, 9976.

(31) Bennett, M. A.; Hockless, D. C. R.; Humphrey, M. G.; Schultz, M.; Wenger, E. *Organometallics* **1996**, *15*, 928.

(32) C. Davies, S.; A. Henderson, R.; L. Hughes, D.; E. Oglieve, K. *Journal of the Chemical Society, Dalton Transactions* **1998**, 425.

(33) Dahlenburg, L.; Kurth, V. *European Journal of Inorganic Chemistry* **1998**, *1998*, 597.

(34) Dzik, W. I.; van der Vlugt, J. I.; Reek, J. N. H.; de Bruin, B. *Angewandte Chemie International Edition* **2011**, *50*, 3356.

(35) Haak, R. M.; Wezenberg, S. J.; Kleij, A. W. *Chemical Communications* **2010**, *46*, 2713.

(36) Das, A. K.; Engelhard, M. H.; Bullock, R. M.; Roberts, J. A. S. *Inorganic Chemistry* **2014**, *53*, 6875.

(37) Le Goff, A.; Artero, V.; Jousselme, B.; Tran, P. D.; Guillet, N.; Metaye, R.; Fihri, A.; Palacin, S.; Fontecave, M. *Science* **2009**, *326*, 1384.

(38) Galan, B. R.; Schoffel, J.; Linehan, J. C.; Seu, C.; Appel, A. M.; Roberts, J. A. S.; Helm, M. L.; Kilgore, U. J.; Yang, J. Y.; DuBois, D. L.; Kubiak, C. P. *Journal of the American Chemical Society* **2011**, *133*, 12767.

3.8 Appendix

3.8.1. Crystallographic details for 10, Ni($P^{PA}_2N^{PH}_2$).

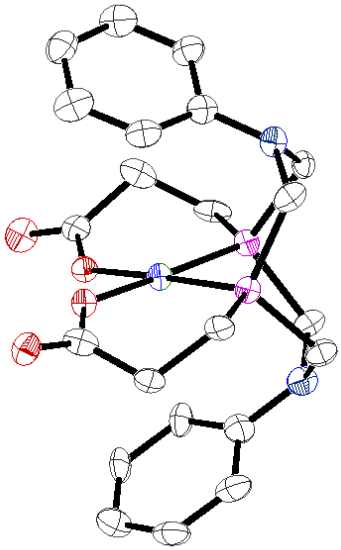

Figure 3.7 Molecular diagram for complex 10, Ni($P^{PA}_2N^{Ph}_2$). Thermal ellipsoids are shown at the 50% probability level. Hydrogens have been removed from this diagram for clarity.

Table 3.2 Crystal data and structure refinement for 10, Ni($P^{PA}_2N^{Ph}_2$).

Report date	2015-08-07	
Empirical formula	C22 H26 N2 Ni O4 P2	
Molecular formula	C22 H26 N2 Ni O4 P2	
Formula weight	503.10	
Temperature	100.0 K	
Wavelength	0.71073 Å	
Crystal system	Orthorhombic	
Space group	$Pna2_1$	
Unit cell dimensions	a = 15.8888(11) Å	□= 90°.
	b = 6.9188(5) Å	□= 90°.
	c = 18.4161(14) Å	□ = 90°.
Volume	2024.5(3) $Å^3$	
Z	4	
Density (calculated)	1.651 Mg/m^3	
Absorption coefficient	1.152 mm^{-1}	
F(000)	1048	
Crystal size	0.211 x 0.203 x 0.102 mm^3	
Crystal color, habit	Yellow Plate	
Theta range for data collection	2.212 to 25.387°.	
Index ranges	-19<=h<=19, -8<=k<=8, -22<=l<=22	
Reflections collected	23567	
Independent reflections	3723 [R(int) = 0.0639]	
Completeness to theta = 25.000°	99.9 %	
Absorption correction	Semi-empirical from equivalents	
Max. and min. transmission	0.0265 and 0.0094	
Refinement method	Full-matrix least-squares on F^2	
Data / restraints / parameters	3723 / 11 / 297	
Goodness-of-fit on F^2	1.094	
Final R indices [I>2sigma(I)]	R1 = 0.0518, wR2 = 0.1395	
R indices (all data)	R1 = 0.0561, wR2 = 0.1424	
Absolute structure parameter	0.20(4)	
Extinction coefficient	n/a	
Largest diff. peak and hole	0.954 and -0.483 $e.Å^{-3}$	

3.8.2 Crystallographic details for 11, [Ni(PAmide2NPh2)](BF4)2.

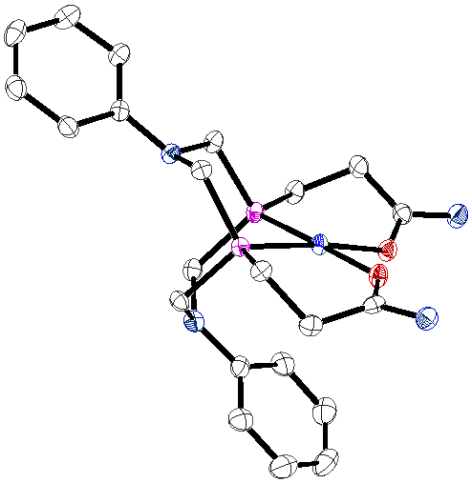

Figure 3.8 Molecular diagram for complex 11, [Ni($P^{Amide}_2N^{Ph}_2$)](BF_4)$_2$. Thermal ellipsoids are shown at the 50% probability level. Counterions, hydrogens, solvent molecules, and have been removed from this diagram for clarity.

Table 3.3 Crystal data and structure refinement for 11, $[Ni(P^{Amide}_2N^{Ph}_2)](BF_4)_2$.

Report date	2015-08-07	
Identification code	MDD20150731	
Empirical formula	C28 H39 B2 F8 N7 Ni O2 P2	
Molecular formula	C24 H33 N5 Ni O2 P2, 2(B F4), 2(C2 H3 N)	
Formula weight	799.93	
Temperature	100.0 K	
Wavelength	0.71073 Å	
Crystal system	Triclinic	
Space group	P-1	
Unit cell dimensions	a = 11.8611(9) Å	□= 73.878(2)°.
	b = 15.3513(12) Å	□= 85.785(2)°.
	c = 20.2721(16) Å	□ = 89.189(2)°.
Volume	3536.4(5) $Å^3$	
Z	4	
Density (calculated)	1.502 Mg/m^3	
Absorption coefficient	0.720 mm^{-1}	
F(000)	1648	
Crystal size	0.217 x 0.208 x 0.11 mm^3	
Crystal color, habit	Yellow Orange Block	
Theta range for data collection	1.048 to 25.405°.	
Index ranges	-14<=h<=14, -18<=k<=18, -24<=l<=24	
Reflections collected	73049	
Independent reflections	13021 [R(int) = 0.0766]	
Completeness to theta = 25.000°	100.0 %	
Absorption correction	Semi-empirical from equivalents	
Max. and min. transmission	0.0870 and 0.0645	
Refinement method	Full-matrix least-squares on F^2	
Data / restraints / parameters	13021 / 102 / 963	
Goodness-of-fit on F^2	1.015	
Final R indices [I>2sigma(I)]	R1 = 0.0420, wR2 = 0.0991	
R indices (all data)	R1 = 0.0638, wR2 = 0.1143	
Extinction coefficient	n/a	
Largest diff. peak and hole	0.538 and -0.302 $e.Å^{-3}$	

3.8.3 CRYSTALLOGRAPHIC DETAILS OF 12, NI($P^{EtE}_2N^{PH}_2$)CL_2.

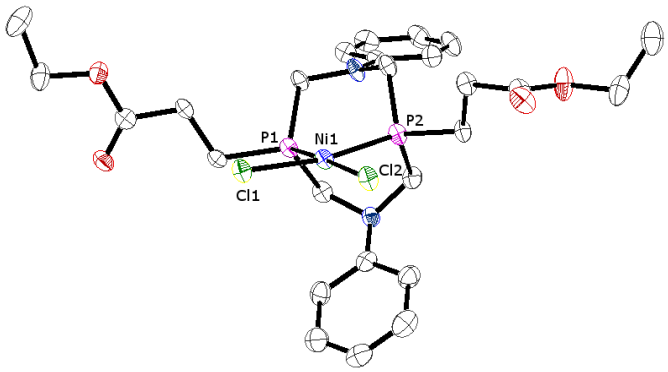

Figure 3.9 Molecular structure of complex 12, Ni($P^{EtE}_2N^{Ph}_2$)Cl_2, as determined by X-ray diffraction studies. Thermal ellipsoids are shown at the 50% probability level. Hydrogens have been removed from this diagram for clarity.

Table 3.4 Crystal data and structure refinement for 12, $Ni(P^{EtE}_2N^{Ph}_2)Cl_2$.

Report date	2015-08-07	
Identification code	MDD140306b	
Empirical formula	C26 H36 Cl2 N2 Ni O4 P2	
Molecular formula	C26 H36 Cl2 N2 Ni O4 P2	
Formula weight	632.12	
Temperature	100.0 K	
Wavelength	0.71073 Å	
Crystal system	Monoclinic	
Space group	P 1 21/c 1	
Unit cell dimensions	a = 13.3211(14) Å	□= 90°.
	b = 19.1057(18) Å	□= 91.929(3)°.
	c = 12.8946(13) Å	□ = 90°.
Volume	3279.9(6) $Å^3$	
Z	4	
Density (calculated)	1.280 Mg/m^3	
Absorption coefficient	0.883 mm^{-1}	
F(000)	1320	
Crystal size	0.205 x 0.113 x 0.108 mm^3	
Crystal color, habit	Dark Red Rod	
Theta range for data collection	2.411 to 25.441°.	
Index ranges	-16<=h<=15, -23<=k<=23, -14<=l<=15	
Reflections collected	28397	
Independent reflections	6013 [R(int) = 0.0848]	
Completeness to theta = 25.000°	99.8 %	
Absorption correction	Semi-empirical from equivalents	
Max. and min. transmission	0.0916 and 0.0664	
Refinement method	Full-matrix least-squares on F^2	
Data / restraints / parameters	6013 / 0 / 336	
Goodness-of-fit on F^2	1.023	
Final R indices [I>2sigma(I)]	R1 = 0.0465, wR2 = 0.1130	
R indices (all data)	R1 = 0.0835, wR2 = 0.1282	
Extinction coefficient	n/a	
Largest diff. peak and hole	0.549 and -0.331 e.$Å^{-3}$	

3.8.4 CRYSTALLOGRAPHIC DETAILS OF 13, $Ni(P^{EtE}_2N^{PhOMe}_2)Cl_2$.

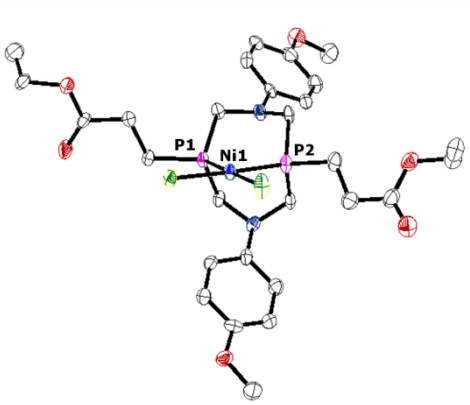

Figure 3.10 Molecular structure of complex 13, $Ni(P^{EtE}_2N^{PhOMe}_2)Cl_2$, as determined by X-ray diffraction studies. Thermal ellipsoids are shown at the 50% probability level. Hydrogens have been removed from this diagram for clarity.

Table 3.5 Crystal data and structure refinement for 13, $Ni(P^{EtE}_2N^{PhOMe}_2)Cl_2$.

Report date	2015-08-07	
Identification code	MDD140306	
Empirical formula	C28 H40 Cl2 N2 Ni O6 P2	
Molecular formula	C28 H40 Cl2 N2 Ni O6 P2	
Formula weight	692.17	
Temperature	100.0 K	
Wavelength	0.71073 Å	
Crystal system	Monoclinic	
Space group	P 1 21/c 1	
Unit cell dimensions	a = 21.9893(10) Å	□= 90°.
	b = 21.2289(9) Å	□= 90.0700(10)°.
	c = 13.6624(6) Å	□ = 90°.
Volume	6377.7(5) $Å^3$	
Z	8	
Density (calculated)	1.442 Mg/m^3	
Absorption coefficient	0.919 mm^{-1}	
F(000)	2896	
Crystal size	0.113 x 0.107 x 0.048 mm^3	
Crystal color, habit	Dark Red Plate	
Theta range for data collection	1.333 to 25.719°.	
Index ranges	-26<=h<=23, -25<=k<=24, -16<=l<=16	
Reflections collected	97171	
Independent reflections	12160 [R(int) = 0.1384]	
Completeness to theta = 25.000°	100.0 %	
Absorption correction	Semi-empirical from equivalents	
Max. and min. transmission	0.0921 and 0.0656	
Refinement method	Full-matrix least-squares on F^2	
Data / restraints / parameters	12160 / 79 / 778	
Goodness-of-fit on F^2	1.031	
Final R indices [I>2sigma(I)]	R1 = 0.0531, wR2 = 0.0956	
R indices (all data)	R1 = 0.1011, wR2 = 0.1097	
Extinction coefficient	n/a	
Largest diff. peak and hole	0.711 and -0.478 $e.Å^{-3}$	

CHAPTER 4
HYDROGEN EVOLUTION ELECTROCATALYSIS BY P_2N_2 COMPLEXES

4.1 Abstract

The nickel complexes of P_2N_2 ligands synthesized by the methods discussed in chapters 2 and 3 are investigated for hydrogen evolution electrocatalysis. The rates of catalysis for different proton sources are compared and analyzed.

4.2 Introduction

Electrochemists have studied the hydrogen evolution reaction (HER) since the electrolysis of water by William Nicholson in the early 1800s.[1] While it has been generally assumed to be one of the simplest electrochemical reactions, there are many experimental and theoretical studies detailing the complexity of its mechanisms.[2-4] Researchers have studied HER in the hopes of storing renewable energy in chemical fuels, the application of which can be more efficient and portable than battery storage.[5] Hydrogen is the simplest chemical fuel[6] and can be the most energy dense as a cryogenic liquid.[7]

$$2\,H^+(aq) + 2\,e^- \rightarrow H_2(g) \qquad E^0 = 0.00 \text{ V vs. SHE}$$

Scheme 4.1 Hydrogen evolution at the standard hydrogen electrode (SHE). The SHE utilizes the hydrogen evolution from platinum as an absolute reference potential.

Platinum cathodes can catalyze HER extremely efficiently at underpotential.[8] The mechanism of this reaction has been the subject of careful study.[9] Essentially, the

platinum surface readily adsorbs protons, and these H_{ads} either combine as adsorbed atoms or react with protons in solution to form H_2, which quickly desorbs and leaves the surface.[10] These reactions are shown in scheme 4.2. The mechanism includes some combination of the Volmer reaction (scheme 4.2a) with the Tafel reaction (scheme 4.2b) or the Heyrovsky reaction (scheme 4.2c).[11]

$$H^+ + e^- \rightarrow H_{ads} \qquad (a)$$

$$2\ H_{ads} \rightarrow H_2 \qquad (b)$$

$$H_{ads} + H^+ + e^- \rightarrow H_2 \qquad (c)$$

Scheme 4.2 The potential mechanisms for electrocatalytic hydrogen evolution on heterogeneous electrodes. A represents the adsorption of protons on the surface, the Volmer reaction; B shows the elimination of two adsorbed hydrogen atoms to form hydrogen gas, the Tafel reaction; and C shows the electrochemical reaction of an adsorbed hydrogen with a proton from solution, the Heyrovsky reaction.

While the platinum electrode is extremely efficient for hydrogen evolution and oxidation, it is a scarce metal on Earth and prohibitively expensive for distributed applications such as fuel cells for transportation.[12] Fortunately, the evolution of living organisms over billions of years has revealed another path to efficiently producing and oxidizing hydrogen gas, using enzymes featuring abundant metals like iron and nickel.[13] The active sites of these hydrogenase enzymes, shown in Figure 4.1, catalyze reactions either to oxidize H_2 for energy processes or to balance redox potentials within the cell.[14] These enzymes are incredibly efficient, both *in vivo* and under electrocatalytic conditions.[15] While bulk metals like Fe and Ni are not efficient heterogeneous catalysts when compared to Pt,[16] the incorporation of these metals within a large enzymatic ligand

framework allows for the rapid delivery of protons and electrons to the active site within the enzyme.[17]

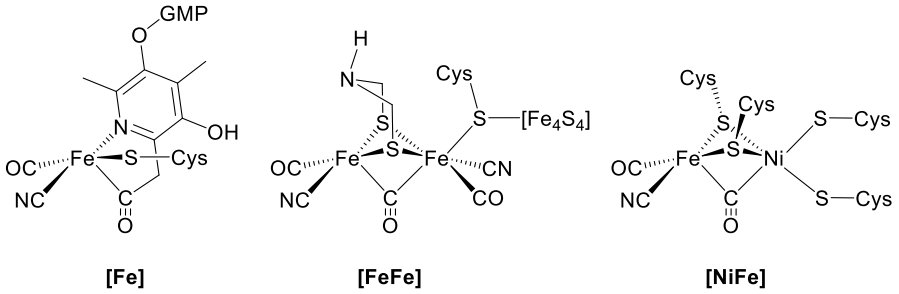

Figure 4.1 Active sites of [Fe], [FeFe], and [NiFe] hydrogenases. Cys represents a cysteine amino acid residue, and GMP stands for a guanosine monophosphate moiety.

The structural lessons of these enzymes have been extremely valuable to modern electrochemists and synthetic inorganic chemists.[18] Many metal complexes have been identified as homogeneous catalysts for HER.[19-21] Nickel P_2N_2 complexes are one of the best examples of incorporating biomimetic design principles into an inorganic catalyst. Dr. Daniel DuBois and his colleagues developed these nickel phosphine electrocatalysts to mimic the active site of FeFe hydrogenase (Figure 4.1).[22] This enzyme catalyzes the reversible oxidation of dihydrogen with great efficiency, due in part to the incorporation of a nitrogen base pendant to the Fe active site, which acts as a proton relay in the second coordination sphere.[23] As shown in Figure 4.2a, the P_2N_2 ligand binds to nickel through its phosphines, positioning the amine nitrogens as above the nickel open coordination site. These "pendant bases" account for the great increases in electrocatalytic rates for proton-coupled electrocatalytic reactions from hydrogen evolution and oxidation to formate oxidation and oxygen reduction, the top rates of which are shown in Table 4.1.

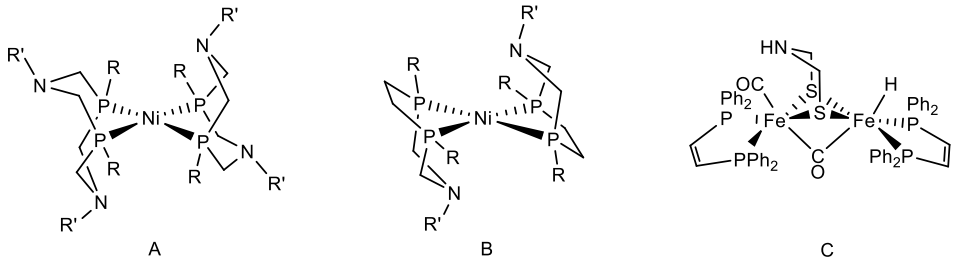

Figure 4.2 Homogeneous electrocatalysts for hydrogen evolution.

Table 4.1 Electrocatalytic rates for $Ni(P_2N_2)^{2+}$ complexes for proton-coupled electron transfer reactions.

Electrocatalytic Reaction	Fastest Rate (s^{-1})
H^+ reduction	6,700
H_2 oxidation	10
HCO_2^- oxidation	16
O_2 reduction	0.1

4.3 Results and Discussion

$Ni(P_2N_2)_2$ complexes were characterized for the electrocatalytic evolution of molecular hydrogen by conducting cyclic voltammetry experiments in acidic electrolyte solution. By starting at a more positive potential and scanning negatively, the $Ni(P_2N_2)_2^{2+}$ is subject to two sequential one-electron reductions. In the presence of acid in the form of titrated CF_3COOH, the doubly-reduced Ni^0 complex reacts with two protons to form gaseous hydrogen. By comparing the catalytic plateau current with the initial peak current, electrocatalytic rates can be determined.

Table 4.2 Reduction potentials for the series of complexes $[Ni(P^{R}{}_2N^{Ph}{}_2)_2(CH_3CN)]X_2$ in benzonitrile. ($X=PF_6^-$ or BF_4^-).

Ligand (R,R')	$E°(Ni^{II/I})$ (V vs $Cp_2Fe^{+/0}$)	$E°(Ni^{I/0})$ (V vs $Cp_2Fe^{+/0}$)
EtE,Ph[a]	–0.85	–1.10
EtE,PhOMe[a]	–0.87	–1.07
Me,Ph[b]	–1.01	–1.30
Et,Ph	-0.91	-1.25
Ph,Ph[b]	–0.79	–1.00

[a] This work. [b] Ref 7

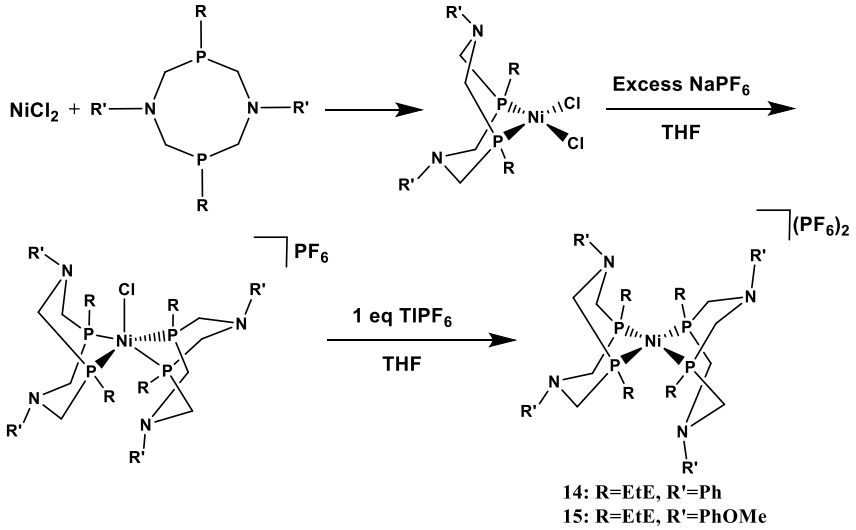

Scheme 4.3 Purification and Isolation for $P^{EtE}{}_2N^{R'}{}_2$ Attachment to Nickel (R' = Ph, PhOMe).

Unlike the amide and carboxylate ligands, these $[Ni(P^{EtE}{}_2N^{R}{}_2)](PF_6)_2$ complexes show characteristic cyclic voltammograms (CV) with two separate 1-electron reductions representing $E°(Ni^{I/0})$ and $E°(Ni^{II/I})$.[24] Table 4.2 compares reduction potentials for $[Ni(P^{EtE}{}_2N^{R'}{}_2)_2](PF_6)_2$ complexes to some previously characterized $[Ni(P_2N_2)_2]^{2+}$

complexes. As expected, the highly donating $P^{Me}_2N^{Ph}_2$ ligand produces the most negative reduction potentials for this group. The two new ethyl ester-substituted complexes also display more negative reduction potentials. The steric bulk of these ligands stabilize the nickel(I) state of the complex. The $E°(Ni^{II/I})$ represents a transition from a 5-coordinate trigonal bipyramidal geometry with a coordinated acetonitrile ligand to a 4-coordinate tetrahedral complex. In this way, the steric bulk of the ethyl-ester-substituted ligands stabilizes the transition to a tetrahedral nickel(I) complex.

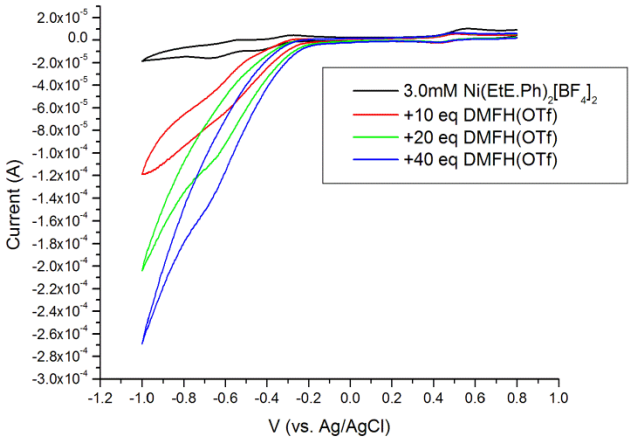

Figure 4.3 Hydrogen evolution catalyzed by 0.2 mM $[Ni(Me.Ph)_2](CF_3SO_3)_2$ in 0.2 M NBu_4PF_6 in benzonitrile with a 3mm gC working electrode and Pt wire counter. 1 M CF_3COOH in electrolyte solution was titrated in 10 uL aliquots.

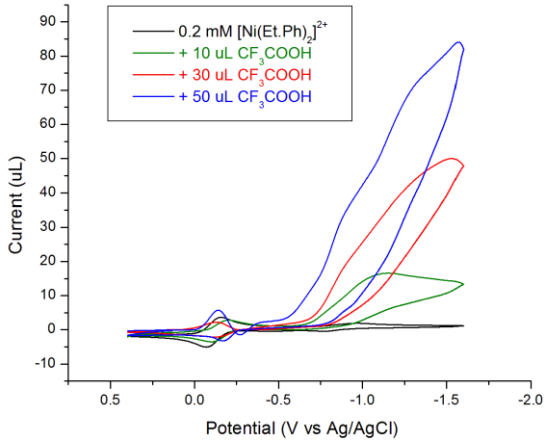

Figure 4.4 Hydrogen evolution catalyzed by 0.2 mM $[Ni(Et.Ph)_2](CF_3SO_3)_2$ in 0.2 M NBu_4PF_6 in benzonitrile with a 3mm gC working electrode and Pt wire counter. 1 M CF_3COOH in electrolyte solution was titrated in 10 uL aliquots.

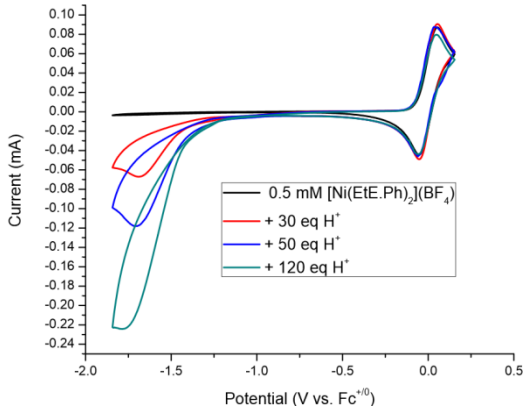

Figure 4.5 Hydrogen evolution catalyzed by 0.2 mM $[Ni(EtE.Ph)_2](BF_4)_2$ in 0.2 M NBu_4PF_6 in benzonitrile with a 3mm gC working electrode and Pt wire counter. 1 M CF_3COOH in electrolyte solution was titrated in 10 uL aliquots.

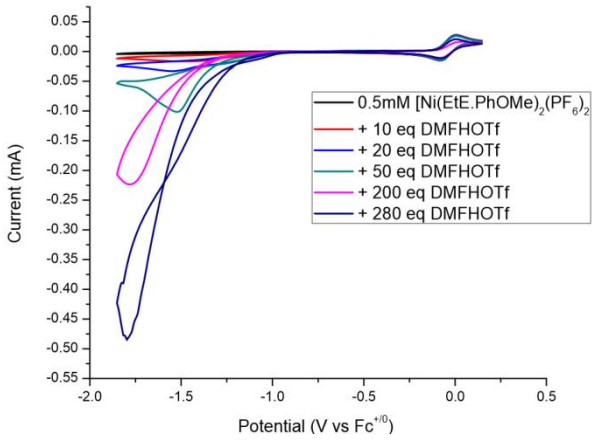

Figure 4.6 Hydrogen evolution catalyzed by 0.2 mM $[Ni(EtE.PhOMe)_2](PF_6)_2$ in 0.2 M NBu_4PF_6 in acetonitrile with a 3mm gC working electrode and Pt wire counter. 1 M CF_3COOH in electrolyte solution was titrated in 10 uL aliquots.

By titrating in protons in the form of 1 M CF_3COOH and applying a potential via cyclic voltammetry, the rate of an electrochemical reaction can be determined. By comparing the initial peak and catalytic plateau currents, an electrocatalytic rate can be determined. The rates for the Me.Ph and Et.Ph ligands are the fastest for any P_2N_2 complexes, which matches with their negative reduction potentials. This level of control of the redox potential is only possible through the direct substitution of the phosphorus atom of the P_2N_2 ligand.

Table 4.3 Hydrogen evolution electrocatalytic rates for the series of complexes $[Ni(P^{R}_{2}N^{Ph}_{2})_{2}(CH_3CN)]X_2$ in benzonitrile. ($X=PF_6^-$ or BF_4^-)

Ligand (R,R')	HER electrocatalytic rate (s^{-1})
EtE,Ph[a]	1,800
EtE,PhOMe[a]	2,000
Me,Ph[b]	6,800
Et,Ph	200
Ph,Ph[b]	4,900

4.4 Experimental

4.4.1 General Considerations

Unless otherwise noted, all reactions and manipulations were performed under a N_2 atmosphere using standard glovebox or Schlenk line techniques. Glassware was dried in an oven overnight prior to use. Acetonitrile and tetrahydrofuran (THF) were purified via passage through alumina and molecular sieves. Ethanol was dried over 4 angstrom molecular sieves. Aniline and triethylamine were distilled from CaH_2. Tetrabutylammonium hexafluorophosphate was crystallized from methanol and dried under vacuum prior to use. Tris(hydroxymethyl)phosphine (THP) was used as obtained from Acros Organics. All other chemicals were used as obtained from commercial suppliers. Electrochemical measurements were performed on a Gamry potentiostat in an air-tight cell with a glassy carbon working electrode, a Pt counter electrode, and a $Ag^{+/0}$ wire pseudo reference electrode. Benzonitrile was used as the solvent and

tetrabutylammonium hexafluorophosphate was used as the supporting electrolyte. ^{1}H and $^{31}P\{^{1}H\}$ NMR spectra were obtained on a 300MHz Varian or a 500MHz Joel spectrometer. ^{1}H and $^{31}P\{^{1}H\}$ NMR spectral data are referenced against the residual solvent signal and are reported in ppm downfield of tetramethylsilane and 85% phosphoric acid, respectively ($\delta = 0$). Elemental Analyses were performed by NuMega Labs in San Diego, CA. Mass spectrometry was performed at the UCSD Molecular Mass Spectrometry Facilty.

4.4.2 Synthesis of $Ni(P^{Me}_2N^{Ph}_2)[BF_4]_2$

In a 10 mL Schlenk flask, 88.0 mg **6** was combined with 67.0 mg $Ni(CH_3CN)_6[BF_4]_2$ in 3 mL acetonitrile. To this cloudy mixture, 3 mL of deoxygenated water was added. Upon stirring overnight, the solution clarified into a yellow solution. Volatiles were removed by evacuation. Yellow, rhomboid crystals suitable for X-ray diffraction were grown by vapor diffusion of acetone into acetonitrile:water (1:1). $^{31}P\{^{1}H\}$ ($CD_3CN:D_2O$) $\delta = +20.39$ ppm. ^{1}H NMR (500MHz, $CD_3CN:D_2O$): $\delta = 7.20$ (t, *J* = 7.9 Hz, Ar*H*, 4H), 7.04 (d, *J* = 8.2 Hz, Ar*H*, 4H), 6.78 (t, *J* = 7.2 Hz, Ar*H*, 2H), 3.33 (d, *J* = 7.0 Hz, PCH_2N, 8H), 2.46 (br, PCH_2CH_2, 4H), 1.04 (t, *J* = 7.0 Hz, CH_2COONa, 4H). Calculated M/z for $[C_{22}H_{27}N_2O_4P_2Ni]^+$: 503.0800; Found: 503.0797.

4.4.3 Synthesis of $Ni(P^{Et}_2N^{Ph}_2)[BF_4]_2$

In a 10 mL Schlenk flask, 88.0 mg **6** was combined with 67.0 mg $Ni(CH_3CN)_6[BF_4]_2$ in 3 mL acetonitrile. To this cloudy mixture, 3 mL of deoxygenated water was added. Upon stirring overnight, the solution clarified into a yellow solution. Volatiles were removed by evacuation. Yellow, rhomboid crystals suitable for X-ray

diffraction were grown by vapor diffusion of acetone into acetonitrile:water (1:1). $^{31}P\{^{1}H\}$ (CD_3CN:D_2O) δ = +20.39 ppm. ^{1}H NMR (500MHz, CD_3CN:D_2O): δ = 7.20 (t, *J* = 7.9 Hz, Ar*H*, 4H), 7.04 (d, *J* = 8.2 Hz, Ar*H*, 4H), 6.78 (t, *J* = 7.2 Hz, Ar*H*, 2H), 3.33 (d, *J* = 7.0 Hz, PC*H*$_2$N, 8H), 2.46 (br, PC*H*$_2$CH$_2$, 4H), 1.04 (t, *J* = 7.0 Hz, C*H*$_2$COONa, 4H). Calculated M/z for $[C_{22}H_{27}N_2O_4P_2Ni]^+$: 503.0800; Found: 503.0797.

4.4.4 Synthesis of Ni($P^{Amide}_2N^{Ph}_2$) (11)

In a 10 mL Schlenk flask, 42.2 mg $Ni(CH_3CN)_6[BF_4]_2$ was combined with 45.8 mg **7** in 5 mL acetonitrile. Upon stirring, the solution turned light red with slight precipitation. After stirring overnight, the solution was filtered and dried to yield 63.4 mg **11**, a yellow-orange powder. (99.5% yield) Yellow, rod-like crystals suitable for X-ray diffraction were grown by vapor diffusion of diethyl ether into acetonitrile. ^{1}H NMR (500MHz, DMSO): δ = 7.47 (br, N*H*$_2$, 2H), 7.44 (t, *J* = 7.9 Hz, Ar*H*, 4H), 7.16 (d, *J* = 8.3 Hz, Ar*H*, 4H), 7.09 (t, *J* = 7.3 Hz, Ar*H*, 2H), 6.96 (br, N*H*$_2$, 2H), 4.12 (d, *J* = 14.5 Hz, PC*H*$_2$N, 8H), 3.71 (dt, *J* = 14.3 Hz, *J* = 4.9 Hz, PC*H*$_2$C, 4H), 2.13 (t, *J* = 13.9 Hz, C*H*$_2$CO, 4H). $^{31}P\{^{1}H\}$ (CD_3CN): δ = 19.76 ppm. Calculated M/z for $[C_{22}H_{29}P_2N_4O_2Ni]^+$: 501.1114; Found: 501.1115.

4.4.5 Preparation of Ni($P^{EtE}_2N^{Ph}_2$)Cl_2 (12)

In a 20 mL scintillation vial, combined 54.2 mg **5** with 12.8 mg anhydrous $NiCl_2$. Upon addition of 5 mL acetonitrile, mixture was stirred and over the course of 10 minutes became dark red. Solution was stirred overnight, then filtered and vacuum dried. This residue was rinsed three times with 10 mL water to remove excess $NiCl_2$. After vacuum drying, 56.4 mg **12** were isolated (90.6% yield). Crystals suitable for X-ray diffraction

were grown from vapor diffusion of diethyl ether into acetonitrile. ^{1}H NMR (CD_3CN): δ = 7.13 (d, *J* = 8.9 Hz, Ar*H*, 4H), 6.94 (t, *J* = 9.1 Hz, Ar*H*, 4H), 6.80 (d, *J* = 8.6 Hz, Ar*H*, 2H), 4.08 (q, *J* = 7.1 Hz, -OC*H*$_2$CH$_3$, 4H), 3.91 (d, *J* = 14, P-C*H*$_2$-N, 8H), 3.76 (dt, *J* = 7.2 Hz, *J* = 3.09 Hz, PC*H*$_2$CH$_2$, 4H), 1.92 (t, *J* = 2.4 Hz, -C*H*$_2$COO-, 4H), 1.21 (t, *J* = 7.1 Hz, COOCH$_2$C*H*$_3$, 6H). ^{31}P{^{1}H} (CD_3CN): δ = +3.54 ppm. Calculated M/z for $[C_{26}H_{36}ClP_2N_2O_4Ni]^+$: 595.1187; Found: 595.1193.

4.4.6 Preparation of Ni($P^{EtE}_2N^{PhOMe}_2$)Cl_2 (13)

In a 20 mL scintillation vial, combined 103.8 mg **6** with 20.0 mg anhydrous $NiCl_2$. Upon addition of 5 mL acetonitrile, mixture was stirred and over the course of 10 minutes became brown-red. Solution was stirred overnight, then filtered and vacuum dried. This residue was rinsed three times with 10 mL water to remove excess $NiCl_2$. After vacuum drying, 0.11 g **13** were isolated (91% yield). Crystals suitable for X-ray diffraction were grown from vapor diffusion of diethyl ether into acetonitrile. ^{31}P{^{1}H} (CD_3CN): δ = +1.35 ppm. ^{1}H NMR: δ = 7.16 (t, *J* = 6.5 Hz, Ar*H*, 4H), 7.00 (d, *J* = 8.8 Hz, Ar*H*, 4H), 6. 84 (t, *J* = 8.4 Hz, Ar*H*, 2H), 4.15 (q, *J* = 7.0 Hz, -OC*H*$_2$CH$_3$, 4H), 3.96 (d, *J* = 14, P-C*H*$_2$-N, 8H), 3.77 (dt, *J* = 21 Hz, *J* = 5.5 Hz, PC*H*$_2$CH$_2$, 4H), 1.97 (t, *J* = 2.3 Hz, -C*H*$_2$COO-, 4H), 1.25 (t, *J* = 5.7 Hz, COOCH$_2$C*H*$_3$, 6H). Calculated M/z for $[C_{26}H_{36}ClP_2N_2O_4Ni]^+$: 655.1398; Found: 655.1409. Anal. Calcd for $C_{28}H_{40}Cl_2N_2NiO_6P_2(H_2O)_2(CH_3CN)_{0.5}$: C, 46.58; H, 6.12; N, 4.68. Found: C, 46.43; H, 5.95; N, 4.83.

4.5 Conclusion

We have demonstrated two new synthetic routes for the production of P_2N_2-type ligands that installs alkyl carbonyl functional groups as the phosphorus substituent. Nickel complexes of the new $P^{R}{}_2N^{R'}{}_2$ ligands have been synthesized and characterized by electrochemical catalysis in the presence of an acid proton source. These rates are among the highest found for a homogeneous catalyst for electrochemical hydrogen evolution.

Parts of the Results and Discussion and Experimental sections for this chapter come directly from a manuscript entitled “Electrocatalytic behavior of alkyl-substituted P_2N_2 complexes" by Michael D. Doud and Clifford P. Kubiak, to be submitted. The dissertation author is the primary author of this manuscript.

4.6 References

(1) Russel, C. *Chemistry World* **2003**.

(2) Breiter, M. W. In *Handbook of Fuel Cells*; John Wiley & Sons, Ltd: 2010.

(3) Fukuzumi, S.; Yamada, Y.; Suenobu, T.; Ohkubo, K.; Kotani, H. *Energy & Environmental Science* **2011**, *4*, 2754.

(4) Lasia, A. In *Handbook of Fuel Cells*; John Wiley & Sons, Ltd: 2010.

(5) Pellow, M. A.; Emmott, C. J. M.; Barnhart, C. J.; Benson, S. M. *Energy & Environmental Science* **2015**.

(6) Lubitz, W.; Tumas, W. *Chemical reviews* **2007**, *107*, 3900.

(7) Winter, M.; Brodd, R. J. *Chemical Reviews* **2004**, *104*, 4245.

(8) Mateo, J. J.; Tryk, D. A.; Cabrera, C. R.; Ishikawa, Y. *Molecular Simulation* **2008**, *34*, 1065.

(9) Gomez, R.; Fernandez-Vega, A.; Feliu, J. M.; Aldaz, A. *The Journal of Physical Chemistry* **1993**, *97*, 4769.

(10) Nichols, R. J.; Bewick, A. *Journal of Electroanalytical Chemistry and Interfacial Electrochemistry* **1988**, *243*, 445.

(11) Meng, Y.; Aldous, L.; Belding, S. R.; Compton, R. G. *Physical Chemistry Chemical Physics* **2012**, *14*, 5222.

(12) Amatya, R.; Ram, R. J. *Journal of Electronic Materials* **2012**, *41*, 1011.

(13) Adams, M. W. W.; Stiefel, E. I. *Science* **1998**, *282*, 1842.

(14) Mulder, David W.; Shepard, Eric M.; Meuser, Jonathan E.; Joshi, N.; King, Paul W.; Posewitz, Matthew C.; Broderick, Joan B.; Peters, John W. *Structure* **2011**, *19*, 1038.

(15) Vincent, K. A.; Parkin, A.; Armstrong, F. A. *Chemical Reviews* **2007**, *107*, 4366.

(16) Hall, D. E. *Journal of The Electrochemical Society* **1981**, *128*, 740.

(17) Lubitz, W.; Ogata, H.; Rüdiger, O.; Reijerse, E. *Chemical Reviews* **2014**, *114*, 4081.

(18) McKone, J. R.; Marinescu, S. C.; Brunschwig, B. S.; Winkler, J. R.; Gray, H. B. *Chemical Science* **2014**, *5*, 865.

(19) Chen, L.; Chen, G.; Leung, C.-F.; Yiu, S.-M.; Ko, C.-C.; Anxolabéhère-Mallart, E.; Robert, M.; Lau, T.-C. *ACS Catalysis* **2015**, *5*, 356.

(20) Fukuzumi, S. *Current Opinion in Chemical Biology* **2015**, *25*, 18.

(21) Marinescu, S. C.; Winkler, J. R.; Gray, H. B. *Proceedings of the National Academy of Sciences* **2012**, *109*, 15127.

(22) Fraze, K.; Wilson, A. D.; Appel, A. M.; DuBois, M. R.; DuBois, D. L. *Organometallics* **2007**, *26*, 3918.

(23) Madden, C.; Vaughn, M. D.; Díez-Pérez, I.; Brown, K. A.; King, P. W.; Gust, D.; Moore, A. L.; Moore, T. A. *Journal of the American Chemical Society* **2012**, *134*, 1577.

(24) Wilson, A. D.; Shoemaker, R. K.; Miedaner, A.; Muckerman, J. T.; DuBois, D. L.; DuBois, M. R. *Proceedings of the National Academy of Sciences of the United States of America* **2007**, *104*, 6951.

CHAPTER 5
FORMATE OXIDATION ELECTROCATALYSIS BY P_2N_2 COMPLEXES

5.1 Abstract

The nickel complexes of P_2N_2 ligands synthesized by the methods discussed in chapters 2 and 3 are investigated for formate oxidation electrocatalysis. The rates of catalysis for different phosphine substituents are determined and compared. The newly synthesized complexes with alkyl- and carbonyl- phosphine substituents oxidize formate more slowly than previously synthesized cyclohexyl- and phenyl- substituted phosphine ligands, due to a more negative reduction potential leading to a decrease in the driving force of formate oxidation.

5.2 Introduction

While current energy production is based in large part on the consumption of fossil fuels, this system is unsustainable and will change within our lifetimes.[1] Supplies of petrochemicals are limited, and increasing combustion of hydrocarbons in the modern era has led to a drastic increase in atmospheric and oceanic carbon dioxide with potentially devastating climatic effects.[2] One of the crucial challenges of science in this generation will be the development of a sustainable energy economy, for which chemistry will play an essential role.[3]

The development of carbon-neutral, renewable energy in the form of wind and solar poses challenges in matching these sources of supply to human energy demands.[4] Both can provide sufficient energy when compared to present demand, yet their

utilization is hindered by intermittent availability.[5] The storage of excess energy in the form of chemical bonds in fuels offers a potential solution to this problem. While batteries can scale competitively for stationary energy storage, nearly 30% of current energy usage in the United States is applied for transportation usage.[6] This is an area where efficient fuel cells can be much more effective than heavier batteries.

Chemical fuels such as hydrogen (discussed in chapter 4) and methanol or formate synthesized from carbon dioxide represent promising replacements in a carbon-neutral fuel cycle. The utilization of these fuels will require developments in electrocatalysts both for the oxidation of formate and its microscopic reverse reaction, the proton-coupled reduction of carbon dioxide.[7] Most examples of formate oxidation reported thus far use expensive and rare noble metals, particularly Pt, Pd, Ru, Au, and Rh.[8-11]

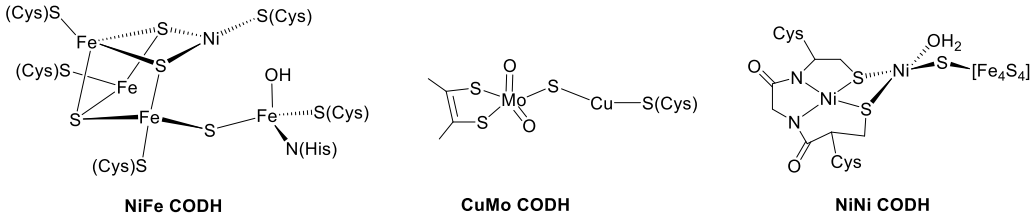

Figure 5.1 Active sites of NiFe, CuMo, and NiNi carbon monoxide dehydrogenase (CODH).[12]

Enzymes have evolved to be highly efficient for the oxidation of formate.[13] For example, formate dehydrogenase (FDH), carbon monoxide dehydrogenase (CODH), hydrogen-dependent carbon dioxide reductase (HDCR), and carbonic anhydrase (CA) all use base metals to catalyze the reversible reduction of carbon dioxide, given appropriate conditions.[12,14-17] The abilities of these active sites to catalyze these important reactions

is facilitated by the enormous protein ligands responsible for delivering substrates to the metal and shuttling products out after the reaction.[18,19]

In this chapter, the new synthetic routes for P_2N_2 ligands discussed in chapters 2 and 3 are used to make competent catalysts for formate oxidation, and the effect of varying phosphorus substituents on the electrocatalytic rate is explored.

5.3 Results and Discussion

Formate oxidation experiments were conducted by titration of a 1 M $HNEt_3OCHO$ solution in acetonitrile electrolyte, followed by cyclic voltammetry. Starting the scan at a negative potential charges the electrode's double layer with Ni^0 complexes. By scanning the potential more positive, two sequential, reversible one-electron couples are observed, representing $E^0(0/I)$ and $E^0(I/II)$. Upon oxidation to the catalytically-active $Ni(P_2N_2)_2^{2+}$ complex, current increases due to the 2-electron oxidation of formate. By comparing the plateau current measured with titrated substrate to the peak current measured beforehand, an electrocatalytic rate can be determined.

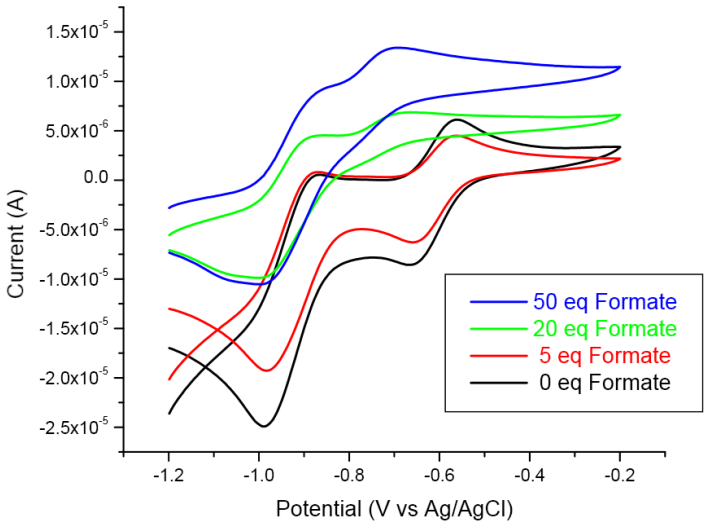

Figure 5.2 Formate oxidation electrocatalysis of $Ni(Me.Ph)_2[BF_4]_2$. 1.0 mM $Ni(Me.Ph)_2[BF_4]_2$ in 0.2 M NBu_4PF_6, formate added in 5 uL aliquots of 1.0 M $HNEt_3OCHO$. 3.0 mm gC working electrode, Pt wire counter electrode. $CoCp_2$ is included as an internal reference.

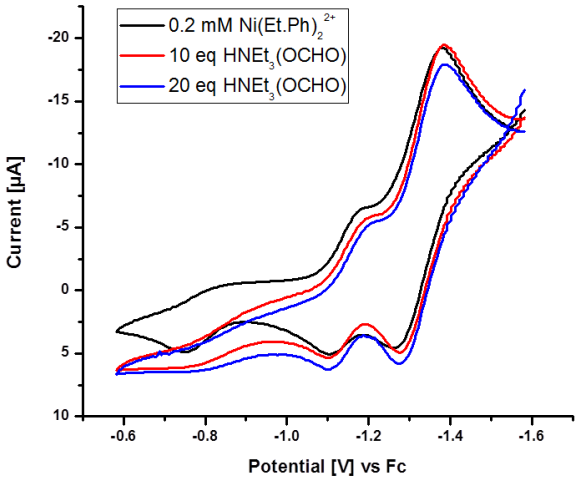

Figure 5.3 Electrocatalytic oxidation of formate by $Ni(Et.Ph)_2[CF_3SO_3]$. 1.0 mM $Ni(Et.Ph)_2[CF_3SO_3]_2$ in 0.2 M NBu_4PF_6, formate added in 5 uL aliquots of 1.0 M $HNEt_3OCHO$. 3.0 mm gC working electrode, Pt wire counter electrode. $CoCp_2$ is included as an internal reference.

Several routes were attempted for the anion exchange; ultimately, a two-step process was utilized. The first step involves the reaction of the $Ni(P^{EtE}{}_2N^{Ph}{}_2)Cl_2$ complex with an excess of sodium hexafluorophosphate. This leads to the exchange of a single chloride anion, and the disproportionation of the mono-P_2N_2 complex into a bis-P_2N_2 complex, observable by $^{31}P\{^1H\}$ NMR. After rinsing with water to remove $NiCl_2$ and $NaPF_6$, this complex can be isolated in nearly quantitative yield. The second anion exchange can be accomplished by reaction with 1 equivalent of thallium(I) hexafluorophosphate. This produces the $[Ni(P^{EtE}{}_2N^{R'}{}_2)_2](PF_6)_2$ complexes, as characterized by NMR, high-resolution mass spectrometry, and characteristic and catalytic cyclic voltammetry.

Table 5.1 Reduction potentials for the series of complexes $[Ni(P^{R}{}_2N^{Ph}{}_2)_2(CH_3CN)]X_2$ in benzonitrile. (X=PF_6^- or BF_4^-)

Ligand (R,R')	$E°(Ni^{II/I})$ (V vs $Cp_2Fe^{+/0}$)	$E°(Ni^{I/0})$ (V vs $Cp_2Fe^{+/0}$)
Me,Ph	–1.01	–1.30
Et,Ph	-0.91	-1.25
Ph,Ph	–0.79	–1.00

Table 5.2 Formate oxidation electrocatalytic rates for the series of complexes $[Ni(P^R_2N^{Ph}_2)_2(CH_3CN)]X_2$ in benzonitrile. ($X=PF_6^-$ or BF_4^-)

Ligand (R,R')	Formate oxidation electrocatalytic rate (s^{-1})
Me,Ph	0.12
Et,Ph	0.2
Ph,Ph[b]	8.0

Ultimately the electrocatalytic rates for formate oxidation of the newly synthesized alkyl- and carbonyl- substituted phosphine P_2N_2 complexes are significantly lower than previously reported P_2N_2 complexes.[20,21] This result likely proceeds from the lower driving force expected from a more negative reduction potential required for these complexes.

5.4 Experimental

5.4.1 General Considerations

Unless otherwise noted, all reactions and manipulations were performed under a N_2 atmosphere using standard glovebox or Schlenk line techniques. Glassware was dried in an oven overnight prior to use. Acetonitrile and tetrahydrofuran (THF) were purified via passage through alumina and molecular sieves. Ethanol was dried over 4 angstrom molecular sieves. Aniline and triethylamine were distilled from CaH_2. Tetrabutylammonium hexafluorophosphate was crystallized from methanol and dried

under vacuum prior to use. Tris(hydroxymethyl)phosphine (THP) was used as obtained from Acros Organics. All other chemicals were used as obtained from commercial suppliers. Electrochemical measurements were performed on a Gamry potentiostat in an air-tight cell with a glassy carbon working electrode, a Pt counter electrode, and a $Ag^{+/0}$ wire pseudo reference electrode. Benzonitrile was used as the solvent and tetrabutylammonium hexafluorophosphate was used as the supporting electrolyte. ^{1}H and $^{31}P\{^{1}H\}$ NMR spectra were obtained on a 300MHz Varian or a 500MHz Joel spectrometer. ^{1}H and $^{31}P\{^{1}H\}$ NMR spectral data are referenced against the residual solvent signal and are reported in ppm downfield of tetramethylsilane and 85% phosphoric acid, respectively ($\delta = 0$). Elemental Analyses were performed by NuMega Labs in San Diego, CA. Mass spectrometry was performed at the UCSD Molecular Mass Spectrometry Facility.

5.4.2 Synthesis of $Ni(P^{PA}_2N^{PH}_2)$ (10)

In a 10 mL Schlenk flask, 88.0 mg **6** was combined with 67.0 mg $Ni(CH_3CN)_6[BF_4]_2$ in 3 mL acetonitrile. To this cloudy mixture, 3 mL of deoxygenated water was added. Upon stirring overnight, the solution clarified into a yellow solution. Volatiles were removed by evacuation. Yellow, rhomboid crystals suitable for X-ray diffraction were grown by vapor diffusion of acetone into acetonitrile:water (1:1). $^{31}P\{^{1}H\}$ (CD_3CN:D_2O) δ = +20.39 ppm. ^{1}H NMR (500MHz, CD_3CN:D_2O): δ = 7.20 (t, *J* = 7.9 Hz, Ar*H*, 4H), 7.04 (d, *J* = 8.2 Hz, Ar*H*, 4H), 6.78 (t, *J* = 7.2 Hz, Ar*H*, 2H), 3.33 (d, *J* = 7.0 Hz, PCH_2N, 8H), 2.46 (br, PCH_2CH_2, 4H), 1.04 (t, *J* = 7.0 Hz, CH_2COONa, 4H). Calculated M/z for $[C_{22}H_{27}N_2O_4P_2Ni]^+$: 503.0800; Found: 503.0797.

5.4.3 Synthesis of Ni($P^{Amide}_2N^{Ph}_2$) (11)

In a 10 mL Schlenk flask, 42.2 mg $Ni(CH_3CN)_6[BF_4]_2$ was combined with 45.8 mg **7** in 5 mL acetonitrile. Upon stirring, the solution turned light red with slight precipitation. After stirring overnight, the solution was filtered and dried to yield 63.4 mg **11**, a yellow-orange powder. (99.5% yield) Yellow, rod-like crystals suitable for X-ray diffraction were grown by vapor diffusion of diethyl ether into acetonitrile. ^{1}H NMR (500MHz, DMSO): δ = 7.47 (br, N*H*$_2$, 2H), 7.44 (t, *J* = 7.9 Hz, Ar*H*, 4H), 7.16 (d, *J* = 8.3 Hz, Ar*H*, 4H), 7.09 (t, *J* = 7.3 Hz, Ar*H*, 2H), 6.96 (br, N*H*$_2$, 2H), 4.12 (d, *J* = 14.5 Hz, PC*H*$_2$N, 8H), 3.71 (dt, *J* = 14.3 Hz, *J* = 4.9 Hz, PC*H*$_2$C, 4H), 2.13 (t, *J* = 13.9 Hz, C*H*$_2$CO, 4H). ^{31}P{^{1}H} (CD_3CN): δ = 19.76 ppm. Calculated M/z for $[C_{22}H_{29}P_2N_4O_2Ni]^+$: 501.1114; Found: 501.1115.

5.4.4 Preparation of Ni($P^{EtE}_2N^{Ph}_2$)Cl_2 (12)

In a 20 mL scintillation vial, combined 54.2 mg **5** with 12.8 mg anhydrous $NiCl_2$. Upon addition of 5 mL acetonitrile, mixture was stirred and over the course of 10 minutes became dark red. Solution was stirred overnight, then filtered and vacuum dried. This residue was rinsed three times with 10 mL water to remove excess $NiCl_2$. After vacuum drying, 56.4 mg **12** were isolated (90.6% yield). Crystals suitable for X-ray diffraction were grown from vapor diffusion of diethyl ether into acetonitrile. ^{31}P{^{1}H} (CD_3CN): δ = +3.54 ppm. ^{1}H NMR (CD_3CN): δ = Calculated M/z for $[C_{26}H_{36}ClP_2N_2O_4Ni]^+$: 595.1187; Found: 595.1193.

5.4.5 Preparation of Ni($P^{EtE}_2N^{PhOMe}_2$)Cl_2 (13)

In a 20 mL scintillation vial, combined 103.8 mg **6** with 20.0 mg anhydrous $NiCl_2$. Upon addition of 5 mL acetonitrile, mixture was stirred and over the course of 10 minutes became brown-red. Solution was stirred overnight, then filtered and vacuum dried. This residue was rinsed three times with 10 mL water to remove excess $NiCl_2$. After vacuum drying, 0.11 g **13** were isolated (91% yield). Crystals suitable for X-ray diffraction were grown from vapor diffusion of diethyl ether into acetonitrile. $^{31}P\{^1H\}$ (CD_3CN): δ = +1.35 ppm. ^1H NMR: δ = 7.16 (t, *J* = 6.5 Hz, Ar*H*, 4H), 7.00 (d, *J* = 8.8 Hz, Ar*H*, 4H), 6. 84 (t, *J* = 8.4 Hz, Ar*H*, 2H), 4.15 (q, *J* = 7.0 Hz, -OC*H*$_2$CH$_3$, 4H), 3.96 (d, *J* = 14, P-C*H*$_2$-N, 8H), 3.77 (dt, *J* = 21 Hz, *J* = 5.5 Hz, PC*H*$_2$CH$_2$, 4H), 1.97 (t, *J* = 2.3 Hz, -C*H*$_2$COO-, 4H), 1.25 (t, *J* = 5.7 Hz, COOCH$_2$C*H*$_3$, 6H). Calculated M/z for $[C_{26}H_{36}ClP_2N_2O_4Ni]^+$: 655.1398; Found: 655.1409. Anal. Calcd for $C_{28}H_{40}Cl_2N_2NiO_6P_2(H_2O)_2(CH_3CN)_{0.5}$: C, 46.58; H, 6.12; N, 4.68. Found: C, 46.43; H, 5.95; N, 4.83

5.5 Conclusion

Nickel complexes of the new $P^R_2N^{R'}_2$ ligand syntheses demonstrated in chapters 2 and 3 have been characterized for the electrocatalytic oxidation of formate. While the new alkyl- and carbonyl- substituted phosphines show lower catalytic activity for the electrocatalytic oxidation of formate, the newly synthesized complexes offer myriad possibilities for iteration. Taking inspiration from natural carbon dioxide reduction enzymes, the development of new bimetallic and heterobimetallic systems can be achieved through synthetic methods. These complexes could allow for new regimes of

bimetallic systems with ligands controlling the secondary coordination sphere of the active site, much like the building up of an enzyme.

Parts of the Results and Discussion and Experimental sections for this chapter come directly from a manuscript entitled “Electrocatalytic behavior of alkyl-substituted P_2N_2 complexes" by Michael D. Doud and Clifford P. Kubiak, to be submitted. The dissertation author is the primary author of this manuscript.

5.6 References

(1) Østergaard, P. A.; Sperling, K. *International Journal of Sustainable Energy Planning and Management* **2014**, *1*, 5.

(2) McGlade, C.; Ekins, P. *Nature* **2015**, *517*, 187.

(3) Pfenninger, S.; Hawkes, A.; Keirstead, J. *Renewable and Sustainable Energy Reviews* **2014**, *33*, 74.

(4) Aslani, A.; Wong, K.-F. V. *Renewable Energy* **2014**, *63*, 153.

(5) Lewis, N. S.; Nocera, D. G. *Proceedings of the National Academy of Sciences* **2006**, *103*, 15729.

(6) Davis, S. C.; Diegel, S. W.; Boundy, R. G. *Transportation energy data book: Edition 23*, United States. Department of Energy, 2003.

(7) Cracknell, J. A.; Vincent, K. A.; Armstrong, F. A. *Chemical Reviews* **2008**, *108*, 2439.

(8) Cuesta, A.; Cabello, G.; Osawa, M.; Gutiérrez, C. *ACS Catalysis* **2012**, *2*, 728.

(9) Chi, N.; Chan, K.-Y.; Phillips, D. *Catalysis Letters* **2001**, *71*, 21.

(10) Jiang, J.; Kucernak, A. *Journal of Electroanalytical Chemistry* **2009**, *630*, 10.

(11) Sathe, B. R.; Balan, B. K.; Pillai, V. K. *Energy & Environmental Science* **2011**, *4*, 1029.

(12) Jeoung, J.-H.; Fesseler, J.; Goetzl, S.; Dobbek, H. In *The Metal-Driven Biogeochemistry of Gaseous Compounds in the Environment*; Kroneck, P. M. H., Torres, M. E. S., Eds.; Springer Netherlands: 2014; Vol. 14, p 37.

(13) Shi, J.; Jiang, Y.; Jiang, Z.; Wang, X.; Wang, X.; Zhang, S.; Han, P.; Yang, C. *Chemical Society Reviews* **2015**, *44*, 5981.

(14) Jormakka, M.; Törnroth, S.; Byrne, B.; Iwata, S. *Science* **2002**, *295*, 1863.

(15) Dobbek, H.; Svetlitchnyi, V.; Gremer, L.; Huber, R.; Meyer, O. *Science* **2001**, *293*, 1281.

(16) Schuchmann, K.; Müller, V. *Science* **2013**, *342*, 1382.

(17) Piazzetta, P.; Marino, T.; Russo, N.; Salahub, D. R. *ACS Catalysis* **2015**, *5*, 5397.

(18) Lu, Y.; Jiang, Z.-y.; Xu, S.-w.; Wu, H. *Catalysis Today* **2006**, *115*, 263.

(19) Lamzin, V. S.; Dauter, Z.; Popov, V. O.; Harutyunyan, E. H.; Wilson, K. S. *Journal of Molecular Biology* **1994**, *236*, 759.

(20) Seu, C. S.; Appel, A. M.; Doud, M. D.; DuBois, D. L.; Kubiak, C. P. *Energy & Environmental Science* **2012**, *5*, 6480.

(21) Galan, B. R.; Schöffel, J.; Linehan, J. C.; Seu, C.; Appel, A. M.; Roberts, J. A. S.; Helm, M. L.; Kilgore, U. J.; Yang, J. Y.; DuBois, D. L.; Kubiak, C. P. *Journal of the American Chemical Society* **2011**, *133*, 12767.

CHAPTER 6
CONCLUSIONS AND FUTURE WORK

6.1 Introduction

The previous five chapters have discussed the synthesis and electrochemical characterization of new P_2N_2 ligands and their complexes. There are a multitude of motivations to continue research into these new P_2N_2 complexes. Practically, P_2N_2 complexes are among the best in the world at catalyzing the hydrogen evolution reaction,[1] and the novel complexes synthesized in chapters 2 and 3, with new phosphine substituents, improve catalytic ability for hydrogen evolution and increase the capability for functionalization of these ligands. Catalyzing hydrogen evolution from acidic solutions is one of the most plausible methods for the generation of a renewable fuel economy, a goal that is of paramount importance for the future of civilization. From the perspective of chemists, catalyst design is an important way to explore mechanisms for facilitating reactions. By understanding how an important reaction mechanism proceeds, even better catalysts can be designed, that once made, work even more efficiently.

6.2 Catalyst immobilization

The development of P_2N_2 ligands with functionalized substituents at the phosphorus atom offers the opportunity to design and synthesize better. Previous studies have successfully attached P_2N_2 complexes via the ligands to surfaces such as glassy carbon and multi-walled carbon nanotubes,[2,3] and others have studied the effect of modifying the amine substituent on the catalytic rates of these complexes.[4] The modified

glassy carbon and carbon nanotubes surfaces with nickel-P_2N_2 complexes show remarkable catalytic activity for heterogeneous hydrogen evolution from acidic solutions, displaying high rates and turnover numbers on the order of 100,000. These heterogeneous systems are desirable from an engineering point of view for the ease of separation between the catalyst and products. Unfortunately, modification of the amine substituent could limit mobility of the pendant amine, the part of the ligand that is responsible for the remarkable coordination of proton transfer to and from the metal active site.[5,6] By immobilizing these electrocatalysts through modification to the phosphine, the amine can retain the mobility that is critical to its function.

6.3 Substitution of phosphine by S_N1 or Michael addition reagents

The new ligand syntheses described in chapters 2 and 3 allow for further innovation in ligand synthesis in the future. Fundamentally, in addition to the nucleophilic substitution (S_N2) and Michael Addition reactions of tris(hydroxymethyl)phosphine (THP) to α,β-unsaturated carbonyls that introduce the phosphine substituent, there are several other types of reactions that could work in a similar fashion.

From the work in chapter 2, it is clear that only the most electrophilic and least sterically encumbered of alkyl halides will undergo S_N2 addition of THP. While methyl iodide, benzyl chloride, and ethyl bromide underwent successful substitution, other reagents including isopropyl iodide, *sec*-butyl bromide, and *tert*-butyl bromide resisted S_N2 addition, even under elevated temperatures and varied solvent conditions. It may however be possible to make ligands with these substituents on phosphine by S_N1

addition of THP. For example, the S_N1 mechanism, employing a reagent such as *tert*-butyl chloride could be used to introduce *tert*-butyl or other tertiary organic substituents.

Michael addition reactions of THP with other α,β-unsaturated carbonyl substituents could also be explored. While the additions of THP to ester acrylate, acrylic acid, and acrylamide in chapter 3 were relatively straightforward, the reaction with acrolein led to additional substitution on the cyano- group, and many byproducts. The use of ethylene oxide as an electrophile for addition to THP[7] could be a way of installing an alcohol group two carbons away from the phosphine, but may also complicate the final step in the ligand synthesis, the condensation with a primary amine.

6.4 Synthesis of asymmetric complexes

Additionally, the carbonate structure shown in figure 3.3 could allow for interesting preparations of ester and other P_2N_2 ligand complexes. The carbonate oxygens could serve as nucleophiles for esterification reactions, for example, reacting this complex with trimethylsilyl chloride should trimethylsiloxy ester substituents, which go on to produce a monoleptic trimethylsilyl ester Ni(P_2N_2) complex. This could be used to prepare asymmetric nickel complexes with two different sets of ligands. By introducing bipyridine ligands, or others that can act as electron reservoirs, the reduction potentials required for the active catalyst could be lowered. Alternatively, by including strong donor ligands such as carbenes, reduction potentials of the complexes should become more negative, and enhance the reduction of carbon dioxide.

The active sites of several carbon monoxide dehydrogenase (CODH) enzymes are shown in Figure 6.1. These enzymes are highly efficient at catalyzing the oxidation of

carbon monoxide and water to carbon dioxide and hydrogen gas, as well as the "microscopic reverse" reaction, the reduction of carbon dioxide.[8] These CODH enzymes are examples of heterobimetallic active sites, where one metal binds to carbon, and the other binds to oxygen during the catalytic process. Key to the synthesis of mimics of these heterobimetallic systems is the combination of two different coordination environments.

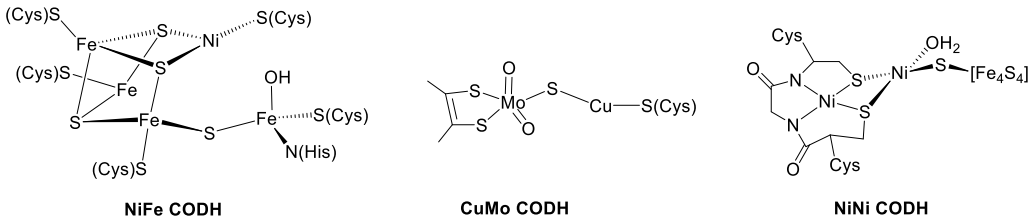

Figure 6.1 Active sites of NiFe, CuMo, and NiNi carbon monoxide dehydrogenase (CODH).[9]

The new complexes synthesized with P_2N_2 ligands via Michael Addition described in chapter 3 resemble half of one of these active sites. One advantage of these modified carbonyl substituents is the relative ease with which the ester or amide can be modified, through transesterification or transamidation.[10] The development of bimetallic catalysts is a complex but promising area of focus of much research.[11] While the challenge of developing biomimetic catalysts is daunting, the development of synthetic techniques for making new ligand-metal complexes and geometries is crucial to the development of new catalysts.

6.5 Testing of metal-P_4N_5 complexes as catalysts

While the novel P_2N_2 ligands were synthesized successfully, they were not the only products of the reactions. Due to the evolution of formaldehyde from the dehydroxymethylation steps, multiple condensation products were observed. The isolation of the $Ni(P_4N_5)^{2+}$ byproduct material from the mixture of products in the complexation reaction to nickel(II) salts enabled it to be identified following the growth of single crystals suitable for X-ray diffraction study.

Tetradentate tetraphosphine byproducts were obtained during the synthesis of selected P_2N_2 compounds. This is likely due to a side reaction involving formaldehyde and the reaction intermediate hydroxymethyl phosphines. If complexes of these ligand show promising catalytic reactivity, they could also be synthesized independently by the reaction shown in Scheme 6.1. As shown in scheme 6.1, two equivalents of unreacted tris(hydroxymethyl)phosphine combine with two equivalents of singly-substituted bis(hydroxymethyl)alkylphosphine and five equivalents of the primary amine to form a tetradentate tetraphosphine ligand without isolation. This mixture was reacted with $Ni[PF_6]_2$ or $Ni[BF_4]_2$ to make the monometallic nickel complexes shown in Scheme 6.1.

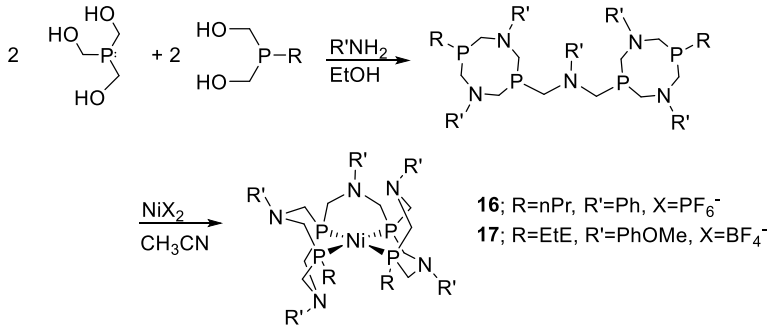

Scheme 6.1 Synthesis of $Ni(P^R_4N^{R'}_5)X_2$ complexes.

Figures 6.2 and 6.3 illustrate two examples of a similar type of complexation byproduct, with these P_4N_5 ligands. Figure 6.2 shows the cation in the nickel(II) hexafluorophosphate complex of the n-propyl substituted tetraphosphine with a phenyl-substituted amine ($[Ni(P^{nPr}{}_4N^{Ph}{}_5)](PF_6)_2$, complex **1**), and figure 6.3 shows the nickel(II) tetrafluoroborate complex of the ethyl-ester-substituted tetraphosphine with a 4-methoxyphenyl-substituted amine ($[Ni(P^{EtE}{}_4N^{PhOMe}{}_5)](BF_4)_2$, complex **2**).

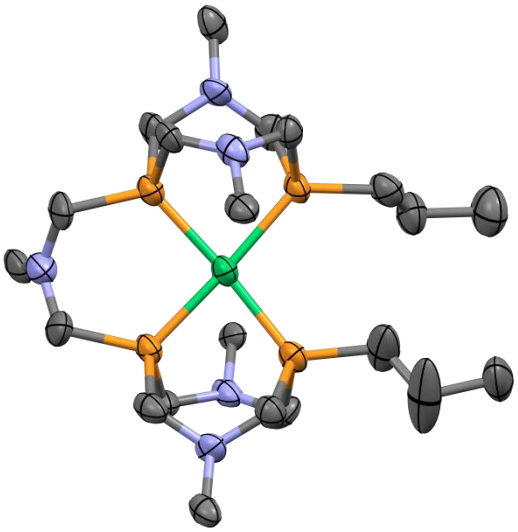

Figure 6.2 Molecular diagram for complex 16, $Ni(P^{nPr}{}_4N^{Ph}{}_5)[PF_6]_2$. Thermal ellipsoids are shown at the 50% probability level. Counterions and hydrogens have been removed for clarity. Only the N-C atoms of phenyl-amine substituents have been shown for clarity.

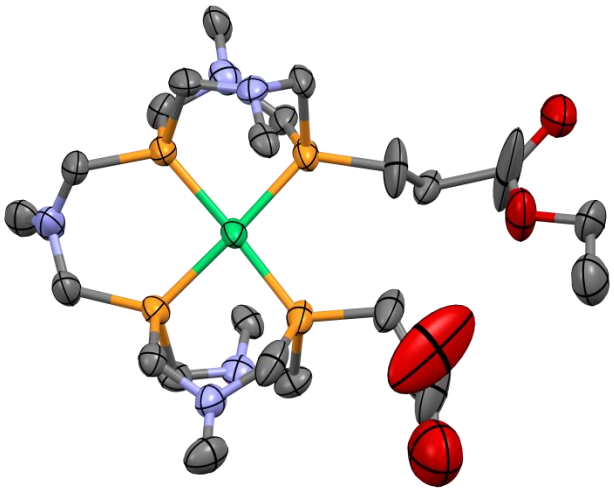

Figure 6.3 Molecular diagram for complex 17, Ni($P^{EtE}_4N^{PhOMe}_5$)[BF_4]$_2$. Thermal ellipsoids are shown at the 50% probability level. Counterions and hydrogens have been removed for clarity. Only the N-C atoms of 4-methoxyphenyl- amine substituents have been shown for clarity.

Each of these complexes, **16** and **17**, were obtained as minor products during the synthesis of nickel-P_2N_2 complexes. Through careful synthesis, as proposed in scheme 6.1, more such complexes could be made and studied. The geometry of the metal-ligand complex suggests the reactivity of the complexes may be similar to $[Ni(P_2N_2)_2]^{2+}$ complexes, with five pendant bases to facilitate proton transfer instead of two. Complexes of other P_4-type ligands with pendant bases have shown promise for electrochemical hydrogen evolution,[12] so the catalytic activity of complexes **16** and **17** for HER should be tested.

6.6 The future of biomimetic catalysis

In this thesis, I have shown that by designing new P_2N_2 ligands and varying the phosphine substituents, new complexes can be synthesized that mimic the activity of

enzymes and are better than existing literature mimics at facilitating the efficient transfer of protons between solution and a substrate. Using our knowledge of the mechanisms of enzymatic catalysts, the design and development of efficient catalytic inorganic systems can become more precise. Ultimately, designing and building chemical systems that are as efficient as enzymes is a major goal, and the development of efficient inorganic technologies may well be more competitive at substrate conversion than nature, due to the complexities associated with the integration of enzymes into living systems.

In this chapter, I have discussed two potentially promising synthetic routes for the development of bimetallic and biomimetic catalysts. There is a great amount of work to be done in the development and exploration of new ligand and metal complex syntheses; hopefully, these can contribute to efficient implementation of a renewable energy paradigm.

6.7 References

(1) Wiese, S.; Kilgore, U. J.; DuBois, D. L.; Bullock, R. M. *ACS Catalysis* **2012**, *2*, 720.

(2) Das, A. K.; Engelhard, M. H.; Bullock, R. M.; Roberts, J. A. S. *Inorganic Chemistry* **2014**, *53*, 6875.

(3) Le Goff, A.; Artero, V.; Jousselme, B.; Tran, P. D.; Guillet, N.; Métayé, R.; Fihri, A.; Palacin, S.; Fontecave, M. *Science* **2009**, *326*, 1384.

(4) Le Goff, A.; Artero, V.; Jousselme, B.; Tran, P. D.; Guillet, N.; Metaye, R.; Fihri, A.; Palacin, S.; Fontecave, M. *Science* **2009**, *326*, 1384.

(5) Solis, B. H.; Hammes-Schiffer, S. *Inorganic Chemistry* **2014**, *53*, 6427.

(6) Seu, C. S.; Appel, A. M.; Doud, M. D.; DuBois, D. L.; Kubiak, C. P. *Energy & Environmental Science* **2012**, *5*, 6480.

(7) Vullo, W. J. *Industrial & Engineering Chemistry Product Research and Development* **1966**, *5*, 346.

(8) Ragsdale, S. W.; Pierce, E. *Biochimica et biophysica acta* **2008**, *1784*, 1873.

(9) Sathe, B. R.; Balan, B. K.; Pillai, V. K. *Energy & Environmental Science* **2011**, *4*, 1029.

(10) Rao, S. N.; Mohan, D. C.; Adimurthy, S. *Organic Letters* **2013**, *15*, 1496.

(11) Das, D.; Mohapatra, S. S.; Roy, S. *Chemical Society Reviews* **2015**, *44*, 3666.

(12) Wiedner, E. S.; Roberts, J. A. S.; Dougherty, W. G.; Kassel, W. S.; DuBois, D. L.; Bullock, R. M. *Inorganic Chemistry* **2013**, *52*, 9975.

6.8 Appendix

Table 6.1 Crystal data and structure refinement for complex 1.

Identification code	$Ni(P^{nPr}{}_4N^{Ph}{}_5)[PF_6]_2$
Empirical formula	$C_{50}H_{80}N_2F_{12}P_6Ni$
Formula weight	1181.69
Temperature/K	100.0
Crystal system	triclinic
Space group	P-1
a/Å	9.2759(6)
b/Å	21.1332(14)
c/Å	28.457(2)
α/°	90.008(5)
β/°	92.870(5)
γ/°	90.144(5)
Volume/$Å^3$	5571.4(6)
Z	4
$\rho_{calc}g/cm^3$	1.409
μ/mm^{-1}	0.597
F(000)	2480.0
Crystal size/mm^3	0.2 × 0.1 × 0.1
Radiation	MoKα (λ = 0.71073)
2Θ range for data collection/°	1.928 to 50.736
Index ranges	$-11 \leq h \leq 11$, $-25 \leq k \leq 20$, $-34 \leq l \leq 33$
Reflections collected	67405
Independent reflections	19873 [R_{int} = 0.2420, R_{sigma} = 0.3407]
Data/restraints/parameters	19873/0/1358
Goodness-of-fit on F^2	1.048
Final R indexes [I>=2σ (I)]	R_1 = 0.1381, wR_2 = 0.2931
Final R indexes [all data]	R_1 = 0.3199, wR_2 = 0.3732
Largest diff. peak/hole / e $Å^{-3}$	1.14/-0.70

Table 6.2 Crystal data and structure refinement for complex 2.

Identification code	Kubiak_MDD131217_EtEPh_Artemis
Empirical formula	$C_{52}H_{58}B_2F_8N_3NiO_4P_4$
Formula weight	1145.35
Temperature/K	273.15
Crystal system	monoclinic
Space group	C2/c
a/Å	38.035(6)
b/Å	11.4418(17)
c/Å	32.669(5)
α/°	90
β/°	123.359(3)
γ/°	90
Volume/Å^3	11875(3)
Z	8
ρ_{calc}g/cm^3	1.465
μ/mm^{-1}	0.622
F(000)	5384.0
Crystal size/mm^3	0.5 × 0.5 × 0.5
Radiation	MoKα (λ = 0.71073)
2Θ range for data collection/°	2.564 to 50.82
Index ranges	-45 ≤ h ≤ 45, -13 ≤ k ≤ 13, -38 ≤ l ≤ 39
Reflections collected	53812
Independent reflections	9854 [R_{int} = 0.1262, R_{sigma} = 0.1427]
Data/restraints/parameters	9854/0/773
Goodness-of-fit on F^2	1.568
Final R indexes [I>=2σ (I)]	R_1 = 0.1168, wR_2 = 0.2764
Final R indexes [all data]	R_1 = 0.2312, wR_2 = 0.3172
Largest diff. peak/hole / e Å^{-3}	2.41/-0.69